Complete characterization of plasma mirrors and development of a single-shot carrier-envelope phase meter

PhD thesis by
Tibor Wittmann

Supervisors:
Prof. Dr. Béla Rácz
Dr. Patrick Audebert

University of Szeged
Faculty of Science and Informatics
Doctoral School in Physics
Department of Optics and Quantum Electronics

Szeged, 2009.

Contents

Chapter 1

Introduction

Delivering a great amount of energy within less than a trillionth of a second is the unique ability of high-power short pulse lasers that made them an invaluable device in experimental high-field physics. The exceptionally high intensity that high-power lasers provide opened a new era in the investigation of matter at extreme conditions. Lasers now routinely generate pulses with multi-TW peak powers and in a few laboratories pulses with petawatt peak powers are available. Focusing such pulses onto a tiny small spot, peak intensities of 10^{22} W/cm^2 [1] can be generated that instantaneously transforms the surface of any solid target into a hot overdense plasma. At these extreme intensities and target temperatures relativistic interactions come to the fore opening the door to the investigation of a wide range of new phenomena. Experiments theoretically predicted for a long, like high-order harmonic generation from oscillating plasma surfaces, or proton acceleration from thin foil films are now routinely performed in many laboratoires. The prerequisite to conduct laser-plasma experiments this kind is to ensure a clean interaction between the exposed solid target and the laser pulse. This practically means that prior to the arrival of the main laser pulse, radiation with a considerable intensity mustn't expose the target. Unfortunately for technical reasons in the amplification process pedestals and leading prepulses are unavoidably generated. Their focused intensity is only a few orders of magnitude lower than that of the main pulse and thus it is well beyond the damage threshold of any target material. As a result prepulses and the pedestal that overtake the main pulse generate a low density preplasma, which expands on the target surface and in place of the steep density gradient solid target the main pulse interacts with the low density preplasma. This unwanted phenomenon has existed since the invention of CPA lasers and has remained the main impediment to study laser-solid interaction at relativistic intensities.

Intensity contrast is the quantity that is used to characterize the temporal cleanness of laser pulses. It is the ratio of the intensity of the main pulse to that of the pedestal. Continuous efforts have been taken to improve the intensity contrast of high-power lasers by several optical methods, and by incorporating all effective techniques into a laser system, the contrast nowadays approaches 10^8 at best [2]. This is several orders below the desired contrast ratios, as prepulses and the pedestal with an inten-

sity above 10^7 W/cm^2 easily alter the interaction and lasers with focused intensities beyond 10^{20} W/cm^2 are now commonplace in many laser laboratories. Moreover with continuous developments available peak intensities are steadily increasing, while available laser contrast have been at the same level for more than a decade now. This shows that improving the laser contrast is one of the foremost challenges in high-intensity laser physics.

Plasma mirror (PM), which is a self-induced ultrafast optical shutter was proposed as a contrast improvement technique already in the early nineties. Its operation is based on the ultrafast ionization of intense laser pulses: a laser pulse is focused onto a transparent bulk target, and while the low intensity prepulses and pedestal traverses the target, the rising edge of the main pulse with its high intensity generates a highly reflective flat plasma layer. The main pulse cleaned from the pedestal and prepulses is specularly reflected off the target thus the contrast of the reflected beam is significantly enhanced.

Although PM has been proposed for long as contrast improvement technique so far only proof-of principle studies have been conducted but no thorough characterization or practical implementation of this technique have been reported yet. My motivation in my Phd studies was to perform a complete experimental characterization of a single PM, and based on this study to take part in the developement of an effective double plasma mirror (DPM) pulse cleaner for the 100 TW laser system at Laboratoire d'Optique Appliquée, and to perform a full characterization of the DPM system.

In chapter 2 first we present the problem of insufficient contrast in laser-solid experiments and we briefly review the existing contrast improvement techniques and show their limitations. Then we describe the principles of PM operation and review some of the proof of principle PM experiments. We conclude at the end of the chapter that in order to construct PMs for high power lasers a thorough quantitative characterization of the PM had been still lacking.

In chapter 3 we provide the theoretical background for plasma mirror generation by high power short laser pulses. We describe the propagation of laser pulses in plasmas by focusing on the fundamental differences between the propagation of S and P polarized beams, and show the role of the critical frequency in reflecting laser light from plasma surfaces. We describe the ionization mechanisms occurring in dielectrics in the presence of intense laser light and briefly review experimental and numerical studies conducted about laser induced breakdown of dielectrics.

In chapter 4 we present a complete experimental characterization of the PM, which was performed at CEA Saclay with the LUCA laser. We describe the experimental setup and present the obtained results: time and space resolved reflectivity and the the onset of plasma formation in function of the incident fluence and the improvement of the spatial profile of the reflected beam.

In chapter 5 we present a double plasma mirror pulse cleaner developed for the 100 TW laser at Laboratoire d'Optique Appliquée. First we discuss the required contrast of laser-solid experiments and then we evaluate the desired contrast level of the laser system. The main part of the chapter presents a complete experimental and nu-

merical characterization of the DPM system including a proof-of-principle experiment on laser-plasma harmonics.

While the first part of my thesis focuses on the improvement of the temporal contrast of sub-picosecond high-power laser pulses – as it has been briefly presented above – the second part of my thesis deals with a fairly different topic, with the development of a single-shot stereo-ATI phase meter.

Thanks to the vast progress in laser technology in the early nineties including such inventions like chirped mirrors [3] and the hollow-fiber compression technique [4], generation of pulses comprising merely a few oscillation cycles of the electromagnetic field became possible. A unique feature of few-cycle pulses in contrast to multi-cycle ones is that the asymmetry in the temporal evolution of the electromagnetic wave within the laser pulse is significant. As virtually all strong field phenomena are directly governed by the electromagnetic field, this feature of few-cycle pulses by providing access to the electromagnetic field in the time domain attracted a great scientific interest in recent years.

The quantity that is used to characterize the evolution of the field within the laser pulse is called the carrier-envelope phase (CEP), which is defined as the offset phase between the electric field and the pulse envelope. Stabilization of the CEP of high repetition rate few-cycle sources became possible a few years ago using f-to-2f interferometers [5]. Phase stable pulses had an enormous impact on time resolved laser spectroscopy as tracking [6, 7] microscopic processes on attosecond time scales became possible. The major limitation of phase stabilization is that it is technically rather complex and it has been demonstrated only up to 0.2 TW peak powers [8], while few-cycle pulses with multi-10-TW peak powers are already available [9, 10]. These unique laser systems hold promise for the generation of isolated attosecond pulses on solid surfaces [11], which due to the several orders of higher intensity of the generated attosecond bursts would open up an entirely new regime for attosecond physics. It would became possible to perform XUV-XUV correlations and to extend attosecond metrology and spectroscopy to attosecond control, with one attosecond pulse releasing the electron and the other controlling its further evolution. However sufficient parameters of the laser pulse's envelope (pulse duration and intensity) are already available, due to the lack of phase stabilization conducting waveform dependent experiments at relativistic intensities is still not possible.

Here in this thesis I demonstrate the development of a measurement apparatus, a single-shot stereo-ATI phase meter, which will enable the characterization of phase dependent processes with few-cycle pulses at any laser intensities. This apparatus is based on the same principles as the previous multishot apparatus [12]. It retrieves the CEP from the left/right asymmetry in the yield of high-energy above-threshold-ionization (HATI) electrons along the polarization axis, but now from a single laser shot. This became possible as a four orders of magnitude increase in the sensitivity of the apparatus was achieved in contrast to the previous multi-shot phase meter. The new design including a completely redesigned vacuum apparatus and magnetic shield-

ing, a digital data acquisition system and an attached imaging system are described in great details in the thesis.

In chapter 6 first we provide a general overview about few-cycle laser pulses and their main applications in attosecond physics. We emphasize the role of waveform controlled few-cycle pulses in the generation of isolated attosecond bursts and describe also the limitations of this technique. We show why a novel measurement method is necessary in order to exploit the potential of state of the art multi-TW few-cycle laser systems to extend waveform dependent experiments to relativistic intensities.

In chapter 7 first we describe the evolution of HATI electrons in the laser field and explain the origins of their pronounced phase sensitivity. Then we describe the principles of phase meter operation and highlight the necessary changes to achieve single shot performance. Following that we describe in great detail the new design of the single-shot phase meter. Then we present the recorded single shot left and right HATI spectra for different CEP values and describe a new representation for their evaluation. At the end of the chapter we introduce the novel measurement method CEP tagging that enables the study of waveform dependent experiments without the need for phase stabilization and compare it with a conventional phase scan on a stabilized laser.

Part I

Complete characterization of plasma mirrors

Chapter 2

General overview

2.1 Short pulse laser technology and intensity contrast

2.1.1 Chirped pulse amplification

Generating pulses with mode locked oscillators, and subsequent amplification of these pulses with multipass and regenerative amplifiers was a common technique up to the mid 80's for producing high-intensity ultrashort laser pulses. Pulses with a duration of a few picoseconds delivering several millijoules of energy were easily attainable this way. After proper focalization the peak intensity could approach 10^{15} W/cm^2 in the focus. The electric field of such extremely intense electromagnetic waves rivals the field inside atoms making possible the ionization of valence electrons by the oscillating laser field. Enabled by this enormous potential the focus of interest in atomic and molecular science turned toward laser induced ionization processes culminating in the discovery of above-threshold ionization by Agostini et al. in 1979 [13]. Experiments to explore ATI and other ionization mechanisms later on, consisted in exposing a dilute gas media to a tightly focused beam. The interaction could have been modeled in frame of atomic physics, as a clean interaction between a single laser atom and the laser field. To proceed further to study the collective behavior of atoms, ions and electrons, which comes to the fore at interaction with materials with higher densities, a significant increase in peak powers would have been necessary. A vast increase though seemed technically unfeasible that time, as lasers and their components were already at a practical limit in size, and pulse intensities inside amplifiers were already close to the damage threshold.

CPA technique

The breakthrough in amplification that overcame these difficulties leading to a revolution in the generation and application of high-intensity laser pulses was chirped pulse amplification (CPA). It was transferred from radar technology, where the same diffi-

culty arose in the creation of short energetic pulses [14]. The concept of this technique is the following: before amplification the pulse is temporally stretched by a large factor in order to reduce its peak power. Then this stretched pulse is sent into the amplifier, where it can be easily amplified to high energies without the risk of detrimental nonlinear pulse distortion or even optical damage. Finally it enters a compressor where it is recompressed to its original duration. The stretching and the compression is done using optical dispersion. Both stretcher and compressor consist of dispersive optical elements, typically of multiple prisms and/or gratings. The dispersion of the stretcher and that of the compressor are with opposite signs, which ideally cancel each other out ensuring that the original pulse duration is retained after amplification.

After the initial demonstration of this technique [15] an intensive progress in output peak powers began. The expansion-compression ratio after a novel stretcher design shortly approached the factor of 3000 [16] and soon pulses at the terawatt level became available [17]. Thanks to CPA, the fast development of high-intensity short pulse lasers has been going on ever since, making possible the generation of higher and higher intensities with relatively compact laser systems.

Application of CPA lasers

Various categories of CPA lasers respect to pulse width and pulse energy emerged, of course for very different applications. The most energetic pulses are produced by petawatt-class laser systems. The first representative of this category delivering sub-kilojoule pulses with some hundred femtosecond pulse duration started to operate in 1999 [18]. However that laser has been shut down and dismantled since, several petawatt lasers were constructed and put into operation in recent years [19–21]. These facilities are dedicated primarily to fast ignition [22, 23], but other phenomena which requires extremely high pulse energies like nuclear effects induced by laser accelerated high energetic protons [24] or the generation of extremely bright coherent X-ray pulses [25] by relativistic harmonics on solid surfaces [26] are also investigated.

Another class of high-intensity lasers with peak powers below one PW down to several terawatts is the most dominant nowadays. These tabletop TW and multi-TW laser systems are commonplace in many laser laboratories. Pulse durations typically range between 25 fs and some hundreds fs, and pulse energies from hundred millijoules up to 15 J. Due to the relatively short pulse duration, focused intensity can reach 10^{21} W/cm^2 [27] or even 10^{22} W/cm^2 in a nearly diffraction limited focus [1]. The sharply increasing temporal profile of the pulses makes these lasers suitable for a wide range of applications including the production of energetic collinear electron [28], multiple-charged-ion [29] and proton beams, generation of X-ray [30] and γ-ray [31] radiation, or the experimental demonstration of relativistic nonlinear Thomson scattering [32].

Thanks to the invention of chirped mirrors [3] and the hollow-core fiber technique [4] a new category of CPA lasers, ultrashort pulse lasers emerged in the late nineties [33]. These lasers are capable of generating pulses which are so short that they contain

only a few oscillation cycles of the electromagnetic field. The motivation behind the generation of shorter and shorter optical pulses is to make timed-resolved spectroscopic investigations at ever shorter time scales. Lasers now routinely generates pulses with sub-two cycle durations [34] and very recently generation of pulses in the so called single-cycle regime has become possible [35]. These pulses with a duration of only a few femtoseconds are short enough to study the dynamics of chemical reactions in real time [36], but still too long to explore the dynamics of subatomic particles which happen on attosecond timescales [37]. Generation of attosecond pulses which are well below the single-cycle limit of Ti:sapphire lasers is only possible in the XUV/X-ray range. Coherent XUV pulses with attosecond duration are synthetised from high-order harmonics [38] emitted from a gas jet irradiated by a few-cycle laser pulse [39]. Taking snaphots of evolving atomic systems [40, 41] or controlling electron wave packets with light [42] had been far beyond the reach with femtosecond laser pulses but became possible with attosecond XUV bursts. The emerging new field attosecond science [43] is a major application field of few-cycle CPA lasers.

2.1.2 Contrast of CPA lasers

Contrast problem

Majority of the scientifically exciting experiments mentioned above requires high intensity, temporally clean laser pulses. CPA opened the gate to the generation of unprecedented laser intensities, but its main limitation is that it is unable to provide the required high temporal cleanness for the amplified pulses. Due to several technical reasons the compressed pulses are overtaken by a long pedestal and some shorter prepulses. In high-intensity laser-solid experiments this preceding part of the pulse ionizes the target material, and creates a so called preplasma. The preplasma expands to low density on the target surface, and in place of the steep density gradient solid target the main pulse interacts with the low density preplasma. This unwanted phenomenon has existed since the invention of CPA lasers and has remained the main impediment so far to the investigation of laser-matter interaction at relativistic intensities. Another drawback of the presence of the pedestal is that in the amplification system it acts as a parasite stealing a large fraction of the energy from the main pulse. However its intensity is low, but due to its long duration, which is typically several nanoseconds, the energy of the pedestal and prepulses according to the estimations of Itatani et al. [44] can be even comparable to that of the main pulse.

The quantity that is used to characterize the temporal profile of laser pulses in respect of the pedestal is the so called intensity contrast ratio. It is the ratio of the intensity of the main pulse to that of the pedestal. As it is a time dependent quantity, the most common way to characterize the contrast of a particular laser is to give the contrast of the pedestal in different time domains in which it is more or less constant, and to specify the contrast of the distinct prepulses. If no corresponding time domain is mentioned (which is very common) the contrast of the pedestal is considered constant

in time. High-dynamic range contrast measurements around the main pulse are usually performed with third-order autocorrelators [45], while for longer time scales plasma shuttered high-sensitivity streak cameras [46] can be used.

Attempts on contrast improvement

There has been an intensive research on eliminating the pedestal and prepulses since the invention of CPA. The ionization threshold of solid targets depending on the pulse duration and type of material is in the range of $10^{10} - 10^{14}$ W/cm^2, hence clean interactions require pedestal intensities to be kept below this level. Several technical issues have been responsible for the presence of this undesired radiation, and those have changed over time with the development of the amplification systems.

In the beginning CPA was based on fiber-grating pulse stretcher-compressor systems. At that time due to the lack of oscillators capable of producing sufficiently short pulses with the corresponding broad spectra, optical fiber was used to increase the bandwidth by self-phase modulation (SPM). As a secondary function, the fiber acted as a stretcher by giving a positive chirp to the pulses. After amplification the pulses were sent into the compressor consisting of a pair of parallel gratings. The main principle of CPA is that the chirps introduced by the stretcher and the compressor stages are identical but with opposite signs, thus the pulse after compression recovers its initial shape and duration. Unfortunately in case of fiber-grating systems this is far from reality. The compressor, a simple device consisting of two optical gratings is a proper negative chirp delay line, but due to the fact that SPM is strongly intensity dependent, the chirp introduced by the fiber is only close-to linear in the central part of the pulse, but strongly nonlinear in the leading and trailing portions of the pulse. This strong discrepancy between the frequency-chirp characteristics of the fiber stretcher and the grating compressor leads to imperfect compression with a poor contrast ratio. This was mitigated by using appropriately long single-mode optical fibers where the combination of the positive group velocity dispersion (GVD) and SPM created a linear chirp over a fairly long part of the pulse [47]. This yielded a contrast ratio of not better than 1:100.

It was apparent that for a considerable improvement of the contrast the nonlinearly chirped leading and trailing portions of the stretched pulse have to be eliminated. The first simple and straightforward solution called spectral windowing simply erased those components from the spectrum [48], while a more sophisticated method employed well-controlled gain narrowing in the amplifier for the same purpose [49]. These simple techniques could increase the contrast up to 10^3, but a further improvement was impossible merely by manipulating the spectrum.

Temporal windowing was the next step in the long struggle for a better contrast. Yamakawa et al. [50] applied saturable absorbers in order to select the positively and linearly chirped central part of the stretched pulses. Removing the nonlinear components this way was a relatively simple and cost-effective method – although the contrast didn't get significantly better than with spectral windowing. Soon the

replacement of the saturable absorbers with fast Pockels cells was reported by the same authors [51]. The contrast was enhanced radically from 10^3 to 10^6, but the degree of sophistication of the laser system, and the expenses became high due to the Pockels cells. An other drawback of that technique was that the transmission rise-time of the available cells were relatively long compared to the duration of the chirped pulses in some laser systems, thus this approach couldn't offer a comprehensive solution to the problem.

It should be noted that the main source of the pedestals on nanosecond scale is amplified spontaneous emission (ASE). Noise photons presence in regenerative and multipass amplifiers follow the same path as the original pulse and due to high amplification ratios are strongly amplified by the nanosecond pump pulses. Each stage of amplification gives rise to this unwanted radiation but the major contribution comes from regenerative amplifiers. The intensity contrast ratio of these long pedestals to the main pulse at the beginning was typically 10^5 [44], thus significant effort has been made from the early times for the removal of this long and consequently rather energetic pedestal.

First attempts on the elimination of the ASE made use of saturable absorbers again by placing them after the compressor [52, 53]. Reducing the ASE this way benefits from the higher intensity contrast ratio of the compressed pulses, which helps the absorber to distinguish the signal from the ASE but at the same time increases the risk of nonlinear effects, which can degrade the pulse temporally and spatially. Other researchers employed birefringent fibers for nonlinear discrimination of the low intensity pedestals from the main pulse [54]. The contrast exceeded 10^7, but at the expense of significant pulse broadening.

In the meantime oscillators were developed those were capable of producing pulses with subpicosecond duration. Consequently fibers in the stretcher became dispensable for the production of high-intensity short pulses. Using fiberless grating-telescope stretchers, pulses with a positive linear chirp could be generated easily, which after amplification and recompression exhibited an intensity contrast ratio of better than 10^7. To attain such high contrast ratios a new concept in amplification called seed pulse injection was also necessary. Even though the major source of pedestals had been already avoided by the fiberless technique, but the presence of the ASE arising mainly from the regenerative amplifier still limited the generation of really clean pulses by CPA. ASE contribution from the amplifier was effectively reduced by injecting intense clean pulses directly from a high energy oscillator into the CPA system thus requiring less amplification [55]. Itatani et al. [44] fully exploited the potential of this method by pre-amplifying the pulses and cleaning them with a saturable absorber before sending them to the CPA.

The fast progress in laser technology was going on, and soon the generation of sub-20-fs pulses became possible. Amplification of such ultrashort pulses to terawatt peak powers with a high contrast ratio became of particular interest. Especially the generation of coherent ultraviolet and soft-X-ray radiation by means of high-order harmonic generation on solid surfaces could benefit a lot from the development of such

sources. Fiberless stretcher-compression configurations canceling the lower order phase errors with a sufficiently large bandpass were already available, but the contrast due to the higher-order dispersion, which were still present in those systems was still too low. This was partly eliminated by a novel all-reflective stretcher, which could enhance the intensity contrast of such broadband pulses up to 10^5 [56]. An other expander with the same performance based on a new approach was reported by Sullivan et al. [57]. In their design the conventional part of the stretchers, the cemented achromat lens or curved mirror was replaced by a tunable air-space doublet. This modification simplified the structure of the stretcher appreciably and made its handling much easier while the high contrast ratio was still ensured. A similar expander to that using only one grating instead of two was made by Cheriaux et al. [58]. Their aberration free stretcher-compressor system permitted the amplification of pulses with nine orders of magnitude to the joule level and subsequent recompression close to the initial duration. To date this is one of the most effective stretchers. It has been in use in one of the word's leading high-intensity laser facility for producing 100 TW pulses at 10 Hz repetition rate, with a contrast ratio better than 10^7 [59].

Limitations of all-optical methods

Due to the extensive research over the past two decades the contrast ratio of high-intensity short pulse lasers was raised from its primary value (10^2) of the first CPA lasers with four orders of magnitude up to 10^7, and distinct prepulses were reduced effectively by using fast Pockels cells. Recently by carefully optimizing the strecher-amplifier-compressor chain a contrast of 10^8 has been reported [2], which can be considered the best available contrast using only optical methods inside the laser. In respect of amplification efficiency these achievements are already satisfactory since only a negligibly small fraction of the pulse's total energy is stolen from the main pulse by the pedestal. But considering the main goal of all contrast enhancement efforts – a clean laser pulse with a sufficiently low pedestal and prepulses below the damage threshold for undisturbed laser plasma experiments – the success was still far away.

Lasers now in many laboratories can generate intensities above 10^{21} W/cm^2, whereas the pedestal with the maximum contrast exceeds 10^{14} W/cm^2. This is at least more than two orders of magnitude higher than the ionization threshold of any well-known target material, and even higher than the optical damage threshold. Despite numerous efforts there are still several sources of pedestals and prepulses in currently operating CPA lasers. These are the following: imperfect compensation of the higher order phase distortions induced by the amplifier, leaking pulses from previous round trips and imperfect recompression. Some of these have been predicted to overcome by a new technology optical parametric chirped pulse amplification (OPCPA) [60–62], which have been implemented in several laser systems in recent years [9, 10, 63]. Although no physical reason for the existence of any pedestal or prepulse was foreseen, recent characterization of the contrast showed the limitations of this technique as well [64].

In summary the desired contrast ratios to conduct experiments on solid surfaces are far beyond the capabilities of currently running CPA systems. Furthermore the progress in output peak power seems continuing in the near future, while no hope for any notable improvement of the contrast is expected. Therefore there is an increasing need for a technique which can increase the contrast of already existing and future high power lasers and keep pace with the development in peak powers.

2.2 Plasma mirror

Most of the contrast enhancement methods those have been described in the previous section were based on the concept, that the pedestal and prepulses should be avoided by the improvement of the laser chain. A different approach to the contrast problem is that the pulse should be cleaned from these leading satellites after compression, out of the laser. Primary attempts for such a filtering applied saturable absorbers, but with a low success, as it was mentioned already. A completely different method that avoids the beam to be sent through any material, what can lead to deleterious nonlinear effects, is the use of a plasma mirror.

2.2.1 Plasma mirror concept

Plasma mirror (PM) is a promising device for the suppression of the pedestal and prepulses of high-energy ultrashort pulse ($<$ 1ps) lasers. It is an ultrafast shutter switched by the laser light itself at the striking edge of the main pulse, so as cleaning the pulse from any leading pedestal. The operation of the PM (illustrated in Figure 2.1). is based on the ultrafast ionization of laser light. The laser pulse strikes a flat transparent target, at a well determined fluence. The fluence is sufficiently low for the leading pedestal and prepulses to be transmitted through the target, but high enough for the striking edge of the main pulse to ionize it. Owing to the very fast ionization, a dense, flat highly reflective plasma layer is triggered on the surface of the target. At the appropriate fluence the ionization takes place within a few optical cycles, and the expansion of this thin plasma layer is negligible during the laser pulse. Thus it remains a flat, metal-like mirror with good optical quality, low divergence and highly reflective for the main pulse. The laser pulse with almost no pedestal is reflected off specularly.

Of course some energy of the main pulse is absorbed by the target material for the creation of the plasma layer, and the reflectivity of the triggered plasma layer is high, but not perfect, as it also partly absorbs the beam. This results in an energy loss of the main reflected pulse. This is characterized by the ovetall reflectivity of the PM which is the ratio of the total energy of the main pulse before and after the PM. Another important characteristic is the contrast enhancement factor. However, the prepulse traverses the target without any reflective plasma formation, due to the Fresnel reflectivity a small fraction of the prepulse is also specularly reflected off the target. The prepulse thus can not be suppressed perfectly. The contrast is improved

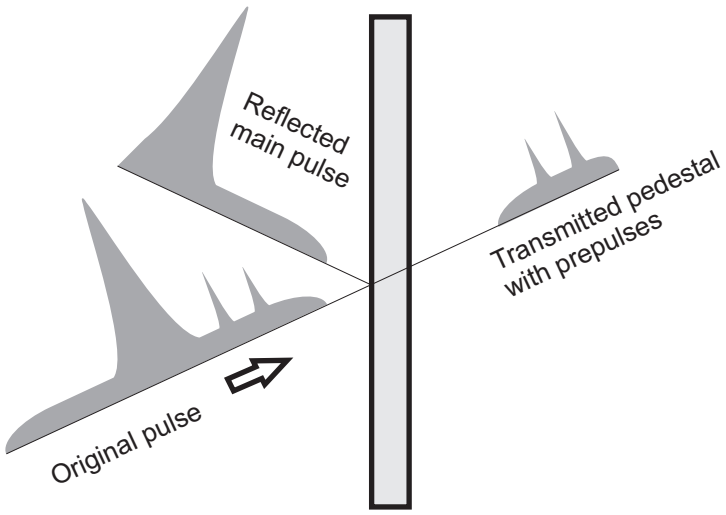

Figure 2.1: Plasma mirror concept. A laser pulse is focused onto a transparent bulk target. The fluence is adjusted so that the the leading pedestal and prepulses traverse the target while the striking edge of the main pulse ionizes it and almost instantaneously generates a highly reflective flat plasma layer on the target's surface. The main pulse and the post pulse cleaned from the pedestal and prepulses are specularly reflected off the plasma mirror.

by the reflectivity ratio of the plasma and the Fresnel reflectivity of the transparent target. Depending on the lifetime of the PM, a certain fraction of the post-pulse is also reflected. However the presence of the post-pulse is also unwanted for several experiments, but PM is only dedicated to the suppression of the prepulse, which is much more a hindrance to nowadays laser-plasma physics than the post-pulse.

Nonlinear reflectivity, contrast improvement

The reflectivity of the PM is strongly dependent on the fluence of the applied laser pulse. Below the threshold fluence, which is several J/cm^2 no breakdown occurs. The target remains transparent with its low Fresnel reflectivity. Pulses above the threshold ionize the target to the breakdown level, and create the reflective plasma layer. The amount of the absorbed energy that is necessary for the generation of the plasma, is a loss, since almost no reflection occurs until the breakdown. This loss is a higher fraction of a low energy pulse than of a high-energy pulse. Consequently, as a rule of thumb the reflectivity increases with increasing fluence of the incident laser beam. To achieve the highest possible reflectivity, the laser fluence has to approach the limit, where the prepulse still can't trigger any plasma formation itself.

Ti:sapphire lasers owing to the applied amplification techniques generates polarized laser pulses. It is the experimentalist choice weather in the particular experiment one utilizes S or P polarized beam. The absorption of light, and thus the generation of

the PM is different for the two polarizations. Therefore the most important features of the PM: contrast enhancement and peak reflectivity are strongly dependent on the polarization. The absorption mechanism will be discussed in greater details in chapter 3, here only a brief overview of the consequences of the polarization on reflectivity and contrast improvement is presented. For P polarization, due to resonance absorption the reflectivity of the plasma is lower than in S. The Fresnel reflectivity is also different for S and P polarization. For S it is higher. Typically, for transparent glass-like targets it is between 4 and 10% depending on the target material and angle of incidence. The prepulse is reflected off the target with that reflectivity. In contrast, for a P polarized beam, in Brewster angle the Fresnel reflectivity is zero. In practice though the polarization of a high power beam is never perfect, thus the reflectivity can not be lower than a few tenths of one percent. This means that in P polarization the contrast improvement can be high, but the reflectivity of the PM is relatively low. For an S polarized beam the reflectivity of the PM can be higher, but due to the high Fresnel reflectivity, the contrast improvement is low. This can be improved significantly by the use of anti-reflection (AR) coated target, leading to a high reflectivity and contrast enhancement simultaneously. A well-fabricated AR target can reduce the reflectivity of prepulse down to some tenth of one percent even for broadband pulses. This leads to a radical enhancement of the contrast thus making S polarization with AR coated targets the ideal choice for plasma mirrors. The AR coating doesn't affect the reflectivity of the PM appreciably. The only negative aspect of this setup are the high cost of AR targets.

To ensure the flatness of the triggered PM, the laser beam always has to strike a flat undamaged target surface. For low repetition rate lasers this can only be provided by shifting the target after each shot. For lasers with high repetition rates this method is hardly feasible. The solution to that can be a liquid jet target, with its self-reproducing flat surface.

Spatial distribution, spatial filtering

The nonlinear dependence of the reflectivity on laser fluence has some important consequences on PM operation. Owing to this nonlinearity, the spatial profile of the reflected beam differs from that of the incident beam. Assuming a Gaussian spatial energy distribution for the focused beam on the PM surface, the reflectivity of the PM is much higher in the center of the focal spot than at the boundary. Therefore the reflected beam's spatial energy distribution will be steeper than that of the original Gaussian beam. As in most laser-solid experiments, where the contrast is the key parameter the energy delivered in the central part of the focus matters rather than the total focused energy, the peak reflectivity, which is higher, characterizes the PM better than the total or overall reflectivity.

Another important feature of the PM is that it spatially filters the beam. Imperfections of the beam appears in the focal plane as low intensity ripples. If the fluence on the PM is ideal to provide the highest reflectivity in the center, the low intensity

ripples will be poorly reflected. The PM act as a pin mirror placed in the center of the focal spot. This slight improvement of the beam profile is a key characteristic from the application point of view, since high-intensity lasers often exhibit a rough profile that considerably limits focusability.

Pulse width reduction, spectral changes

The lifetime of the triggered plasma sets a temporal limit to the applied pulse duration. Even during short pulses the plasma expands and the density gradient declines. Up to a certain pulse duration, the expansion is negligible, respect to the optical quality of the PM. The reflectivity is specular and no degradation to the beam occurs. The only alteration caused by the expansion on account of the Doppler effect is a blue shift of the spectra [65]. The extent of the blue shift is a function of the expansion velocity and the pulse duration. For longer pulses it is obviously larger. For long pulses that are so long, that the hydrodynamic expansion is not planar any more, the plasma stops being a highly reflective flat metal-like surface. The expansion of the plasma can be calculated from the pulse width and the expansion velocity, which equals approximately the plasma sound speed. Comparing the calculated expansion with the focal spot size, enables to estimate weather the PM is still applicable on a particular laser, or not.

Even for high-energy pulses the generation of the plasma layer requires some energy and takes some time. In the case of a pulse with the appropriate fluence (corresponding to the maximum peak reflectivity as described above), the striking edge of the pulse creates the plasma within a few optical cycles. However during plasma formation, the absorption dominates, and the reflectivity gradually increases from its initial value, which is given by the Fresnel formula. This results in a steeper rising edge and a shorter pulse duration of the reflected pulse.

2.2.2 Evolution of the plasma mirror idea

Primary plasma mirror studies

However the principles of plasma mirror seems simple, for the proper, effective operation of the PM many hurdles had to be overcome. Pioneer experiments using PM for contrast improvement was carried out first in the early nineties [66–69]. Encountering the prepulse problem in the generation of short X-ray pulses emitted from laser produced plasmas inspired Kapteyn et al. [66] to the installation of a PM into their experimental setup. Ultrashort high-intensity laser pulses with sufficiently high contrast focused on a solid target can create a nearly solid-density plasma that emits short X-ray bursts. The pulse width of the X-ray pulse typically falls into the ps range. With lower contrast the prepulse energy can exceed the breakdown threshold, and vaporize the solid target prior to the arrival of the main pulse. Thus the main pulse instead of the solid target interacts with the lower density plasma, and this results in significantly longer pulse widths of the emitted X-ray bursts. To demonstrate that

PM is an appropriate device for contrast improvement a comparative study was made: X-ray pulses were generated by laser pulses (150 fs, 3 mJ) having different intensity contrasts and the X-ray pulse durations were compared. A pulse with an artificially increased ASE (from 0.1% to 15%) was cleaned by a PM and were focused onto a target to generate X-ray bursts. It was found that these bursts have the same duration as those generated with the original unmanipulated laser beam (with 0.1% ASE) at half the output energy. (The reflectivity of the PM is approximately 50%, hence for the accurate comparison, the energy of the initially high contrast beam had to be reduced.) Removing the PM from the beam path of the pulse with 15% ASE resulted in a significantly longer pulse duration of the X-ray burst. These results demonstrated, that the PM is beneficial to the generation of high density laser plasmas, as it reduces the pedestal intensity without markable spatial or temporal degradation of the laser pulse. In this pioneering paper, the proof of principles of plasma mirror operation for the supression of the pedestal were presented.

A comprehensive research article of the PM operation was published by Gold et al. [67]. In that paper fundamentals of PM were described, relevant work was thoroughly reviewed and new results were also presented. Experiments for characterizing the reflectivity, the spatial filtering and pulse width reduction were carried out. The average reflectivity was measured in function of the focused laser energy. The angle of incidence was 45 °. Above the breakdown threshold with increasing energy the average reflectivity rises sharply and peaks at 60% with an input energy of 1.5 mJ . The corresponding intensity (calculated assuming a Gaussian profile) was $1.4 \cdot 10^{15}$ W/cm^2. Reflected spatial profile measurement was done at different pulse energies. Images of the reflected beam met expectations: high frequency spatial intensity ripples and diffraction rings were diminished. The reflected beam remained nearly Gaussian, with a steeper intensity slope at high energies. Measurement of the pulse width reduction using a single shot second-order autocorrelator was also reported. Unfortunately neither a detailed description of the experimental setup nor information on how the pulse width was retrieved from the autocorrelation trace was given in the paper. This lack of information makes the reader think that however the temporal asymmetry of the reflected pulse was discussed in the paper, it wasn't considered at the autocorrelation measurement and simply an ordinary autocorrelation was performed. Since pulse symmetry is a prerequisite of second order autocorrelation, it is an inappropriate method here for the correct detection of pulse width reduction. Consequently the reported experimental findings on shorter reflected pulse width are unreliable.

Liquid jet as a promising plasma mirror target for high repetition rate lasers was investigated by Backus et al. [68]. The jet was found to be a trouble free solution with its stable, fast recovering flat surface. Measurement of the average reflectivity of the PM at different polarization, and angle of incidence was carried out. The contrast improvements were inferred from the cold (Fresnel) and plasma reflectivities. As it was expected the average reflectivity was significantly higher and the contrast enhancement was much lower at S polarization than at P. At P polarization in Brewster angle the highest measured average reflectivity was 38% with an inferred contrast improvement

of 380. The calculated peak intensities used at S polarization for approximately the same reflectivity was found to be more then an order of magnitude higher than in [67].

Another study of PM operation was performed by Gold [69]. Measurements of spatial filtering and smoothing, spectral blue shift and broadening agree well with previous results. The intensity contrast for the first time was directly measured with a high-dynamic-range autocorrelator. The instrument limited measurement showed a massive > 625 improvement of the contrast for P polarized beams when the angle of incidence was carefully set to Brewster angle.

In summary these early PM experiments demonstrated the proof of concept of PM operation, that it can effectively improve the contrast of high-power lasers. Contrast improvement factor of better than 625 was achieved, while no degradation but rather a slight improvement in the reflected beam's spatial profile was observed. The energy loss on the PM was relatively modest. The fundamental differences between S and P polarization were experimentally demonstrated although the ideal combination of an S polarized beam and AR coated target, as it was proposed in [66] hasn't been used. In all measurements the average reflectivity was measured and the fluence wasn't directly measured but calculated assuming a Gausian beam profile. Regarding the spatial distortions of high-power lasers these results can be very approximate. Therefore the construction of PMs for high power state-of-the-art laser systems based on these studies was not possible. Accurate quantitative measurements for the exploration of PM operation still had to be performed.

Time resolved plasma mirror studies

The first time resolved plasma mirror reflectivity measurement have been conducted by Bor et al [70]. In their experiment a pump-probe arrangement was used to measure the reflectivity change on various polymer (PMMA, Mylar, Kapton) surfaces after ablation by an UV excimer laser (248 nm) beam. A low intensity dye laser (496 nm, 500 fs) at 57.5° angle of incidence probed the target. The reflected probe was imaged onto a screen with a hole in its center. The energy of the reflected dye beam was measured behind the hole. This ensured that not the average but the peak reflectivity was measured. It was found that after ablation the reflectivity increases within 0.4–1 ps to its peak value (94% for Kapton). After the short rise time it decreased gradually (within 10–20 ps) significantly below the initial value, which was attributed to the roughening of the ablated surface. With a different experimental setup spectral changes were investigated. The reflected spectra was blue shifted and broadened (1 nm).

A somewhat modified setup was used to probe the reflectivity of the triggered PM on liquid [71] and solid [72] surfaces. The probe dye laser beam was focused onto the target with a cylindrical lens at 45° angle of incidence. The pulse front in the line focus scanned along the irradiated surface. Temporal changes of the reflectivity modified the spatial energy distribution of the reflected beam which was monitored by a diode array connected to a fast oscilloscope. Polysilicone oil, methyl(metacrylate), styrene, and water [71] exhibited a fast change in reflectivity with a 0.4–0.7 ps rise time. The

peak reflectivity of the plasma was 1.5–2.5 times higher than the initial cold or Fresnel reflectivity of the sample, that after 2–6 ps life time fell back to the initial value. Similar results were obtained for solid polymeric and semiconductor targets [72]. In both study the UV absorbtion was increased by doping the sample with naphthalene. The reflectivity vs. dopant concentracion curve for liquid methyl(metacrylate) increased up to 2% of concentration and sharply fell beyond that. For solids a reflectivity increase was observed for doped PMMA and a decrease for doped glass as compared to undoped samples. The reflectivity increase of doped liquids was attributed to the increased absorption coefficient and to contribution of 2-photon absorption of the naphthalene. At higher concentration an observed thin solid film on the liquid surface, that was induced by UV irradiaton, was accounted for the sharp fall of the reflectivity. Similar to liquids the reflectivity increase of doped PMMA could be explained by faster ionization while the reflectivity decrease of doped glass was attributed to the expansion of the plama as the dominant effect.

The significance of these time resolved studies is that a conclusive experimental evidence for the first time of the instantaneous nature of the PM generation was provided. Even at the relatively low incident pulse energies the PM was triggered within a few picoseconds. Furthermore although it was not the prime objective of the measurement in [70] but the first direct measurement of peak reflectivity was also performed. The close-to-perfect (94%) reflectivity clearly demonstrated that the peak reflectivity can be significantly higher than the overall reflectivity that had been measured in previous studies. The measured reflectivity dependence on the dopant concentration in [71, 72] provides a deeper insight into the competeing processes involved in reflective plasma generation. Moreover in [71] the generation of the reflective plasma is thoroughly reviewed.

2.2.3 Goal of the single PM study

My first goal is to perform a complete experimental characterization of a single PM. So far in the above reviewed proof of principle experiments only the time and space integrated (overall) reflectivity was measured which depends on the spatial parameters of the applied laser, therefore such measurements can not be used as an absolute reference. My primary goal was to perform a complete space and time resolved experimental study that can provide the necessary parameters for designing an effective PM system for the 100 TW laser at Laboratoire d'Optique Appliquée.

The experimental characterization aimed for measuring: time and space resolved, time integrated and space resolved (peak) and time and space integrated (overall) reflectivity in function of the incident fluence at various pulse durations. My goal was to measure the plasma triggering threshold at various pulse durations and demonstrate that by applying the optimal fluence on the PM, it can effectively enhance the intensity contrast of high-power laser pulses, while focusability and spatial characteristics of the reflected beam are also improved.

Chapter 3

Plasma generation with short laser pulses

This chapter discusses the theoretical aspects of plasma mirror generation by high-power short laser pulses. In the first section the electromagnetic wave propagation in plasmas is studied. First, waves impinging at right angles to the vacuum-plasma interface are examined and by deriving the dispersion relation the role of the critical density in the reflection of light is discussed. Then more generally the propagation of obliquely incident laser pulses is presented and the fundamental differences between the propagation of S and P polarized beams in plasmas are highlighted.

In the second short section ionization mechanisms occurring in dielectrics in the presence of intense laser light is presented and at the last section experimental and numerical studies about the breakdown of dielectrics are briefly reviewed.

3.1 Electromagnetic wave propagation in plasmas

When an electromagnetic wave propagates in a medium it induces a material response - each particle in the medium emits a small e. m. wave - and the wave inside and outside the material is constructed by the superposition of the original wave and the small induced e. m. waves. In case of low density gases the calculation of the transmitted and reflected wave is fairly simple since interactions between rare particles can be neglected. For higher density materials like dielectrics such simplification can not be made but the effect of each particle on the others should also be taken into account. When plasmas are considered the situation is even more complicated since plasmas as ionized gases besides the neutral particles contain a large number of charged particles. The free electrons and ions collide freely with each other and with the neutral particles, and due to the collisions change the magnitude and direction of their speed and travel zigzag orbits. However these collisions and other processes those lead to the ionization of solid material are in the focus of our interest, but for the derivation of the wave propagation equations, first the two-fluid model will be applied, which models collisions between the different species simply by a set of collision frequencies. Collisional processes in a

simplified form will emerge at the end of this section for the calculation of the dielectric function of plasmas but in depth discussion of this effect and other dominant ionization mechanisms will be presented comprehensively only in the next section.

The two fluid model considers the plasma as two interpenatrating fluids consisting in purely electrons and ions and derives equations for the evolution of the different parameters (i. e. density, pressure). The most important characteristic of the plasma that can be investigated satisfactorily with this model is the high frequency Langmuir oscillation of the electrons which according to the above explanations have a serious effect on e. m. wave propagation.

3.1.1 Electron and ion oscillations

An important mechanism in plasmas that makes them so different from ordinary gases is that besides the transversal e. m. waves, longitudinal electrostatic waves of ions and electrons are also present. Both charged species, the ions and electrons themselves constitute resonant systems and oscillate about their equilibrium positions with their own characteristic frequencies. On the macroscopic level these oscillations manifest themselves as periodic charge density vibrations which are mainly responsible for the unique features of plasma. Our intention here is to assess how these electrostatic vibrations influence the propagation of e. m. waves in plasmas.

First let us consider the oscillation of the electrons. When the electrons are displaced from their equilibrium positions an electrostatic force between the ions and electrons try to pull them back to the ions. Owing to the much greater mass of the ions compared to the electrons the movement of the ions is insignificant, thus it is straightforward to consider that the restoring force induces an oscillation of the electrons around the fixed ions. However this oscillation is a truly three-dimensional movement, for the derivation of the characteristic frequency it can be treated as a simple one dimensional resonant oscillation. Since this derivation is a simple exercise of classical mechanics [73], which holds no interest regarding our purposes here just the result is presented. The characteristic frequency of the electron plasma oscillation or with other name the Langmuir frequency is given by:

$$\omega_{pe} = \sqrt{\frac{e^2 n_e}{\epsilon_0 m_e}} \tag{3.1}$$

where e and m_e is the charge and the rest mass of the electron respectively, n_e is the plasma electron density and ϵ_0 is the permittivity of free space also known as the electric constant.

On a much longer time scale than that of the electron oscillations, the ions also support resonant vibrations. As these longitudinal oscillations don't have a considerable influence on e. m. wave propagation in plasmas, it is beyond the scope of this study to investigate the supporting mechanisms in details. It is only worth to mention here that these waves are often called as ion sound waves referring to the fact that their

propagation is analogous to sound propagation in gas media. In plasmas produced by short laser pulses electrons transfer only a very small amount of energy to the ions.

3.1.2 Wave equations in plasma

Now by considering longitudinal electron plasma oscillations, we can derive the wave equations for plasma. Of course for this, the well known Maxwell's equations will be used:

$$\boldsymbol{\nabla} \cdot \boldsymbol{E} = \frac{\rho}{\epsilon_0} \tag{3.2}$$

$$\boldsymbol{\nabla} \cdot \boldsymbol{B} = 0 \tag{3.3}$$

$$\boldsymbol{\nabla} \times \boldsymbol{E} = -\frac{\partial \boldsymbol{B}}{\partial t} \tag{3.4}$$

$$\boldsymbol{\nabla} \times \boldsymbol{B} = \mu_0 \boldsymbol{j} + \frac{1}{c^2} \frac{\partial \boldsymbol{E}}{\partial t}, \tag{3.5}$$

where $\boldsymbol{E}$ is the electric field strength, $\boldsymbol{B}$ is the magnetic flux density, $\boldsymbol{j}$ is the electric current density and ρ is the volume charge density. Solution of these equations in combination with a model for the polarization response of the medium provides the exact description of the field propagation. Such a calculation is far beyond the capabilities of present computers, thus an approximative treatment is required. A significant simplification can be made by using the quasi-stationary approximation, which considers the electric field to be harmonic in time all along the plasma. The necessary requirement of this is that the temporal evolution of the dielectric function have to be slow on the timescale of the incident laser pulse's optical cycle. In our experiment due to the relatively long pulse durations (≥ 60 fs) this was the case. This approximation is reasonable for even shorter laser pulses, except for really short few-cycle pulses [9, 10]. In case of such ultrashort pulses the change of plasma parameters (like electron density and temperature) are almost instantaneous, which leads to a parallel swift change in the dielectric function and that can be already comparable to the period of the laser light oscillation. For this case a more sophisticated treatment of the problem has been developed [74] that is valid even for the shortest available pulse durations. It extends concepts used in perturbative regime of nonlinear optics into high intensity laser-matter interactions. By deriving a first-order propagation equation from the scalar wave equation without any assumption in respect to the pulse duration it provides a powerful tool for the simulation of ultrashort pulse-plasma experiments. In our case due to the relatively long pulse widths this method wouldn't offer a notable improvement in accuracy. However in the future for the understanding of PM operation with few-cycle pulses [75, 76] this model should be seriously considered.

In summary, the quasi-stationary approximation provides a relatively simple and exact treatment of the current problem by assuming that the electric field at any point is harmonic in time. So let us consider that a high frequency harmonic wave:

$$\boldsymbol{E} = \boldsymbol{E}(\boldsymbol{r})\, e^{i\omega t - kr}, \tag{3.6}$$

where $k = 2\pi/\lambda$ is the wave number with λ for wavelength, and r denotes scalar displacement propagates in an underdense plasma with ω frequency, which is larger than the plasma frequency. Here an other approximation was also made that the harmonic wave is monochromatic, which considering the narrow bandwidth of our lasers is reasonable. On these fast time scales only the electrons move and the ions can be considered to be at rest. The derivation of the wave equation will follow the following procedure: First the simplest case when the beam impinges at right angles to the vacuum-plasma interface will be examined. The initial step will be the investigation of the electronic response of the medium to the high frequency field - in particular the electric current density will be derived. Relating this to the electric field will allow us to write Ampere's law in a suitable form that contains only known parameters. This together with Faraday's law after some mathematical treatment - those are common in electrodynamics to derive the wave equation - will give us the wave equation for the electric field in plasma, which is of our interest. Then we will proceed toward the more general case and investigate the propagation of obliquely incident light waves: both S and P polarized beams will be examined.

Since ions are considered to be fixed, the electric current density consist in only the movement of the electrons: $\boldsymbol{j} = -n_e e \boldsymbol{u_e}$, where $\boldsymbol{u_e}$ is the mean velocity of the electrons. An other beneficial consequence of this approximation is that the momentum balance equation will obtain a more convenient form. The standard form of this equation for electrons, which can be found in most textbooks on plasma physics [77, 78] is:

$$-m_e n_e \left(\frac{\partial \boldsymbol{u_e}}{\partial t} + (\boldsymbol{u_e} \cdot \boldsymbol{\nabla}) \boldsymbol{u_e} \right) = n_e e \left(\boldsymbol{E} + \boldsymbol{u_e} \times \boldsymbol{B} \right) + \boldsymbol{\nabla} \cdot \boldsymbol{P} + m_e S \boldsymbol{u_e}, \tag{3.7}$$

where $\boldsymbol{P}$ is the pressure tensor, and S is the volume source rate. This equation is also known as the Navier-Stokes equation for plasmas. Comparing it with the ordinary Navier-Stokes equation that describes the flow of Newtonian fluids, one can conclude that they are very similar in many respects except for the electric and magnetic terms. Let us investigate this equation and neglect some terms in order to obtain a more simple form.

Basically this equation is a force equation that gives the acceleration of the electrons in function of the different forces. On the left-hand side we see the acceleration of the electrons in terms of the total derivative multiplied by the electron mass. The reason for using the total derivative here is that in a motion equation of course we need the acceleration of a moving particle and not the acceleration of a fixed point in the fluid, which is simply the normal derivative of the velocity. As the difference is very small between the two, i. e. $(\boldsymbol{u_e} \cdot \boldsymbol{\nabla}) \boldsymbol{u_e}$ is a negligibly small term, we can eliminate it from the equation.

The first terms on the right side, which don't appear in the ordinary N.-S. equation are the contributions by the electric and magnetic fields. The next term is a momentum flux term related to the pressure which can be associated with the momentum transfer by the moving particles, and the last term represents the new electrons produced by ionization and the electron loss by recombination. To keep the derivation relatively

short, we don't elaborate upon the contribution of all these terms and only state without proving it, that all of them except for the one describing the contribution of the electric field, in the current case are insignificant and thus can be omitted. (However in plasma mirror generation the increase of electron density due to ionization have a key role, but to simplify the problem that will be taken account only in the next section. Here we consider a constant number of electrons, and thus the source term can be omitted.) By keeping only the electric term on the right side of the equation the Navier-Stokes equation for the treatment of the current problem obtains the following pretty simple form:

$$m_e \frac{\partial \boldsymbol{u_e}}{\partial t} = e\boldsymbol{E} \tag{3.8}$$

As can be seen this is the linearized equation of motion of the electrons. With a less rigorous approach to the problem this equation can come directly without considering the fluid equation.

Solving this for $\boldsymbol{u_e}$ and substituting into (3.8) we obtain the relation between the current density and the electric field:

$$\boldsymbol{j} = \frac{i n_e e^2}{m\omega}\boldsymbol{E} \tag{3.9}$$

Now we can substitute this expression for $\boldsymbol{j}$ into Ampere's low. Using that together with Faraday's low (3.4) after some mathematical treatment we obtain the following wave equation for $\boldsymbol{E}$:

$$\boldsymbol{\nabla}^2\boldsymbol{E} + \frac{\omega^2}{c^2}\epsilon\boldsymbol{E} = 0 \tag{3.10}$$

where $\epsilon = 1 - \omega_{pe}^2/\omega^2$ is the dielectric function of the plasma. In the more general non-isotropic discussion of the problem the dielectric function is of course a tensor, but in our 1 dimensional treatment we can simply consider it a scalar. ϵ in this form is valid only for collisionless plasmas, the effects of collisions on wave propagation will be taken into account later in this chapter, which will modify substantially the above expression for ϵ. Searching the solution of (3.10) in the form of (3.6) we obtain the dispersion relation:

$$\omega^2 = c^2k^2 + \omega_{pe}^2, \tag{3.11}$$

that reveals essential information on e. m. wave propagation in plasmas. It is obvious regarding (3.11) that not any wave can propagate in a plasma with a frequency smaller than ω_{pe}. Thus the electron plasma frequency act as a critical frequency: waves with a larger frequency can penetrate into the plasma, while waves with a smaller frequency are reflected back. As in the case of laser produced plasmas the frequency is usually constant and the density is increasing, it is practical to define a so called critical density (n_c) in terms of light frequency, which is a density limit below a particular wave can travel in a plasma.

$$n_c = \frac{m_e\epsilon_0\omega_{pe}^2}{e^2} \tag{3.12}$$

It is important to note again that these results are valid only for high-frequency waves impinging at right angles to the surface and due to the applied quasi-stationary approximation the mentioned restrictions on the temporal evolution of the dielectric function also have to be taken into account.

Now we can proceed further and examine what happens when the angle of incidence is different from 0°. In case of obliquely incident laser pulses - similarly to the derivation of the classic laws of reflection and transmission i. e. the Fresnel formulas - it is convenient to treat the problem separately for the S and P polarized waves. The general case, a wave with arbitrary plane of polarization can always be created of the combination of this two. The reason of doing so is that in case of S polarization (also called perpendicular polarization) the electric vector is perpendicular to the plane of incidence thus it has no component to excite electron oscillations, which makes the treatment of the problem relatively simple. Whereas at P polarization (or parallel polarization) $\boldsymbol{E}$ is parallel to the plane of incidence, thus the field drives Langmuir waves in the plasma that leads to resonant absorption. This in total establishes a rather complex problem which is much more difficult to explore. Another point that makes this separate treatment even more appropriate is that lasers due to the applied regenerative amplifiers generate polarized pulses which can be directly used in experiments. Hence comparing the S and P polarized cases - as will be done here also - is also of great experimental interest.

Let us begin with S polarization. Figure 3.1 (a) depicts the incident wave (its electric vector $\boldsymbol{E}$ and wave vector $\boldsymbol{k}$) in a coordinate system where the plasma surface lies in the x-y plane and the density gradient $\boldsymbol{\nabla} n_e$ points in the z direction. Choosing the y-z plane to the plane of incidence, the angle of incidence θ will be the angle between the wave vector and the density gradient. With this layout the x and y components of the electric field: $\boldsymbol{E_y}$ and $\boldsymbol{E_z}$ are both zero, and k_x will be constant so the solution of the general wave equation can be searched in the following form:

$$\boldsymbol{E} = E(z)e^{i\omega t - k_y y} \tag{3.13}$$

where k_y is the wave vector's y component: $k_y = k \sin\theta$. Substituting this into (3.10) we obtain the wave equation for S polarized light waves in plasmas:

$$\frac{\partial E(z,t)}{\partial z^2} + \frac{\omega^2}{c^2}\left[\epsilon(z,t) - \sin^2\theta\right] E(z,t) = 0 \tag{3.14}$$

The obvious difference compared to the general equation is that the $\epsilon(z,t) - \sin^2\theta$ factor replaced the dielectric function, which means that the wave is reflected when $\epsilon(z,t) = \sin^2\theta$. This as it is illustrated at Figure 3.1 (b) happens at an electron density lower than the critical density at: $n_e = n_c \cos^2\theta$.

Equation (3.14) describes the propagation of S polarized electromagnetic waves in plasmas in terms of the dielectric function. Complementing this with a sophisticated model for ϵ that considers also plasma collisions, will allow us to obtain a complete model of S polarized wave propagation in underdense plasmas. This will be done soon, but before that obliquely incident P polarized waves will be examined.

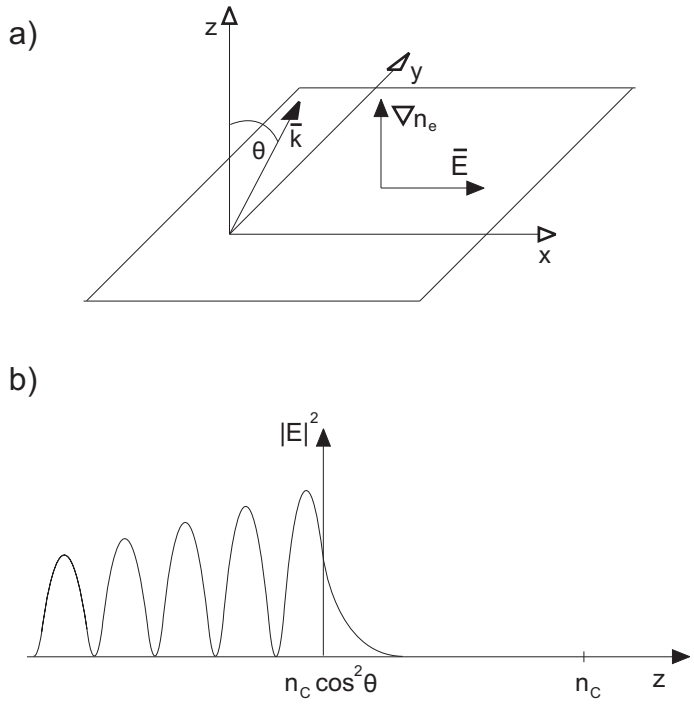

Figure 3.1: Obliquely incident S polarized electromagnetic wave propagation in plasmas. (a) Vector arrangement: x-y plane - plasma surface, y-z plane - plane of incidence, θ - angle of incidence, density gradient $\boldsymbol{\nabla} n_e$ points in the z direction. The wave vector ($\boldsymbol{k}$) lies in the x-y plane and electric vector due to S polarization points in the x direction; (b) electric field square along the plasma. The electric vector is reflected at the plasma layer of $n_c \cos^2\theta$ electron density

Since at P polarized waves the electric vector lies in the plane of incidence, it has a component parallel to the density gradient, which means that $\boldsymbol{E} \cdot \boldsymbol{\nabla} n_e \neq 0$ in this case. This parallel component excites longitudinal Langmuir oscillation of the electrons, which implies that the wave propagation is not purely electromagnetic but a rather complicated phenomenon occurs where a considerable fraction of the wave's energy is transfered to the driven electron oscillations. Considering our interest which is the highest available reflectivity of the generated plasma mirror this energy loss has important consequences on the effectivity of plasma mirror generated by P polarized laser beams.

First it is worth to demonstrate with a simple calculation from Giulietti et. al. [79] that resonant absorption only occurs at P polarization. Using the collisionless formula for ϵ:

$$\epsilon = 1 - \frac{\omega_{pe}^2}{\omega^2} = 1 - \frac{n_e}{n_c}, \tag{3.15}$$

which for the current problem provides a reasonable approximation and the Poisson

equation in plasmas $\boldsymbol{\nabla} \cdot (\epsilon \boldsymbol{E}) = 0$ with some vector calculations it can be shown that

$$\boldsymbol{\nabla} \cdot \boldsymbol{E} = \frac{\boldsymbol{\nabla} n_e \cdot \boldsymbol{E}}{n_c - n_e}. \tag{3.16}$$

Applying Gauss law for the electron density perturbation of the plasma wave δn_e: $\boldsymbol{\nabla} \cdot \boldsymbol{E} = 1/\epsilon(-e\delta n_e)$, it follows from (3.15) and (3.16), that

$$\delta n_e = \frac{\boldsymbol{\nabla} n_e \cdot \boldsymbol{E}}{n_c}. \tag{3.17}$$

This conclusively demonstrates that at S polarization where the field is perpendicular to the density gradient no excitation of plasma waves occurs while at P polarization the component parallel to $\boldsymbol{\nabla} n_e$ drives Langmuir waves.

For the better understanding of resonant absorption mechanism and its effect upon plasma generation, it is beneficial to examine the frequency of the excited plasma oscillations and their position along the electron density gradient. Making use of the Poission equation and (3.15) again it can be easily derived that

$$\boldsymbol{\nabla} \cdot \boldsymbol{E} = -\frac{1}{\epsilon} \frac{\partial \epsilon}{\partial z} E_z, \tag{3.18}$$

where the coordinate system and vector orientations are shown in Figure (3.2) (a). It is apparent from (3.18) that as ϵ goes to 0, the electric field exhibits a singularity. This all happens according to (3.15), where ω equals to ω_{pe} i. e. at the critical density. Thus electrons in this thin region around n_c are resonantly excited, which accounts for the name of this phenomenon: resonance absorption. The parallel component of the electric field along the density gradient is illustrated in Figure (3.2) (b). Due to absorption mechanisms of course the field doesn't increase to infinity but remains finite, and even by low absorption coefficients a considerable amount of the laser energy is absorbed, that will be all converted into thermal energy. It is important to note that the component of the electric vector perpendicular to $\boldsymbol{\nabla} n_e$ is reflected of course at an electron density of $n_c \cos^2 \theta$, thus the parallel component have to tunnel through the dense plasma to resonantly excite electron plasma waves.

The most comprehensive studies [80–84] describing resonant excitation of plasma waves by obliquely incident P polarized electromagnetic waves focus their attention on the excitation efficiency of these longitudinal oscillations. Although our interest in respect of plasma mirror generation is the opposite, it is worth to present a brief summary of the main findings of these publications here: With an increasing θ the width of the dense zone between the reflection point and the critical density point, that the parallel component have to tunnel through is increasing, so due to the absorption during propagation only a weak absorption phenomenon can be observed at large angles of incidence. On the contrary toward small angles the width of the dense zone is decreasing, but the parallel component of the electric field also, which results again poor excitations. Therefore there should be an optimum position between this two cases, which according to detailed calculations [84] is approximately at an angle of incidence of 60°.

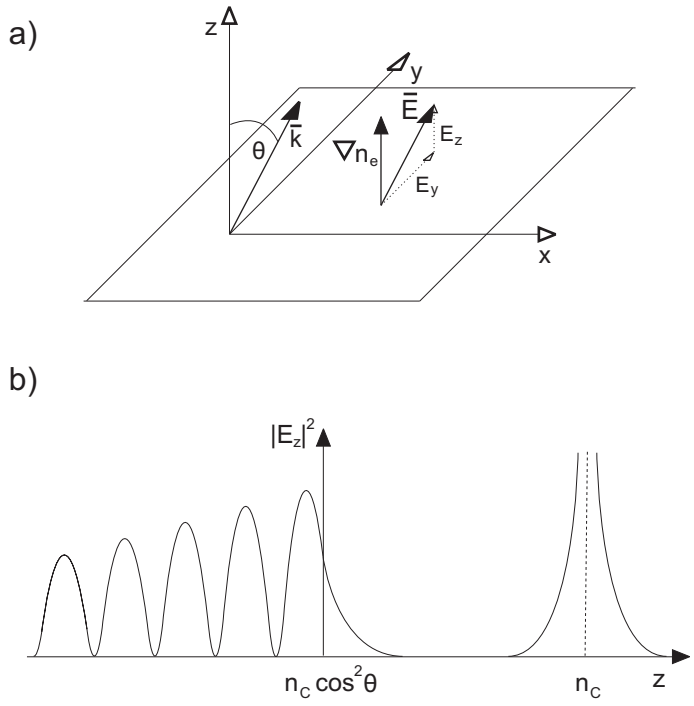

Figure 3.2: Obliquely incident P polarized electromagnetic wave propagation in plasmas. (a) Vector arrangement: as at Fig. 3.1 but with an electric vector lying in the y-z plane.(b) Square of the electric field component (E_z) parallel to the density gradient along the plasma. It tunnels through the dense plasma from the reflection point of the perpendicular component (i. e. at el. density of $n_c \cos^2\theta$) up to the thin volume at the critical density, where it exhibits a singularity. Electron plasma waves are resonantly excited here.

3.1.3 Dielectric function

This chapter covered so far the electromagnetic wave propagation in plasmas. The dielectric function that has a central role in the description of electromagnetic processes, in the above calculations was estimated with a formula derived from a simple model by considering a quasi collisionless plasma. Collisions were taken into account merely through a pressure term that represented a sort of interaction by momentum transfer between different species of particles. However this simple model has been used successfully for the interpretation of several phenomenon so far, to understand wave propagation requires a more sophisticated model on epsilon that considers also collisional processes in the plasma.

The most accurate treatment of the problem would be of course to go back to the fluid equation (Eq. (3.7)) that describes the motion of the electron fluid and by modifications making it valid for plasmas with collisions, and then the wave equations can be derived again. Fortuitously due to the fact that electron-ion collisions can be

defined in terms of collision frequency that otherwise rather elaborate method becomes much more simpler. Using a collision frequency (ν_{ei}) for the collisions between moving electrons and fixed ions, a collisional term emerges on the right side of the (Eq. (3.7)) representing the momentum transfer through collisions. We follow now the less rigorous approach as it was mentioned there and write immediately the linearized equation of motion:

$$m_e \frac{\partial \boldsymbol{u_e}}{\partial t} = e\boldsymbol{E} + m_e \nu_{ei} \boldsymbol{u_e}. \tag{3.19}$$

Since the field is harmonic in time (Eq. (3.6)) after some calculations we obtain the following expression for the current density:

$$\boldsymbol{J} = -en_e \boldsymbol{u_e} = \frac{i\omega_{pe}^2}{4\pi\omega\left(1 + i\nu_{ei}\right)} \boldsymbol{E} = \sigma \boldsymbol{E} \tag{3.20}$$

From the Maxwell equations we can derive the electromagnetic wave equation. Substituting the above expression for $\boldsymbol{J}$ into the wave equation, it reads as follows:

$$\nabla^2 \boldsymbol{E} + \frac{\omega^2}{c^2}\left(1 - \frac{\omega_{pe}^2}{\omega^2 + i\omega\nu_{ei}}\right)\boldsymbol{E} - \nabla(\nabla \boldsymbol{E}) = 0 \tag{3.21}$$

in which the dielectric function is:

$$\epsilon(z,t) = 1 - \frac{\omega_{pe}^2}{\omega^2 + i\omega\nu_{ei}}. \tag{3.22}$$

The above model was formulated by the German physicist Paul Drude in 1900 and was named Drude-model after him. It is a relatively simple but very powerful model that has been widely used for more than a century now for the interpretation of physical processes related to electromagnetic wave propagation in metals and in plasmas.

3.2 Ionization mechanisms

So far the electromagnetic wave propagation in plasmas have been discussed. To provide a complete picture about the ultrafast plasma generation in this section the ionization mechanisms occurring in dielectrics in the presence of intense laser light will be presented.

There are two ionization mechanisms tunnel or multiphoton ionization and impact ionization, those are widely considered as being the sources of free electrons in laser induced plasma generation process. Let us consider first tunnel and multiphoton ionization. According to the Keldysh model for a certain wavelength and target material it is the laser intensity that clearly separates tunneling and multiphoton ionization. The Keldysh parameter is $\gamma = \omega\sqrt{2mE_{ion}}/eE$ where E_{ion} is the ionization energy. For values of $\gamma < 1$ tunnel and for > 1 multiphoton ionization occurs. This in practice means that for a fixed target and laser wavelength tunneling occurs at higher and

multiphoton ionization at lower intensities. In our case even for the shortest pulses (60 fs) below the damage threshold which is the intensity range of our interest γ remains greater than 1, thus it is multiphoton ionization that we have to be considered. The physical picture of multiphoton ionization is that it occurs when an atom submitted to laser radiation absorbs multiple photons and thus an electron subduing the ionization threshold is released to the conduction band. The electron excitation rate from the valence band to the conduction band by multiphoton ionization W_{MPI} has an exponential dependence on the instantaneous laser intensity. Quantitatively:

$$W_{MPI} = \sigma_n \left|E(z,t)\right|^{2n}, \tag{3.23}$$

where n is the minimum number of photons required to cross the band gap, and σ_n is the corresponding cross section. At 800 nm the photon energy is 1.57 eV thus the absorption of an n=6 photons is necessary in fused silica (10 eV) for multiphoton ionization.

Now that we have the excitation rate by multiphoton ionization we have to take it also for avalanche ionization to obtain the total electron excitation rate. Avalanche ionization occurs when an electron in the conduction band, that is accelerated by the laser field transfers another electron from the valence band to the conduction band via impact ionization. The electron excitation rate by avalanche ionization W_{av} scales linearly with the laser intensity and the conduction electron density, and is given by the following expression:

$$W_{av} = \beta \frac{n}{n_0} \left|E(z,t)\right|^2, \tag{3.24}$$

where β is the avalanche coefficient and n_0 is the bound electron density.

3.3 Breakdown models

Numerous experimental and theoretical studies of laser induced (or optical) breakdown were conducted in the past fifteen years. The experimental works mainly focused on the measurement of the threshold fluence in function of various laser parameters and the fitted numerical models tried to draw conclusion on the dominant ionization process from the experimental findings. The extensive research of the breakdown mechanisms was mainly driven by practical considerations: with the increasing laser intensities, damage of the optical components of lasers became a problem of primary importance.

The threshold fluence was investigated in a very broad pulse duration range spanning from 5 fs up to several nanoseconds. However the experimental conditions and methods were very diverse, the obtained results correlated for pulses longer than some tens of picoseconds. It was found that the threshold fluence in this duration range scales with $\sqrt{\tau}$, where τ is the laser pulse duration. In contrast to this agreement, for shorter pulses ($< 10ps$) significant discrepancies both in tendency and value of the measured damage threshold have been observed. The only agreement reached in this duration range was that the $\sqrt{\tau}$ scaling is not valid any more. In their preliminary study Du

et al. [85] reported a sharp minimum of the threshold at 1 ps and detected a further increase toward shorter pulse durations. These findings were contradicted soon by Stuart et al. in their extensive investigations on the breakdown phenomenon [86–89]. They've found a monotonic decrease of the threshold fluence with decreasing pulse width over the entire pulse duration range, but with a continuously declining rate of decrease below 20 ps. All further investigations [90–92] confirmed their findings in respect of the tendency but the measured thresholds showed a substantial diversity. As it was raised in some of the later studies (especially in [92]) this is probably due to the very different experimental methods and conditions. The most significant difference was that some measurements were carried out with single pulses, while others applied multiple shots (up to a number of 600), that can lead to very different thresholds due to incubation, as it was demonstrated in [90]. An other difference was that various techniques were used to detect the damage. Some experiments defined the damage threshold as the appearance of detectable plasma emission, while others observed the surface with a Nomarski microscope. Other circumstances like surface roughness of the target were also suspected being responsible for the deviations. Another influential experimental condition was the spatial profile of the incident pulse. This was well demonstrated by the measurements in [91, 93] where the same group with almost the same laser, target and setup reported threshold fluences with a factor of two difference in their two publications. The only difference between the two measurements was that an additional hollow-core fiber was applied in [91], which improved the beam quality via spatial filtering. Due to the diverse experimental conditions these measurements were not reproducible, therefore they can not serve as absolute references.

Numerical models on the optical breakdown showed a great diversity about the dominant ionization mechanism due to the discrepancy of experimental results used for the validation. Most of the models used a rate equation to predict the conduction electron density by multiphoton/tunnel and impact ionization. The first model [85] based on their data showing a minimum in the damage threshold at 1 ps found that it is the avalanche ionization mechanism that dominates the damage in the enture sub-10 ps range. Other studies [86–91] based on the monotonic decrease of the threshold fluence with decreasing pulse duration concluded that seed electrons are produced by multiphoton ionization at the peak of the pulse, and it is the avalanche in the second part of the pulse that boosts the conduction electron density up to the critical density.

A complex model that resolves this inconsistence in previous studies was developed by Tien et al. [92]. They used Thornber's [94] expression for the calculation of the avalanche rate instead of the commonly used avalanche rate that linearly scales with the intensity. Instead of an also commonly used multiphoton rate they used Keldysh's calculation [95] for the photoionization rate. With this model a pronounced sensitivity of the damage threshold on the initial carrier electron density was observed. The results show that at low carrier densities the damage threshold decreases with decreasing pulse duration, while with increasing carrier density a minimum in the damage threshold versus time curve is becoming more and more pronounced at 1 ps of pulse duration. They conclude that for long pulses the avalanche is the dominant ionization mechanism,

while for shorter pulse durations the role of multiphoton ionization by generating the seed electrons is becoming increasingly important.

3.4 Summary

In this chapter the theoretical background of plasma mirror generation by high-power short laser pulses was presented. First by employing a quasistationary approximation the wave equation was derived for light waves impinging at right angles to the vacuum-plasma interface and then the more general case, the propagation of obliquely incident laser pulses in plasmas was studied. It was shown that an S polarized beam is superior over a P polarized for the generation of a highly reflective plasma mirror, as in P polarization the resonance absorption eats up a considerable portion of the energy. Examining the dispersion relation for electromagnetic waves in plasmas it was shown that electron plasma frequency acts as a critical frequency: waves with a frequency larger than the critical frequency can penetrate into the plasma, while waves with a smaller frequency are reflected back.

The two major ionization mechanisms which are widely considered as being the sources of free electrons in laser induced plasma generation process: tunnel or multiphoton ionization and avalanche ionization were also briefly reviewed, and their different characteristics have been shown. A rate equation describing the evolution of the free-electron density by these two ionization mechanisms have been used in the presented numerical models, which due to the discrepancy in experimental results lead to rather different conclusions about the role of the two ionization mechanisms in ultrafast plasma generation.

Chapter 4

Experimental characterization of a plasma mirror

4.1 Experimental setup

The experiment was conducted at Saclay Laser Interaction Center (SLIC) with the LUCA laser, which is a high-power short pulse Ti:sapphire laser, that delivers 60 fs nearly transform limited pulses with energies up to 100 mJ at 800 nm central wavelength. The key parameter of the laser in respect of our PM experiment was its intensity contrast. Pre-plasma formation due to an inappropriate contrast could have seriously mislead the experiment. To avoid that, the laser contrast was checked regularly during the experiment with a third order correlator. A 1 ns and a 2 ps long pedestal with a contrast of $\approx 10^6$ and $\approx 10^4$ respectively were detected. Since the highest peak intensity that was used in the experiment was 10^{15} W/cm^2, the corresponding pedestal fluences 1 J/cm^2 and 0.2 J/cm^2 respectively were well below the damage threshold of dielectrics at the corresponding pulse widths according to references [86–93]. Therefore in the experiment it was the main pulse and not the pedestal that triggered the PM. This was double checked by irradiating the target with the oscillator switched off, when only the leading pedestal was emitted. It was found that the pedestal alone didn't cause any optical damage, even for multiple exposures.

Two types of targets were used in the measurements: a non coated, and an AR coated bulk quartz. The laser beam was S polarized and the angle of incidence was 45 ° during the whole experiment. The AR coated target was manufactured for this angle of incidence and exhibited an initial reflectivity of 0.3 %. These parameters (S pol., AR) were chosen to maximize the efficiency of the PM in respect of reflectivity and contrast improvement factor. The quartz had a Fresnel reflectivity of 10 %, at this angle of incidence. The targets were stored and handled with care to avoid surface contaminations and damages, thus no cleaning of them prior to the experiment was necessary.

The experimental setup is depicted in Figure 4.1. The repetition rate of the laser was 20 Hz. A mechanical shutter was used to select single pulses from the emitted pulse

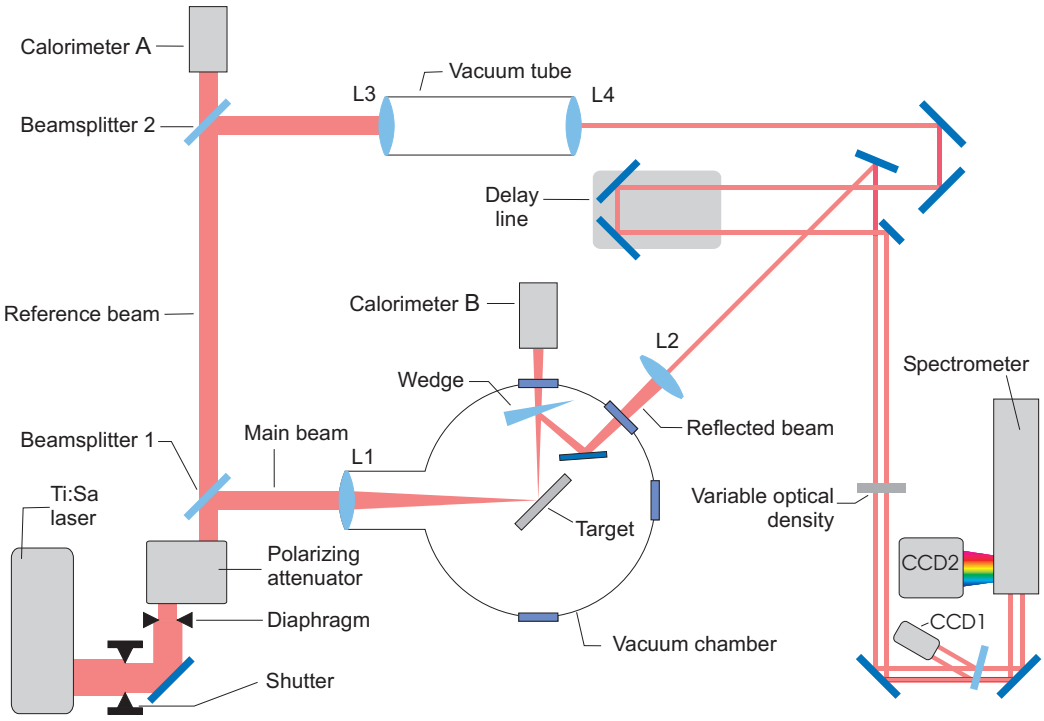

Figure 4.1: Experimental setup. The S-polarized laser pulse was split into a reference beam and a main beam that illuminated the target. The fluence of the laser beam was attenuated by a polarizing attenuator and a variable diaphragm. The pulse energy of the reference and reflected beam was measured with calorimeter A and B respectively. Both beams were imaged onto a high-dynamic CCD (CCD1) to monitor the beam profile and onto the entrance slit of an imaging spectrometer. The latter diagnostic was used to measure the onset of plasma formation with linearly chirped pulses.

train. A single-shot measurement has several advantages over multi-shot methods. As damage can occur during the first shots, with a multi-shot method the threshold can not be accurately determined, and incubation can lead to further inaccuracies. Furthermore multi-shot methods inherently average over fluctuations of laser pulses. To avoid these, the target after each shot was shifted with a translation stage perpendicular to the beam, so as ensuring a fresh undamaged target surface for the next single-shot exposure.

An important objective of the experiment was the accurate measurement of the fluence of the incident and reflected beam. In previous experiments the fluence was only roughly estimated: the total incident pulse energy and damage spot size on the PM was measured and the fluence was calculated assuming a perfectly Gaussian intensity profile. Conducting an accurate measurement is much more cumbersome, it requires simultaneous monitoring of both the intensity profile and energy of the incident and reflected pulses. This allows the determination of the fluence from point

to point in the incident and reflected beams. As there is a nearly one and a half orders of intensity difference between highly reflective plasma generation and the damage threshold on solids, accurate attenuation of the laser beam in a rather broad range was necessary. Several common methods in laser-matter interaction experiments are used to attenuate the laser fluence, like moving the target out of focus, aperturing the incident beam or using neutral density filters or polarizing attenuators, but none of them can provide the sufficient broad variability itself. Hence in the experiment an appropriate combination of some of these techniques was the solution: right after the compressor a polarizing attenuator and a variable diaphragm were used and elsewhere neutral density filters were inserted into the incident beam. The polarizing attenuator consisted in a half waveplate and polarizer permitting the continuous attenuation of the fluence, and two diaphragms with a diameter of 18 mm and 25 mm were used for attenuating the beam in larger steps.

For the simultaneous monitoring of the incident and the reflected fluence, the beam after attenuation was split into two with a 90/10 beamsplitter: into a high intensity main beam, and a low intensity reference beam. The main beam was focused onto the target with a long focal length (L1, f=1200 mm) lens. Special care was taken in the design of the experiment to avoid nonlinear effects. To this end the focusing lens was made of MgF_2, which exhibits a low non-linear refractive index, and the target was placed into a vacuum chamber. The intensity on the windows of the vacuum chamber was low enough to prevent nonlinearities. The pressure in the chamber during experiment was kept below 10^{-3} mbar. The reflected beam at high incident fluences due to high reflectivity was very intense, thus strong attenuation was necessary before sending it out of the chamber. For that a reflection on a wedge was used. The transmitted part of the beam through the wedge was used for measuring the reflected energy. It was collected to a single shot calorimeter (Calorimeter B). The reflected part, outside of the chamber was sent through a lens (L2), which imaged the beam onto a 16 bit dynamic-range CCD camera (Princeton Instruments, CCD1) for monitoring the reflected beam profile. The camera was carefully protected from background light. The reference beam was split further with a 50/50 beam splitter. The transmitted part again was used for energy measurement with an identical calorimeter (Calorimeter A), and the reflected part was focused and imaged with a telescope (lenses L3 and L4) onto CCD1. Calorimeter A was calibrated with a power meter, placed in the main beam for measuring the energy incident on the target surface. The CCD was protected by a set of optical densities. High vacuum inside the telescope (L1;L2) prevented the generation of nonlinear effects by the relatively high intensity between the lenses. The overall magnification factors of lenses L1 and L2 (in the reflected beam) and lenses L3 and L4 (in the reference beam) were identical. For the determination of the reflected and reference fluence the magnification of the system had to be known with a great accuracy. That was easily obtained by a simple calculation using the distance of the spots reflected from the front and rear surfaces of the target. The smallest focal spots obtained in the experiment had an FWHM of larger than 30 μm.

For the observations of spatial profile of the beam in the near field, which enabled

to conclude on the PM induced distortion, an additional lens was inserted into the reflected beam (not shown in the figure). Together with lens L2 it imaged the plane located 60 cm after the target.

Time resolved study of the PM operation was conducted by applying a linear chirp on the incident pulses. This naturally resulted in longer pulse durations (1.7 ps and 4 ps) allowing us to study the dependence of the reflectivity and breakdown threshold on the duration of the incident laser pulse. Furthermore to provide direct experimental evidence for the ultrafast nature of plasma formation the chirped pulses were imaged onto a spectrometer. The chirp was introduced by setting the distance between the two gratings of the compressor that resulted in a quadratic spectral phase (linear chirp) in the laser pulse. For pulses with a duration large compared to the Fourier limit (as in our case), a linear chirp provides a one-to-one mapping between time and frequency. The reflected and reference chirped pulses were both imaged onto the entrance slit of an imaging spectrometer (800 lines/mm, 1 m focal length) equipped with a high-dynamic CCD camera. The two beams were separated on the entrance slit so that their spectra could had been captured simultaneously with the CCD. This way the onset of plasma formation was obtained at different incident fluences by comparing the corresponding pair of recorded spectra.

4.2 Experimental results

Plasma mirror operation was characterized from many aspects in this complex experiment. In this section a very brief description of the data analysis will be given and the experimental results will be presented and discussed in great details.

4.2.1 Peak and overall reflectivity

For the peak and overall reflectivity curves, the incident and reflected fluence had to be determined. Calorimeter A was calibrated to the incident energy of the main beam, and the spatial profile of the reference beam was monitored with the CCD1 camera. The cooled high-dynamic CCD chip had a better signal-to-noise ratio than the calorimeter especially at low fluences thus it was more accurate to use the CCD for energy measurement. After background suppression the illuminated pixels of the reference beam's spot were integrated and plotted versus the Calorimeter A data. The dependence was linear with only a small deviation at lower fluences. The linear fit was used for the calibration of the CCD to measure the energy of the main beam. The next step was the determination of the incident fluence. Knowing the CCD pixel size, the overall magnification of lenses L3 and L4 and the total energy of the pulse, the spatially resolved fluence of the main beam on the target could had been easily calculated from the reference spot. The peak fluence indicated on the reflectivity graphs is the spatial peak measured at the center of the focal spot.

After the calculation of the incident laser fluence the corresponding peak and overall

reflectivities of the PM were determined. Thanks to the relatively high initial reflectivity of the quartz target, that was a quite simple procedure. Instead of performing again the same calculation to obtain the reflected fluence, and then the reflectivity, a much easier method was used: numerous shots have been taken in the low fluence regime where no plasma triggering occurs and the bulk target reflects the laser beam with its initial 10% Fresnel reflectivity. These shots were used to calibrate the peak and overall reflectivity curves. After calibration, the peak reflectivity was obtained by dividing the pixel value of the central pixel of the reflected spot with its reference counterpart while for the overall reflectivity the ratio of integrated pixels were divided. The AR coated target is not suitable for such a calibration with its very low intial reflectivity, but as there was no modification on the experimental setup between measurements with the two types of targets, the calibration performed with the quartz target was valid also for the measurements with the AR target.

Figure 4.2 shows the peak reflectivity (the time-integrated spatially resolved reflectivity measured in the center of the focal spot) of quartz and AR as a function of the incident peak laser fluence for 60 fs incident pulses. Both quartz and AR exhibits a

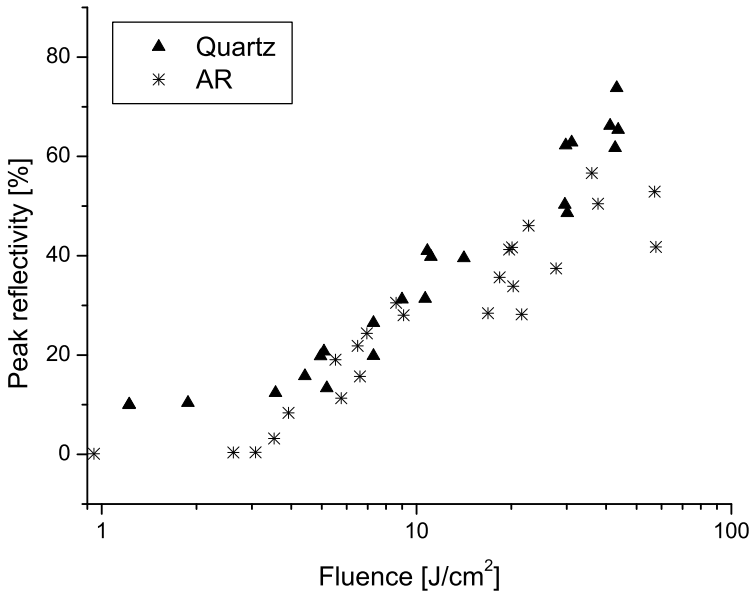

Figure 4.2: Peak reflectivity of bulk quartz and AR coated target versus incident fluence for 60 fs pulses.

constant reflectivity below the breakdown threshold. This initial reflectivity of quartz (which was used for the calibration of the reflectivity) is 10 %, while AR as it was expected shows a much lower (0.3 %) cold reflectivity. We defined the breakdown threshold fluence in this experiment as the fluence at which the reflectivity starts a

sharp rise from its initial value. This increase happens when the electron density exceeds the critical level (n_c) during irradiation and the plasma begins to reflect. As it can be seen in the figure the measured thresholds are the same 4 J/cm^2 for both targets. Not depicted here but the damage thresholds of AR and quartz targets were found being the same also at longer pulse widths (1.7 ps and 4 ps). This finding is seemingly in contrast to the findings of Stuart et al. [88, 89]. They compared the breakdown thresholds of multilayer dielectric polarizers to that of fused silica samples with S polarized laser light over a wide pulse duration range (from 200 fs to 70 ps). At all pulse durations a lower threshold for dielectric mirrors was found than for high purity fused silica samples. In the picosecond regime with approximately a factor of two lower. The investigated dielectric targets consisted of 20 individual layers of thickness 0.1-0.3 μm, deposited by e-beam evaporation to the substrate. The authors believe that so many layers due to the imperfect evaporation technology probably contain a lots of defects, large in size and density in the material. These defects via a faster ionization become sources of free electrons already at lower fluences leading to an earlier breakdown. In contrast to their targets our AR plates were made up of only a few layers with similar thickness, which couldn't induce a significantly earlier ionization. We believe that this is the reason that the breakdown at our AR coated targets occur at the same fluence as that with ordinary bulk quartz.

Above the breakdown threshold with the increasing fluence a sharp rise in the reflectivity of both targets was observed. However, the rate of this rise decreases towards higher fluences, in the high-fluence regime metal like reflectivities were approached (74 %, quartz). The two curves show the same tendencies above the breakdown threshold, with only a negligible difference in reflectivity values. This is due to the fact that after the generated plasma gets overdense the laser doesn't see any more the AR layers. The contrast enhancement in case of quartz was only a factor of 7, but with the AR target an improvement of higher than 200 was achieved. This is a significant increase of the contrast in the center of the beam, moreover due to the high reflectivity only a small portion of the inccident fluence is lost.

Figure 4.3 shows the experimental peak and overall reflectivities of the bulk quartz target in function of the laser fluence for 60 fs pulses. The overall reflectivity, which was measured overall the whole focal spot contains also the low intensity boundary parts, thus it is a bit lower than the peak reflectivity. The overall reflectivity though in experiments is usually of lower importance than the peak reflectivity.

The next figure (Fig. 4.4) depicts the overall reflectivity of quartz versus incident fluence for various pulse durations: for 60 fs, 1.7 ps and 4 ps long pulses. Almost no difference between the reflectivity curves can be observed: the slope of the reflectivity increase is the same for all pulse durations, only the starting point of the increase, the breakdown threshold varies slightly with the duration. The threshold fluences are 4 J/cm^2, 9.5 J/cm^2 and 12.5 J/cm^2 for pulse durations of 60 fs, 1.7 ps and 4 ps respectively. This is of great practical importance in the construction of plasma mirrors that the reflectivity doesn't and the breakdown only slightly varies with the pulse duration.

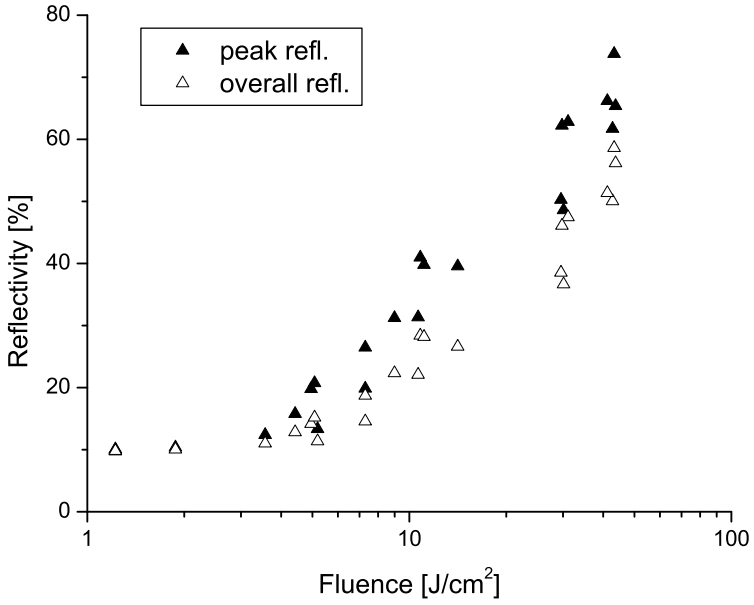

Figure 4.3: Peak and overall reflectivity of bulk quartz versus incident fluence for 60 fs pulses.

4.2.2 Beam profiles

Figure 4.5 shows the energy distribution in the far field of the beam on the target surface when the PM wasn't (c), and when it was (d) triggered. Corresponding line-outs (a) and (b) through the center are also shown. The target was quartz and the incident pulse had a duration of 60 fs with a high peak fluence of 65 J/cm^2 when a highly reflective PM (b,d) was generated, and with a low fluence below breakdown threshold when no PM was triggered (a,c). In the latter case the target reflected the beam with the Fresnel reflectivity. The incident beam's far field profile on the target is close to an Airy function (a), which is the Fourier transform of the top-hat profile that arrives on the lens L1. The first Airy ring is visible in the incident beam's profile. Below the damage threshold the reflectivity of the quartz is low, thus the Airy-rings of the beam that doesn't trigger the PM are poorly reflected. This means that the spatial effect of the PM is similar to that of a low-pass spatial filter placed in the Fourier plane of the focusing lens. The filtering effect is also visible on the near field images. Figure 4.6 shows the profiles and energy distributions in a plane located 60 cm after the target recorded at the same fluences as the far field images. Profile and spot (a,c) shows the near field when the PM wasn't triggered, and profile and spot (b,d) when the PM was triggered. As the beam was apertured between the two spots to attenuate the fluence only a qualitative comparison can be made. Due to the filtering the profile of the beam

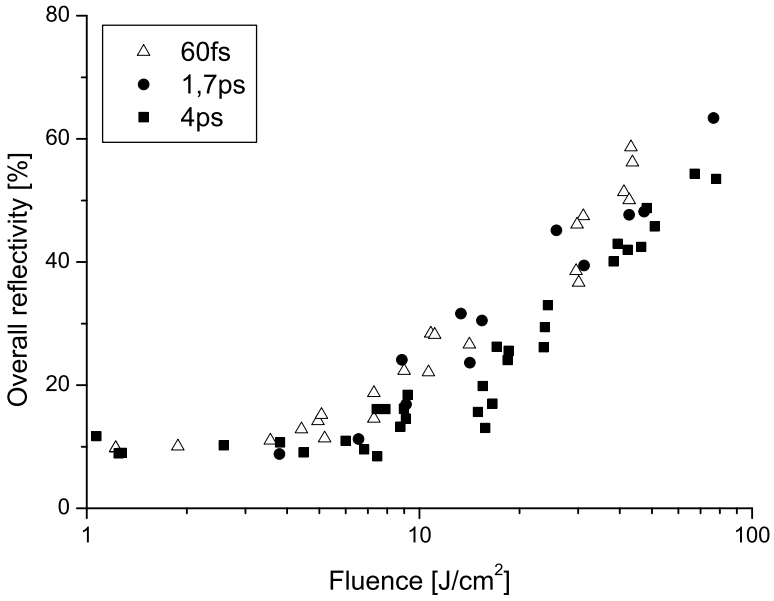

Figure 4.4: Overall reflectivity of bulk quartz versus incident fluence for incident pulse durations of 60 fs, 1.7 ps and 4 ps.

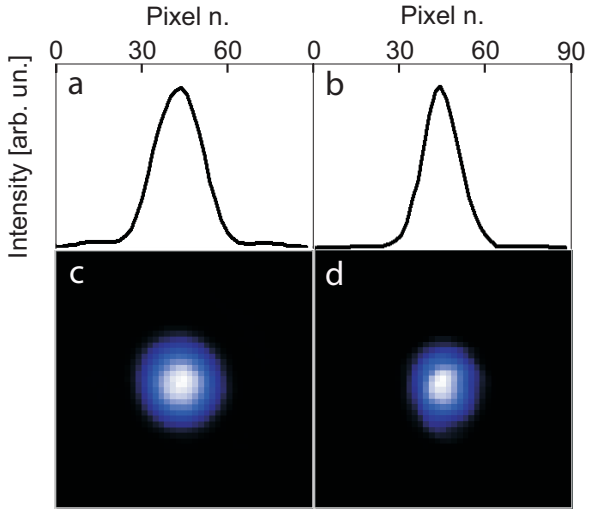

Figure 4.5: Spatial profile (lineout) (a) and energy distribution (c) of the beam in the far field when the PM wasn't triggered, and spatial profile (b) and energy distribution (d) in the far field when the PM was triggered.

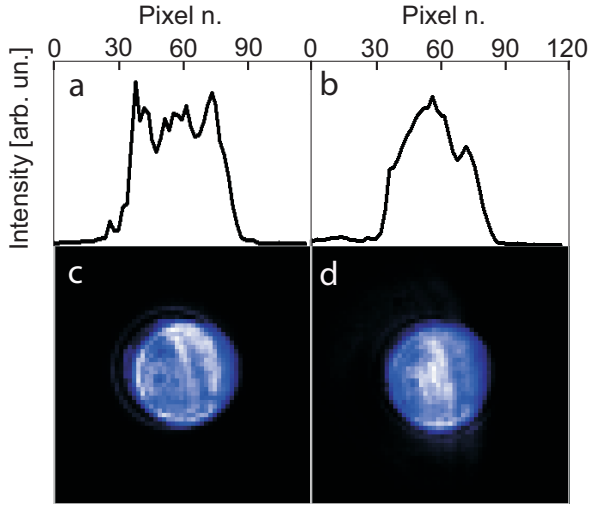

Figure 4.6: Spatial profile (lineout) (a) and energy distribution (c) of the beam in the near field when the PM wasn't triggered, and spatial profile (b) and energy distribution (d) in the near field when the PM was triggered.

reflected from the triggered PM (b) becomes considerably smoother.

4.2.3 Time resolved reflectivity

Time resolved study of the reflectivity increase was performed with chirped pulses. The PM was triggered with 1.1 ps long linearly chirped pulses, and the spectra of the reflected pulse and that of the reference pulse were monitored with a spectrometer. The reflected spectra normalized by the incident fluence are shown in Figure 4.7. The prerequisite for the spectrum to directly provide the temporal profile of the pulse is a sufficiently big chirp with a pulse duration significantly bigger than the Fourier limit. In this case this requirement was met as the chirped pulse was 18 times longer than the original (60 fs) unchirped pulse, which was close to the Fourier-transform limit. The instantaneous frequency $\omega(t)$ has been converted into time t using the relation: $\omega(t) = t/\Phi'' + \omega_0$ where ω_0 is the central frequency and Φ'' is the group delay dispersion. ($\Phi'' = 2.4 \times 10^4$ fs^2 in this case)

It can be readily seen that the reflectivity at all fluences start from the initial cold reflectivity of the PM (0.3% with AR coating), thus it is the main pulse and not the prepulse or pedestal that triggers the PM. Another important observation that the onset of reflectivity increase happens earlier with increasing fluence. On the lowest fluence curves this sharp rise in reflectivity happens later then the temporal peak of the incident pulse, while at appropriately high incident fluences for effective plasma mirror generation this sharp reflectivity increase leads to front-edge steepeing of the reflected pulse.

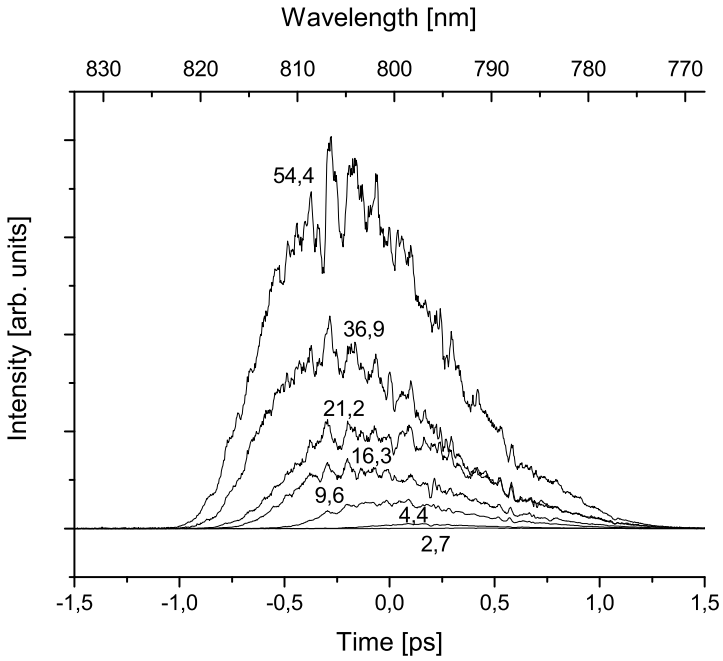

Figure 4.7: Spectra of 1.1 ps long chirped pulses after reflected off the plasma mirror. The target was AR-coated quartz. The original unchirped pulse, which was close to the Fourier-transform limit had a duration of 60 fs. The spectra were normalized with the incident fluences, which are indicated on each curve. The time scale has been obtained using the linear relationship between time and frequency for a chirped pulse as it is explained in the text.

4.3 Summary

In this chapter I provided a complete experimental characterization of a single plasma mirror. I described the experimental setup that was used to measure the following characteristics of the plasma mirror: space and time-integrated (overall) reflectivity, space resolved time-integrated (peak) reflectivity, time and space resolved reflectivity and the onset of plasma formation in function of the incident laser fluence. Distortion of the beam spatial profile in the far-field and the near-field was also characterized.

With these measurements I demonstrated that PM can effectively improve the contrast of high-power laser pulses. I measured a peak reflectivity of 74% and ≈60% on quartz and AR coated quartz targets respectively at 60 J/cm^2 incident laser fluence. This provides a contrast improvement factor of nearly 200 with AR targets with a reasonable energy loss. (The contrast improvement factor is the ratio of the reflectivitiy after and before (0.3% for AR) plasma formation).

I found that the plasma triggering threshold is slightly increasing with increasing

pulse duration. I demonstrated that the spatial profile of the reflected beam is improved due to the fact that the PM acts as a low-pass spatial filter in the Fourier plane of the focusing lens. With time resolved measurements I showed that the onset of plasma formation and reflectivity increase happens earlier with increasing fluence, and even at the highest applied fluence it is the rising edge of the main pulse that triggers the PM and not the prepulses or the pedestal.

Chapter 5

Ultra-high contrast laser pulses - complete characterization of a double plasma mirror

The destructive effects of prepulses and leading pedestals preceding the main laser pulse have been the major obstacle in laser-solid interaction experiments for nearly two decades now. As it was presented in chapter 4, plasma mirror provides an effective solution to this problem offering a contrast improvement by more than two orders of magnitude at a relatively low cost in pulse energy and by no degradation of temporal and spatial pulse parameters. An intriguing question remained to be answered though before its application, whether the contrast enhancement provided by the use of a single plasma mirror is fully sufficient to avoid preplasma generation in experiments, or a more elaborate setup containing multiple plasma mirrors have to be used.

5.1 The need for ultra-clean laser pulses

5.1.1 Prepulse effects

Experiments for the evaluation of the effect of pedestal and leading prepulses were conducted already shortly after the invention of CPA technology [15]. The reason for that was although this technique revolutionized the amplification of short laser pulses leading to never seen intensities on target surface, expectedly clean hot dense plasmas could not had been produced due to the inherently present prepulses and leading pedestal.

The most intriguing phenomenon of those early times that was expected to benefit the most from the boosted laser performances was the production of bright, short X-ray pulses. The generation of such pulses by thermal emission from hot dense plasma have been the subject of numerous studies [96–98]. This was mainly motivated by their potential application for the observation of ultrafast microscopic processes which require pulse durations preferably in the sub-picosecond range. Therefore considerable

effort had been invested into the shortening of these pulses. The most notable work in this field have been performed by Murnane et al [98]. In their study pulse duration of the X-ray pulses generated by laser pulses with significantly different intensity contrasts have been compared. However the temporal resolution of the measurements was limited by the streak camera, it was clearly shown that in the presence of a relatively high ASE the decay time of the X-ray signals is significantly longer than with a low ASE. This was interpreted as emission coming from the lower density preplasma generated by the pedestal. Additional spectroscopic measurements confirmed that the higher the laser contrast the higher density plasma is produced. Reflectivity measurements were conducted as well. These demonstrated that plasma mirror created by ns pulses have a reflectivity significantly lower than that created by ps pulses, which is due to the coupling into the preformed plasma by the extended rising edge of the long pulse. These early qualitative studies including their later work as well [66], which was briefly reviewed at subsection 2.2.2, show that a low contrast pulse owing to low density preplasma generation is highly undesirable for experiments aiming for hot high density plasma.

The phenomenon that has been providing the greatest impetus since the beginnings to short pulse laser developments is the generation of high-order harmonics on solid surfaces. It has been already observed before CPA with long laser pulses [99, 100] and even relatively efficiently generated with them reaching up to the 46^{th} harmonic [101], but effective harmonic generation became possible only with the emergence of short pulse lasers. While in gas harmonics the applicable intensities are limited by the ionization threshold to 10^{14}-10^{15} W/cm^2, solids can withstand arbitrarily high intensities. Moreover the conversion efficiency of laser light to harmonics on solids is significantly higher and increases with intensity. Although due to these attractive features solid harmonics have been in the center of interest, and even necessary laser intensities have been available for a long, no considerable progress was made due to the imperfect temporal profile of the laser pulses. The effect of pedestal and prepulses on harmonic generation has been extensively investigated by Zepf et al. [102]. In their study pulses with vastly different intensity contrast have been used and corresponding harmonic conversion efficiencies have been measured and modeled. In general it was found that the lower the contrast of the laser pulse the weaker the $I\lambda^2$ scaling [103] of the harmonic conversion efficiency. With second harmonic generation of the fundamental laser pulse the investigated intensity contrast range was extended far beyond the capabilities of today's lasers, reaching 10^{10} at ns scale. 160 fs pulses with 60 mJ of energy at 395 nm central wavelength with this immense contrast produced a preplasma that's density scale length 150 fs before the main pulse peak was 0.2. In this case it was found that by keeping other parameters constant but varying the peak intensity have only a negligible effect on the onset of plasma formation, unlike in case of pulses with a typical intensity contrast (10^7) at 800 nm. These findings clearly demonstrated that effective high harmonic generation with multi-TW lasers require an intensity contrast far beyond the capabilities of today's lasers.

Besides high-order harmonics generation the other major topic that is of particular

interest in high-field physics is particle acceleration with high-intensity lasers. Laser wakefield acceleration of electrons from rarefied gases [104–106] and laser-driven proton acceleration from thin foils hold promise for future table-top laser accelerators. Since electrons are accelerated from a gas medium one would presume that a lower laser contrast shouldn't have any effect as opposed to laser-solid experiments where preplasma generation is a critical issue for apparent reasons. Recent investigation of beam propagation in gas in conditions of interest for wakefield acceleration of electrons [107] corroborated these assumptions. It was found that however pulses with a typical Ti:Sa contrast ($10^3 - 10^4$ in ps scale and 10^6 in ns scale) preionize the gas a few ps before the main pulse, this has only a marginal effect on subsequent beam propagation and acceleration mechanisms. Another recent study conducted on the same subject [108] is however somewhat controversial to that. Electron beam profile measurements performed with different lasers with different contrasts clearly show a difference in the spatial profiles. Electron beams produced with fairly high contrast pulses (3×10^7) exhibits a perfect profile and a great pointing stability, while the profile of those produced by pulses having a lower contrast but otherwise similar parameters exhibits multiple beamlets with a larger pointing stability. More important to that the stability of the electron spectrum, the key issue of laser driven electron acceleration shows a definite improvement at the highest contrast over the lower ones. This key feature alone justifies the need for high temporal contrast in electron acceleration experiments. The authors believe that the noticeable degradation of the beam profile and energy and pointing stability with a lower intensity contrast can be explained by the ionization instability of the leading pedestal, that's intensity lies above the optical breakdown threshold. This means that preplasma generation should be prevented even in electron acceleration from gases, which is a somewhat new and unexpected recent development.

Proton acceleration from thin foils is the emerging hot topic of the recent years, which doesn't have such a long history as electron acceleration [109]. Due to its novelty and complexity just the underlying mechanisms have been explored so far, and still even some of the basic features are a matter of discussion. The origin of fast protons have been such an indecisive question between front and rear surface acceleration, till Mackinnon et al. [110] proved conclusively that high energy photons are mainly accelerated from the back side of the target: changing the plasma scale length on the rear of the target by irradiating it from the back with another laser pulse have a strong influence on the highest energy protons. The most energetic proton beam was generated from an unperturbed target i. e. with the the shortest plasma scale length - implying that the temporal contrasts have a pivotal role in proton acceleration as well. Measurements trying to optimize proton production by searching for the optimal target thickness confirmed this. Comparing measurements on different laser systems with rather different temporal contrasts (see Spencer et al. [111] and references therein) showed that the highest energy protons were accelerated from the thinnest foils with the highest contrast pulses. The benefit of thinner targets is well explained by the target normal sheath acceleration (TNSA) model. According to that in thinner targets

the transversal spreading of the hot electrons is smaller resulting in a higher density accelerating electron sheath on the rear surface leading to a higher energy proton beam. A high temporal contrast is an essential prerequisite for this as any preplasma formation drastically weakens the steep accelerating gradient. Systematic experimental and numerical investigation conducted on the influence of ASE [112] agreed well with the aboves. The duration of the ASE and the the target thickness were varied and a linear correlation between these two parameters were found. The optimal target thickness is decreasing with smaller ASE durations providing better conditions to high energy proton acceleration.

Inertial confinement fusion is truly the primary project of large laser facilities, which deliver rather long pulses with extreme energies, nevertheless multi-TW fs lasers always played an important role in the advancement of fusion research. Their most notable contribution was performed in the design of the ignition targets, which are typically capsules containing hydrogen isotopes in a gaseous fuel, coated with a thin Al layer on the outside surface. It is a well accepted fact that prepulses and pedestal impair the effectivity of fusion experiments by damaging this outer coating, therefore a high contrast is necessary for successful fusion experiments as well. The desired contrast level has been determined lately in an experiment [113] that has been conducted on the OMEGA laser. This throughout investigation included measurements of the neutron yield, optical probing of the target reflectivity and determination of the damage threshold by a change in transmission – all in function of the pedestal fluence. It was found that already $0.2\mathrm{J/cm^2}$ laser radiation emitted prior to the main pulse worsens the target performance therefore the cumulative fluence of pedestals and prepulses should be kept below this threshold. This fluence corresponds to a contrast of 10^7 in the ns scale on the OMEGA laser. It is important to note that the authors found that the damage threshold doesn't depend on the intensity but only on the laser fluence applied to the coating. This agrees very well with the main finding of our experiments. (see subsection 4.2.1 at page 37)

In summary, the scientifically most intriguing experiments: high-order harmonic generation in solid surfaces, laser driven proton and electron acceleration and target design experiments for inertial confinement fusion are all inhibited in progress by the imperfect temporal profile of laser pulses. Therefore improvement of the contrast became the most vital task in high-power laser development.

5.1.2 Desired contrast level

The higher the contrast the cleaner the experiment - one can simply conclude from the aboves - which is certainly true; but one should keep in mind that the improvement of contrast by any known improvement method leads to a degradation of other laser parameters. However plasma mirror is undoubtedly excels in retaining the temporal and spatial characteristics of laser pulses, which are essential in most experiments, even it has a serious drawback of reducing the delivered laser energy and thus peak intensity in the focus. Therefore a careful evaluation of these drawbacks and benefits

considering the requirements of particular experiment was necessary in the design of our plasma mirror setup to establish the ideal trade-off between energy loss and contrast improvement.

Our goal was to construct a plasma mirror setup for a large laser facility, for the 100 TW Salle jaune laser at LOA, that would significantly improve the conditions of most laser-solid experiments, primarily that of high-order harmonic generation. As it was discussed above this phenomenon is highly sensitive to the contrast but at the same time its effectivity scales with intensity, thus finding the ideal trade-off between contrast improvement and energy conservation was difficult. The desired contrast level can be estimated from [114] which studies the interaction of low intensity prepulses with solids. However it had been generally presumed that the pedestal and prepulses are dangerous only above the ionization threshold in [114] this was disproved by showing that even below this threshold nonionizing prepulses can significantly alter the interaction. Prepulses at an intensity as low as $10^8 - 10^9$ W/cm^2 vaporized the target and this neutral vapor outgased from the surface gets ionized by the rising edge of the laser pulse. This can significantly mislead the experiment. It was proposed to use opaque targets for reducing the absorption of ASE so that vaporization occurs at somewhat higher fluences. Similar concerns were raised in [115] using a high intensity excimer laser [116]. Material evaporation couldn't had been excluded at an intensity of 10^6 W/cm^2 at 248 nm. These studies clearly show that for a proper laser-solid interaction, where no alteration in the conditions of the experiment happens prior to the arrival of the main pulse, an ASE intensity of not higher than $\leq 10^7$ W/cm^2 is desirable at 800 nm.

5.1.3 Goal of the double PM study

The Salle Jaune laser delivers 25 fs pulses of energies up to 2.5 J at 780 nm wavelength with up to 10 Hz repetition rate. Such parameters with tight focusing allows for the generation of 10^{20} W/cm^2 in the laser focus. The peak-to-background contrast of the laser, according to third order autocorrelation measurements, slightly exceeds 10^7 on a nanosecond scale and it is 10^4 on the picosecond scale. Considering the requirements of a clean laser-solid experiment [114, 115], a minimum contrast improvement of 10^4 or higher is necessary. The contrast improvement factor of a single plasma mirror is limited to 200, therefore employing two plasma mirrors in sequence was necessary. Provided that both plasma mirrors operate at peak performance such a double plasma mirror setup could potentially offer a contrast improvement factor of a few times of 10^4, with a fairly moderate 50% of loss of the peak intensity.

My goal was to set up and fully characterize a double plasma mirror system for the 100 TW laser "Salle jaune" laser at Laboratoire d'Optique Appliquée. My goal was to optimize the fluence on both PMs to exploit the most from the system in order to improve the initial contrast of the laser with several orders of magnitude. My goal was to perform a complete experimental and numerical characterization of the system. In particular I wanted to demonstrate that placing the first plasma mirror into the

near field - which is a critical part of the design but unavoidable due to the high pulse energy (2.5 J) - doesn't impair the focusability but together with the second PM's spatial filtering effect the final beam's profile is rather improved.

5.2 The double plasma mirror setup

The major consideration taken in the design and construction of the a double plasma mirror (DPM) setup was providing the optimal conditions for the operation of each plasma mirror in a way that at the same time other experimental and practical requirements in the laboratory were also met. These design guidelines were the following:

- Both plasma mirrors should have operated in S polarization which ensures a higher reflectivity and contrast improvement than P. The drawback of this solution is that AR targets manufactured for S polarized beams with 45 ° angle of incidence are rather costly, especially with a really low 0.3-0.4% of reflectivity. Considering however that both contrast improvement and reflectivity of the DPM are obtained as the product of the single plasma mirrors' respective parameters, even a small drop in these would have led to a poor total performance. Therefore for large scale facilities where high intensity beams are produced at great expenses, S pol. is the right choice.

- The first plasma mirror based on our previous investigations should have been exposed to the optimal 100 J/cm^2 laser fluence, that temporally cleans the pulses with a factor of 200 and provides at least a reflectivity of 70% at peak, and 50% in average. The second PM thanks to this pre-cleaning by the first mirror can be exposed to a higher fluence without the risk of preplasma formation. This higher fluence is expected to yield a somewhat higher reflectivity. The ideal fluence range for the second PM is a few hundred J/cm^2.

- The operation and performance of a single PM strongly depends on the spatial and temporal characteristics of the irradiating beam. Using two plasma mirrors in sequence vastly increases this sensitivity, and daily fluctuations of the laser makes the situation even more difficult. This can be handled effectively if the laser fluence on the plasma mirrors, which is the key parameter of plasma mirror operation can be adjusted easily.

- The setup should have fitted into the allocated room in the laboratory and should have been easily removable from the beam path, making possible the use of the laser without the DPM for experiments which don't benefit from an increased contrast but require the highest possible pulse energy.

The experimental setup, which was designed to fulfill these criteria is depicted in Figure 5.1. Due to the high energy of the laser a long focal length (10 m) spherical mirror was used to focus down the beam and the PMs were placed into the long focus

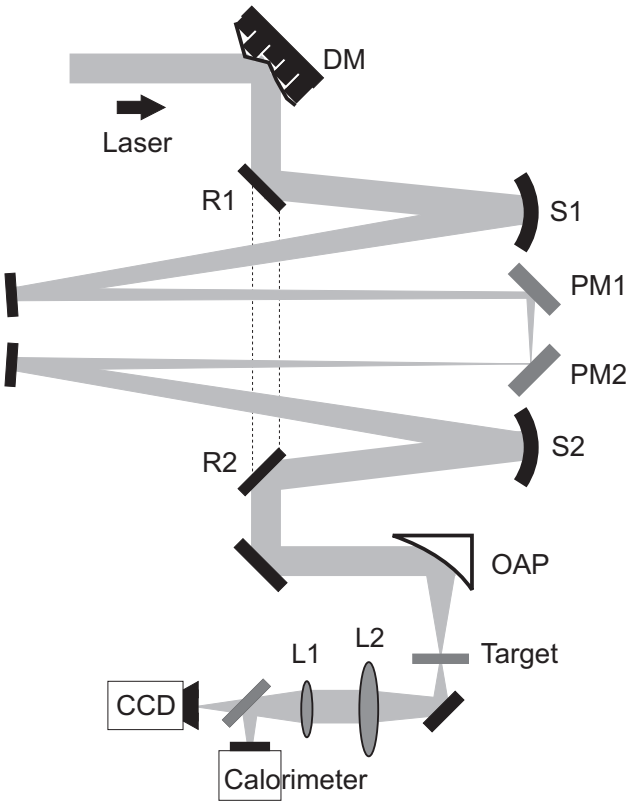

Figure 5.1: Experimental setup of the double PM system. An f = 10 m null-telescope (spherical mirrors S1 and S2) creates an intermediate focus for the laser beam and then recollimates it; near this focus, the plasma mirrors (PM1 and PM2) are situated. The fluence on the PMs was varied by changing the radius of curvature of the deformable mirror (DM). Mirrors R1 and R2 on a kinematic slide permit the DPM to be inserted (solid line) or bypassed (dashed line). Final focus was created by an off-axis-parabolic mirror (OAP), and monitored by a CCD and a calorimeter.

at right angles to each other. The first PM was in the near field, while the second was placed 14 cm from the first toward the focus for being exposed with a higher fluence. It was found by preliminary calculations that by setting this distance the fluence is ∼six times higher on the second PM. Both were exposed at 45 ° angle of incidence with the S polarized laser beam. The beam leaving the PMs was recollimated with another 10 m focal length spherical mirror, thus the whole setup formed a null telescope, with the PMs lying close to the intermediate focus. Both PMs were 10 cm × 10 cm AR coated quartz plates to minimize intrinsic reflectivity, and maximize contrast improvement. Computer-controlled stages translated the PMs parallel to their surface to provide a fresh undamaged surface for each shot – several thousands of shots are possible with one set of mirrors. The whole DPM system was installed in a cross tube of the main vacuum beamline and an ultrahigh precision mirror-slide switchyard was used to add

it into and removed from the beam path on a shot-to-shot basis.

The highest reflectivity and best beam-profile were optimized as a function of the incident fluence on the PMs. For this, the fluence was scanned by changing the radius of curvature of the deformable mirror (BIM36, Cilas), whose standard function in the laser is the correction of the spatial phasefront. We were able to change the position of the null-telescope's focal spot over a range of 80 cm, changing the fluence simultaneously on both PMs.

The fluence on each PM as it is shown in Figure 5.2 was monitored using ordinary webcameras (360 USB 2.0 Spacec@m, TRUST). However webcameras have a relatively

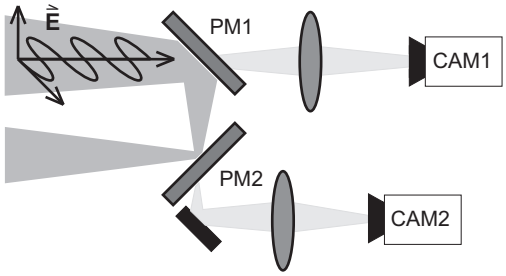

Figure 5.2: Schematic of fluence measurement on PMs: *s*-polarized beam reflects from PM1 and then PM2. The laser spots on both PMs were imaged onto webcameras (cam1 and cam2).

high noise compared to scientific CCDs, their advantages over those are their low price and easy handling. They have a resolution comparable to CCDs and where noise is not an issue but the risk of damage is high they can be considered as a suitable alternative to professional devices. Originally we wanted to use them merely as a simple online diagnostic tool that allowed the monitoring of the beam profile on the PMs, but later the captured webcam images were found suitable for further processing to determine the fluence on the PMs with a relative accuracy of not worse than 20%.

The most important parameter of the optimization, the reflectivity of the system was detected by measuring the laser energy incident on and reflected through the DPM system. Each was measured with a calorimeter placed in the target chamber, first bypassing the DPM and then deploying it. The incident fluence on the first PM was calculated using the spatial profile measured with the webcameras.

The final focus at the target plane was imaged onto a 16 bit CCD camera (Andor), and like other parameters it was recorded while varying fluence conditions. Small displacements of the position of the final focus beam-waist, caused by the varying divergence of the beam during optimization with the deformable mirror, were compensated for by moving the imaging CCD.

5.3 Characterizing double plasma mirror reflectivity

5.3.1 Modeling optical transport of a double plasma mirror

The computer simulation to model the DPM operation was developed by Jean-Paul Geindre. The purpose of the optical model was to provide a full understanding of the system and allow us to conclude on experimentally not acessible parameters and aspects of the DPM system. This fully optical model is a simple paraxial diffraction/propagation model coupled with the response of the PMs. The model calculates the optical field on each element sequentially up to the focus in the final target plane; the steep fluence-dependence of the PM reflectivity R is phenomenologically approximated by a step-like response $R = 75\%$ above 6 J/cm^2 and $R = 0$ below it. The fluctuation of the spatial uniformity in the experimental beam quality was taken into account in our modelling by adding 0.7-wave RMS random phase-disturbance to the optical field. This value was obtained from the Shack-Hartmann sensor that was used to control the deformable mirror. The random phase perturbation was different for each run of the simulation, producing the scatter observed in the data-sets presented below.

5.3.2 Reflectivity and contrast improvement

The following section with a couple of figures provides a thorough characterization of the reflectivity and contrast improvement of the double plasma mirror. Figure 5.3 shows the time- and space-integrated reflectivity (overall efficiency), and the time-integrated reflectivity measured at the center of the final target focus (spatial peak reflectivity) as a function of the plasma-mirror focal position. The same reflectivity curves obtained from the theoretical modeling are also depicted. The position of the focus is determined with respect to the PMs: the zero of the axis corresponds to the focal spot positioned on the second PM. For values less than zero, the focus approaches the first PM; –14 cm corresponds to focusing onto the first plasma mirror. For values greater than zero, the focus shifts behind the second PM. As can be readily seen, the optimal position with the highest reflectivity —31% overall and 47-57% peak reflectivity —is at the zero position, as anticipated in the design. At this position the first PM is subject to a peak fluence of 200 J/cm^2 while the second PM sees 800 J/cm^2. For these fluences, the corresponding peak reflectivities from the preceding single PM study are predicted to be higher than 70%. Together with the low-intensity reflectivity known for the antireflection coatings, these reflectivities lead to contrast enhancements of ~ 200 overall, and ~ 250 peak, for each plasma mirror in succession.

Examining further the reflectivity curves, moving in either direction away from the ideal zero position shows a decrease in both overall and peak reflectivity, and consequently in contrast improvement. This decrease indicates that at the zero position both PMs were optimally positioned to operate at the ideal fluence regime, *i.e.,* where the pedestal is just below the breakdown threshold. Higher fluence on either mirror

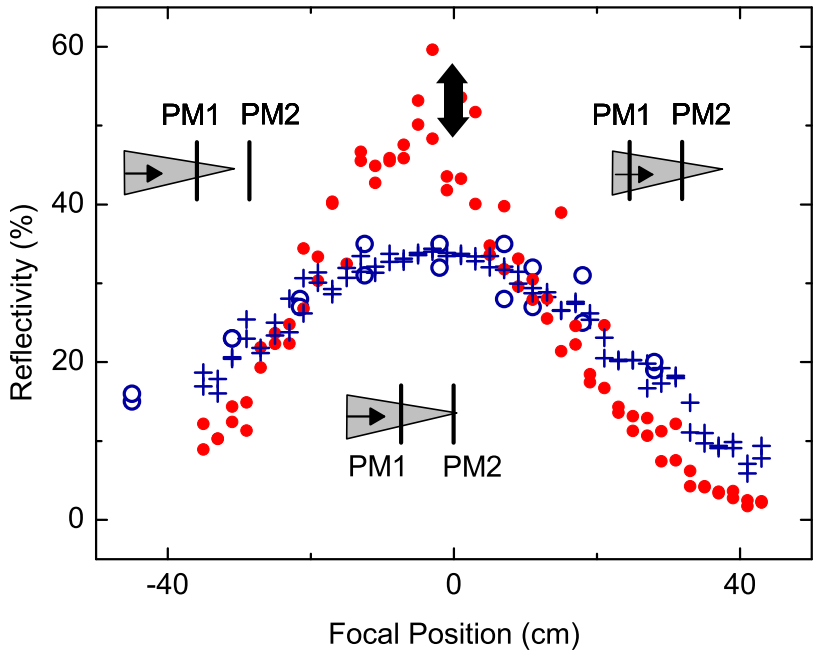

Figure 5.3: Spatial peak and overall reflectivity of the DPM system versus focal position. Spatial peak reflectivity: experimental results at the maximum reflectivity position (black arrow), and numerical results over the whole range (red solid circles). Overall reflectivity: experimental (blue open circles) and numerical results (blue crosses). The position of the focus is referenced with respect to the PMs: the zero of the axis corresponds to the focal spot positioned on the second PM. The random phase perturbation was different for each run of the simulation as discussed in the text, producing the scatter observed in the numerical data sets.

would lead to too-early triggering of the plasma layer, while a lower fluence unnecessarily reduces plasma reflectivity and contrast enhancement. The peak and overall reflectivity curves agrees well with the experimental results showing that we have managed to understand the behavior of this complex system. In summary, the DPM setup was shown to improve the contrast by a factor of 5×10^4 with a loss in peak intensity, at the center of the focal spot, of $\sim 50\%$.

As high-power lasers are dedicated to achieving extremely high intensities on the target surface one of their major characteristic is the focusability of the delivered beam. Any optical system added to the laser is highly anticipated to preserve this key feature. To demonstrate the double plasma mirror's capabilities in this aspect we have conducted a detailed characterization of the beam quality evolution through the

DPM system up to the final focus. This extensive investigation consisted in parallel experimental measurements and computer modelling of the development of the fluence distribution in propagation through the whole setup. Figure 5.4 shows the calculated and measured fluence distributions on the first PM versus focal position on the second PM. The first PM was placed 14 cm from the second one, thus the smallest spot size can be observed at -14 cm in the figure. The solid curve on the figure is a guide to the eye drawn through the corresponding measured overall reflectivity values of the DPM system. Here as in previous reflectivity calculations the same 0.7-wave RMS random phase-disturbance has been added to the optical field, that leaded to severe beam distortion in intermediate field further from the focus, well reproducing the measured profiles. These modulated beam profiles show the drawback of placing the first PM in the intermediate field of the beam. The rough profile leads to spatial variations in PM reflectivity, imparting further amplitude distortions. Moreover due to the strong dependence of the time of reflective plasma formation on laser fluence the reflected waveform will potentially exhibit significant distortions as well. These two major effects can impair the focusability of the reflected beam.

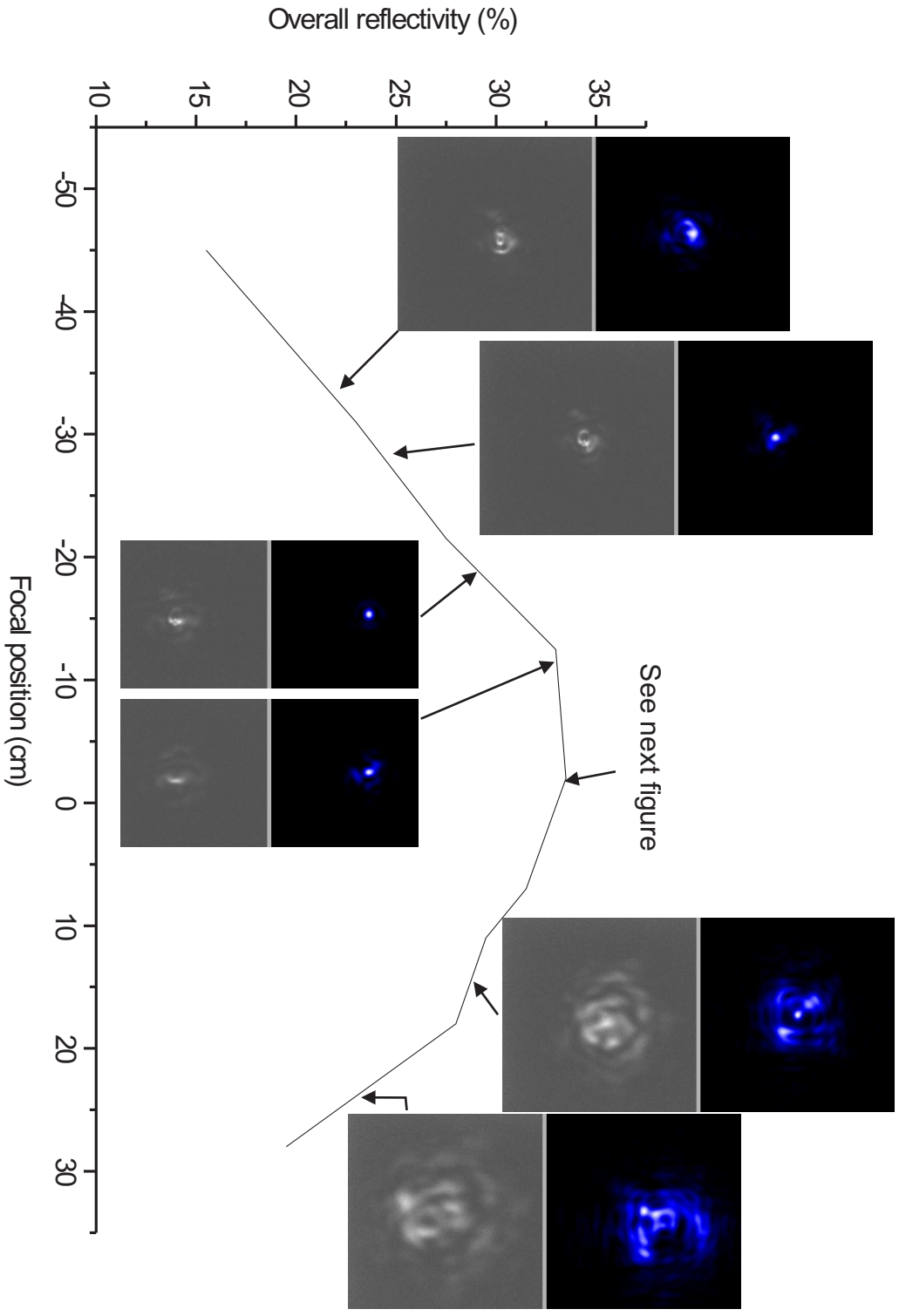

Figure 5.4: Calculated and measured fluence distribution on the first plasma mirror versus focal position. The solid curve is a guide to the eye drawn through the corresponding measured overall reflectivity values of the DPM system.

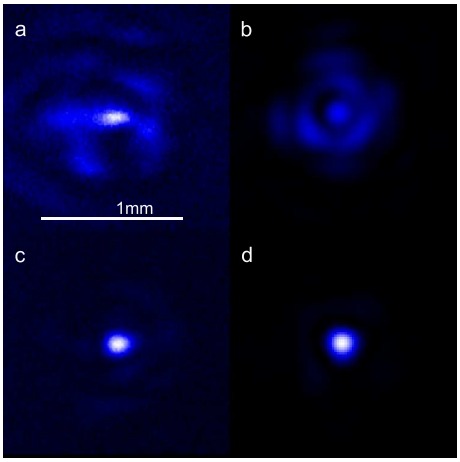

Figure 5.5: Calculated and measured fluence distribution on both the plasma mirrors in the best reflectivity condition. (a) and (c) experimental observation, (b) and (d) numerical simulation of fluence distribution on PM1 and PM2 respectively.

Figure 5.5 shows the beam profiles on both PMs, both measured and modeled, using the maximum-reflectivity condition i. e. the beam was focused onto the second plasma mirror. The beam diameter on the first PM is $\sim$ 1.2 mm with an average fluence of 200 J/cm^2 and as it can be readily seen the profile merely 14 cm from the focus still exhibits strong modulations. In our previous study of the single PM in good agreement with the results of Dromey *et al.* [117] we found that these distortions are weak and don't significantly impair the reflected beam quality. The focus on the second PM is circular with a smooth profile. The diameter of the focus is $\sim$ 200 μm and the average fluence is 800 J/cm^2. This higher fluence made possible by the contrast improvement of the first PM resulted in a higher reflectivity on the second PM.

The most important quality of the DPM system how it affects the final focus is shown by Figure 5.6, which depicts the final focal spot at the target plane, recorded by the 16-bit CCD camera, with and without the DPM system. It also shows the equivalent focal spot images obtained by our numerical model. It is evident taking a glance on the focal images that no visible degradation of the focus can be seen after the plasma mirror, rather a small improvement can be perceived. The sizes of the foci are practically the same, and no worsening in the beam profile is observable but a marked enhancement is that the energy in the foot around the focal spot is reduced significantly by the DPM. This is because the second PM was operating in the beam's far field, and acted as a spatial filter. This effect can also be clearly seen in the images produced by the numerical simulation.

A more quantitative comparison is provided by figure 5.7 that shows the normalized intensity distribution and radial integrated energy in the focus for a few shots with and without plasma mirror. The energy distribution around the peak is strikingly similar with and without the PM but in the wings around the resemblance ends. The

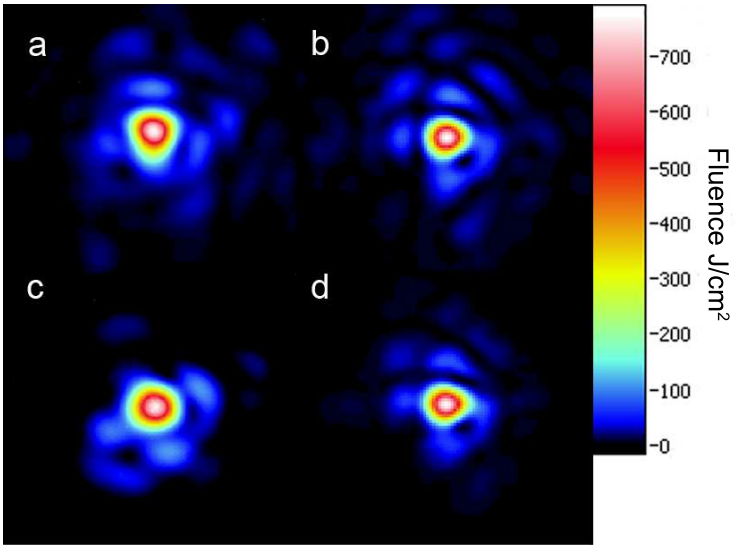

Figure 5.6: Focal spots in final target plane without and with the DPM system: (a) experimental observation and (b) numerical simulation of the final focus without the DPM system; (c) and (d) experimental and numerical results obtained for the final focus with the DPM system.

DPM changes the balance of energy of the focal peak, relative to the wings of the focal spot, while tending to preserve the peak. However the overall reflectivity of the DPM system isn't particularly good (31%), thanks to this spatial filtering effect the peak reflectivity which is of our interest is significantly higher ($> 50\%$).

For a complete characterization of the effect of the DPM on the beam's spatial characteristic an imaged z-scan was performed around the final focus, and the change in peak intensity was investigated. Figure 5.8 depicts the z-scan made with and without the DPM. The peak fluence is plotted versus the displacement from the object plane of the focal position. The curves for ease of comparison are normalized to unity. However only a few measurement points were taken and the peak intensity of the intermediate field doesn't provide as much information as necessary for an accurate characterization a rough comparison still can be made. The slope of the curves moving further from the focus, obtained with or without the DPM are very similar implying that the DPM system preserves the quality of the intermediate field.

5.4 High-order harmonics generation with the double plasma mirror system

We've performed a short proof-of-principle experiment to demonstrate the benefits of the double plasma mirror system in high-order harmonics generation on solid surfaces. We tightly focused the beam onto the surface of the final target to generate

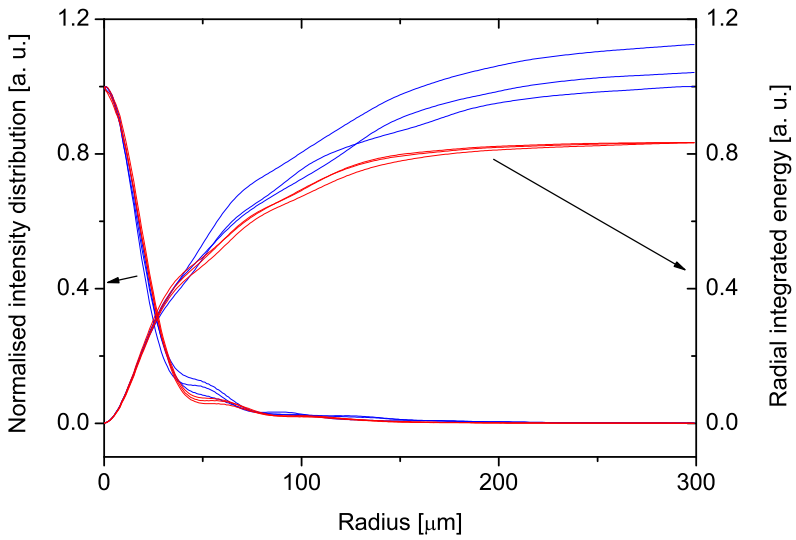

Figure 5.7: Spatial filtering effect of the DPM. Normalized intensity distribution for three experimental shots with plasma mirror and three experimental shots without plasma mirror (left side of graph) and corresponding radial integrated energy (right side of graph) for the six shots. Blue line: without DPM; red line: with DPM. The addition of the DPM reduces the energy deposited outside the focal spot, as compared to the case without DPM.

harmonics with and without the DPM system. The beam reflected from the target and the generated harmonics were imaged onto a diffuse screen at the input to an XUV spectrograph.

First we compared the optical characteristics of the reflected laser beams. In this aspect the final target functioned as a first and as a third plasma mirror without and with the DPM system respectively. The fluence on it was orders of magnitude higher than on the mirrors of the DPM system. With the DPM system in the beam path the light was reflected specularly with a forward cone angle that roughly equals that of the focusing angle. The good optical quality of the reflected beam implied that the generated plasma mirror on the final target's surface remained flat during reflection. In contrast the reflected laser light without the DPM was spreading into a forward-cone angle greater than 90°. The scattered light was diffuse and speckled. We can interpret this as with the tight focusing onto the final target as a first plasma mirror the fluence of the pedestal and the prepulse exceeds the damage threshold of the target, and thus a preplasma is generated. Due to the thermal pressure the preplasma expands on the target surface that leads to a poor optical quality of the reflected main pulse.

The generated harmonics were also compared. With the DPM system we observed a

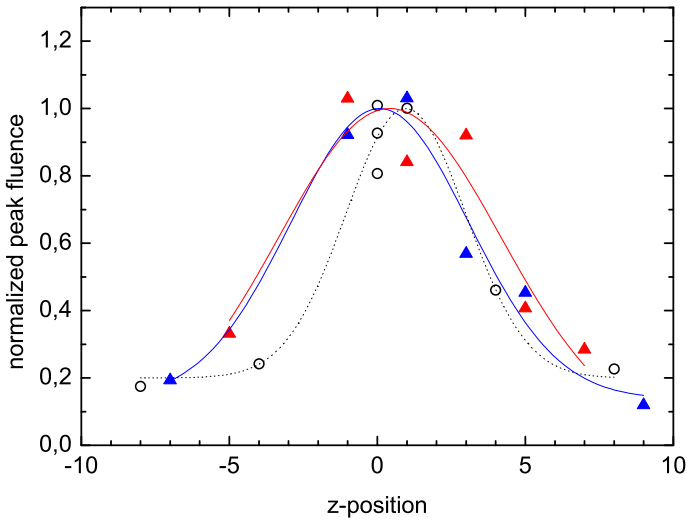

Figure 5.8: Imaged z-scan around the final focus with and without DPM: The peak fluence is plotted versus displacement of the object plane from the focal position. Beam z scan without the DPM (red and blue triangles and solid lines); with the DPM (open circles, dotted line). All curves are normalized to unity. The curves are guide to the eye.

narrow harmonic beam, and preliminary harmonic spectra with the XUV spectrometer. Without the DPM system, although the intensity was higher with a factor of two in this case (due to the lack of the DPM losses) we couldn't observe harmonics. We interpret this as the pulse instead of the steep electronic density gradient target met with a low density pre-plasma, and thus generation of harmonics by the oscillating mirror model was prevented.

Although this was only a short quick measurement, we were able to demonstrate the benefits of higher contrast pulses generated by the DPM system, and show for the first time, that the use of two successive plasma mirrors considerably improves the conditions of laser-solid interactions.

5.5 Summary

I provided a complete experimental and numerical characterization of the double plasma mirror system. I optimized the fluence on both PMs and achieved a 47%-57% peak and 31% overall reflectivity for the system. I improved the initial contrast of the 100 TW laser by a factor of $5 \cdot 10^4$ to a record high $5 \cdot 10^{11}$.

I've used an optical propagation code to model the optical transport of the beam and found a good agreement between modelled and measured results including beam

profiles on both PMs and focus in the final target plane. Extensively studying the fluence distribution on the first PM, which is in the intermediate field, I found that the beam profile as it was expected is somewhat rough. Although this unavoidably leads to some distortion of the reflected beam profile, this slight degradation is overly compensated by the second PM. The second PM was positioned into the intermediate focus, thus it acts as a spatial filter. Due to this I observed no degradation of beam quality or focusability in the final target plane, but on the contrary, a slight improvement in the spatial characteristics. As high-power lasers are built to maximize peak intensity on target surface, retaining or rather improving the focusability of the beam is the key feature of the DPM system.

The DPM was engineered as a standard system feature and is easily added or bypassed with a single kinemtic stage in the 100 TW Ti:sapphire research laser. The AR targets can be shifted from shot to shot to provide a fresh undamaged surface for each laser shot.

I've compared high-order harmonic generation with and without the DPM system. Temporally cleaning the pulses with the DPM system a narrow beam of harmonics was generated and the laser light was reflected specularly. Without the DPM no harmonics were observed and the reflected beam was diffuse and inhomogeneous. With this I demonstrated that high contrast pulses produced by the DPM system preserves the steep electronic density gradient, which is compulsory for conducting clean laser-solid interactions.

Part II

Development of a single-shot carrier-envelope phase meter

Chapter 6

General overview

6.1 Ultrashort laser pulses and applications

The progress in ultrafast laser technology was enormous over the past decades. With the invention of mode locking [118] and its application to lasers [119], generation of ultrashort laser pulses with peak intensities rivaling the field inside atoms at high repetition rates became possible. Table-top lasers with such performance are nowadays commonplace in many laboratories and find applications primarily in time resolved spectroscopic experiments. In these experiments gaseous targets are exposed to intense light pulses (pump pulse) to trigger a reaction repeatedly and an other laser pulse split from the main beam (probe pulse) is used to probe the reaction. The probe is temporally delayed to the pump and by scanning the time delay in a series of high repetition rate exposures one can track the temporal evolution of the reaction. The possibility of studying the dynamics of chemical reactions in such pump-probe experiments with ultrashort laser pulses was first recognized by Ahmed Zewail [36] who has been awarded with the Nobel-prize in 1999 for his pioneering work in femtochemistry. As molecular dynamics take place on the femtosecond scale a temporal resolution of a few femtoseconds or higher is required for their study. The temporal resolution in a pump-probe experiment is limited by the pulse duration of the optical pulse therefore there has been great motivation for the generation of shorter and shorter optical pulses. While molecular interactions can be observed with femtosecond pulses, inter-atomic processes occur on the attosecond scale calling for a pulse duration of the optical pulse which is well below the single-cycle limit at visible and NIR wavelengths.

6.1.1 Attosecond physics

The generation of optical pulses in the attosecond regime required further progress both in technology and in fundamental science. A single-cycle pulse at Ti:Sa wavelength (800 nm) would have a duration of 2.6 fs thus it is obvious that an attosecond pulse can only be generated at significantly shorter wavelengths. The phenomenon that makes possible the generation of coherent optical pulses in the far-UV is high-order

harmonic generation which is well described by the semi-classical three step model from Paul Corkum [38]: an electron liberated from the atom after some evolution in the continuum may recollide with the parent ion and releases an XUV photon. This happens at each half-cycle of the oscillating laser field resulting in a series of XUV bursts with attosecond durations. Although a train of attosecond pulses [120, 121] are suitable for particularly intriguing measurements [122], for pump-probe experiments a single attosecond pulse is desirable which can be achieved if only one half-cycle releases the highest energy XUV photons. This can be provided by using few-cycle laser pulses for harmonic generation as it will be described below.

Isolated attosecond pulses

Any laser pulse has a finite duration which means that as the envelope changes in time the maxima of the half-cycles varies along the pulse. If the laser pulse is so short that it contains only a few oscillation cycles of the electromagnetic field the difference between the neighboring maximum is significant, which plays a key role in several experiments. In the above described high-order harmonic generation process for example such a few-cycle laser pulse with an appropriate waveform can generate an isolated attosecond XUV pulse. If the electromagnetic field within the pulse is positioned so that the maximum of the central half-cycle coincides with the maximum of the pulse envelope, the energy of the XUV photons generated by the central half-cycle will be higher than of those generated by the other half-cycles. This so called continuum in the harmonic spectrum in the time domain constitutes an isolated attosecond pulse.

As a rule of thumb the shorter the laser pulse the bigger the difference between the neighboring maxima which generates a broader harmonic continuum and that in turn leads to a shorter attosecond pulse. This relation demonstrates that the generation of intense few-cycle pulses was a prerequisite in establishing high precision attosecond pump-probe measurements. With the invention of chirped mirrors [3] in the early-nineties and the hollow-core fiber compression technique [4] a few years later the generation of intense few-cycle laser pulses in the NIR range became possible. With such pulses the proof of principles of isolated attosecond pulse generation was for the first time demonstrated by Hentschel et al. [41]. In their pump-probe measurement the attosecond pulse was cross-correlated with the NIR laser pulse to measure its duration. It is important to note that in the early attosecond experiments [39–42] the pulses were sufficiently short for isolated attosecond pulse generation but there was no control above the waveform of the laser field, which is a prerequisite for a controlled generation of attosecond pulses.

Carrier-envelope phase

The waveform of a laser pulse can be written in the following form: $E(t) = E_0(t)\cos(\omega t + \phi)$, where ω is the frequency of the carrier wave, and ϕ is the carrier-envelope phase (CEP), which is the offset phase between the carrier wave and the pulse envelope. One can readily see from the definition that an isolated attosecond pulse

requires a so called "cosine" pulse with a CEP of close to 0. In the early attosecond experiments due to the lack of CEP stabilization the CEP of the pulses varied randomly from shot-to-shot, which severely hindered the interpretation of the experiments and the exploitation of the potential of pump-probe attosecond measurements.

A few years ago using phase stabilized oscillators and an additional f-to-2f interferometer for controlling the phase drifts of the amplifier, phase stable generation of intense few-cycle lasers become possible [5]. This technical development opened new prospects for attosecond metrology and spectroscopy. It became possible to generate attosecond pulses in a controlled manner, which facilitated attosecond streaking [123], a measurement method that can be used for the measurement of atomic and interatomic processes [7].

6.1.2 Limitations of phase stabilization

Although a great many of experiments have been performed with attosecond streaking there is a major limitation in this field which comes from the very low intensity of the generated attosecond bursts. XUV pump-XUV probe measurements can not be performed with XUV pulses having only nanojoule energies. Therefore in attosecond streaking measurements so far, due to the very low intensity of the gas harmonics, the NIR laser pulse was used to probe the phenomena triggered by the attosecond pump pulse. This increases the complexity of the experiments and severely limits the interpretation of the experimental results and understanding of sub-fs processes. Furthermore with two relatively intense attosecond pulses it would be possible to extend attosecond metrology and spectroscopy to attosecond control, with one attosecond pulse releasing the electron and the other controlling its further evolution. Increasing the intensity of isolated attosecond bursts is therefore of top-most interest in attosecond physics.

Isolated attosecond pulse generation by HOHG on solid surfaces based on the oscillating mirror model has been envisaged for a while [11]. As solid targets can withstand arbitrarily high intensities and the conversion efficiency of laser light to harmonics is significantly higher than for atomic harmonics, this process is expected to produce isolated attosecond bursts with several orders of higher intensities. Moreover numerical simulations suggest that the intensity of the harmonics scales with the intensity of the driving laser field thus unlike at gas harmonics there is no fundamental limit for the intensity of the attosecond burst. Simulations also show [11] that generating an isolated attosecond pulse by HOHG on solids requires a few-cycle pulse with an appropriate waveform but with several orders of higher pulse energies than for gas harmonics. Until very recently these requirements have been far beyond the capabilities of ultrafast laser technology.

Few-cycle multi-TW OPCPA lasers have recently become available with sufficient pulse duration and pulse energy [9, 10], but phase stabilization of such large scale systems hasn't been demonstrated yet. Due to the technical complexity of phase stabilization, the highest peak power that is available from a few-cycle phase stabilized

laser is 0.2 TW [8], which is more than an order of magnitude less than required to extend waveform-dependent experiments to relativistic laser plasma interactions.

As phase stabilization is not available for large scale systems the only technically feasible solution could be to fully characterize the temporal structure of the waveform of each few-cycle laser pulse, and then by simple CEP tagging it would be possible to study waveform dependent experiments even at relativistic intensities. As laser pulses with sufficient parameters are available now, in order to exploit the potential of these sources the development of an accurate and precise single-shot method for the temporal characterization of few-cycle waveforms became of foremost interest.

Chapter 7

Single-shot stereo-ATI detector

7.0.3 Goal of single-shot phase meter development

The temporal structure of a few-cycle laser pulse is characterized by the pulse envelope and the carrier-envelope phase. The pulse envelope is determined by the intensity and the pulse duration. The pulse duration can be measured by standard all-optical diagnostics such as autocorrelation [124] or FROG [125] and the intensity can be inferred from the pulse duration and the fluence in the interaction volume. In contrast to the pulse envelope characterization, the measurement of the carrier-envelope phase can only be performed by all-non-optical methods. The reason is that f-to-2f interferometers which are commonly used to stabilize the phase of few-cycle lasers can only detect the rate of change of the CEP, but they are blind to its actual value. Measurement of the actual CEP therefore requires a completely different approach.

In recent years several experiments exploiting various phase sensitive phenomena such as quantum interference in photocurrents [126], Thz emission [127] or half-cycle cutoffs in harmonics spectra [128] have been successfully demonstrated to retrieve the carrier-envelope phase of phase stabilized few-cycle laser pulses. While single-shot diagnostics for the determination of the pulse envelope are available for long, single-shot measurement of the carrier-envelope phase hasn't been demonstrated to date. All the measurement methods presented so far [126–129] required several thousands of laser shots for a single measurement point, and all of them work on a proof-of-principle level. Therefore they are applicable only on high repetition rate few-cycle sources with relatively low pulse energies - which are commonplace in many laboratories - as currently only those can be phase stabilized. My goal is to develop the first single-shot measurement apparatus that can record the phase of consecutive non-phase stabilized laser shots, and therefore can be used also on high-power few-cycle lasers, which are non-phase stabilized.

7.1 High-energy above-threshold-ionization electrons

The best known multi-shot method is by no doubt the stereo-ATI phase meter [12]. The single-shot measurement apparatus and method presented in this thesis is a completely rethought and redesigned version of the previous multi-shot apparatus.

The single-shot stereo-ATI phase meter uses the left/right asymmetry in the yield of high-energy above-threshold-ionization (HATI) electrons along the polarization axis to retrieve the CEP. Above threshold ionization is a multi-photon ionization mechanism. It occurs when multiple photons ionize the atom with a total energy higher than required for the ionization, leaving the electron with some kinetic energy after the ionization process. Due to the asymmetry of the electric field different number of electrons leave the atom in the left and right directions with different kinetic energies. Since these directly ionized electrons arrive to the detectors in relatively large numbers, measuring the left and the right direct electron spectra would provide a fairly easy way for determining the CEP. Unfortunately due to deflections of the direct electrons in the laser field after ionization their left/right spectra exhibit only low sensitivity to the phase [12]. As CEP-tagging requires a robust and accurate measurement of the waveform of the electric field a higher phase sensitivity is required which can be only provided by the so called HATI electrons also known as rescattered electrons. These electrons are generated in the following way: A small portion of the ionized electrons after some evolution in the laser field revisit the ion core. Some of them backscatters from the core and if the laser field after the scattering is high they can obtain a kinetic energy that is significantly higher than that of the directly ionized electrons. The enhanced phase sensitivity of the rescattered electrons comes from their rather complex evolution in the laser field. In order to obtain a significant number of rescattered electrons firstly the field strength have to be high during the initial ionization, just as in the case of direct electrons. Secondly to be accelerated to high energies, the electric field have to be high also after backscattering. Since the scattering event follows the moment of initial ionization by approximately three quarters of an optical cycle, a high electric field strength for both event can not be perfectly ensured for a few-cycle laser pulse. The trade-off between these two conditions leads to an increased phase sensitivity of the rescattered left and right electrons [130], that in turn provides a high precision to the CEP measurement. The main drawback of using the HATI electrons in a single shot measurement is that these electrons due to their complex evolution are generated in almost two orders of magnitude smaller numbers than the direct electrons. Therefore detecting sufficient number of highly phase sensitive HATI electrons in a single laser shot poses a significant experimental challenge.

7.2 Experimental apparatus

The multishot stereo-ATI phase meter was invented by Gerhard G. Paulus. The stereo-ATI scheme with two opposing detectors was successfully employed to detect for the first time phase effects with few-cycle laser pulses [131] and later with the apparatus

the first CEP measurement was performed [12]. After that proof-of-principle measurement the same apparatus was used to study the Gouy-phase shift for few-cycle laser pulses [132] and it was also employed for long term CEP stabilization with an external stabilization loop [133]. All these measurements have been performed with the multi-shot phase meter that needed at least ten thousands of laser shots for a single measurement point. Therefore in order to reach single shot detection a four orders of magnitude increase in signal yield i.e. in the number of detected electrons was necessary.

The scheme of the multishot apparatus was relatively simple [12, 133]. The central part of the vacuum apparatus was an ISO-K 160 vacuum cube with a gas nozzle in the center. The front and the back sides of the cube was covered with vacuum flanges with a small central thin glass entrance and exit windows for the laser beam. The drift tubes were attached to the left and the right sides of the vacuum cube, and the turbomolecular pump to the bottom side. The horizontally polarized focused beam entered the apparatus through the entrance window and ionized the xenon atoms slightly before the focus with a peak intensity of nearly 10^{14} W/cm^2. ATI electrons ejected from the xenon jet in left and right directions after 40 cm of flight in the drift tubes reached the MCP detectors. Computer-hosted multiscaler cards connected to the MCPs measured the arrival times of the electrons. The left and right ATI energy spectra were calculated from the TOF signals.

In order to reach four orders of magnitude increase in signal yield considerable changes were necessary. These changes were the following:

- redesigning the magnetic shielding and the vacuum apparatus to increase the number of electrons arriving to the detectors
- changing the data acquisition system from electron counting to digital voltage detection to be able to detect a large number of simultaneously arriving electrons in a single laser shot at high repetition rates
- installing an imaging system that allows for a precise alignment of the laser beam in the interaction volume and optimization of the laser intensity

7.2.1 Vacuum design and magnetic shielding

The most important modification was done on the vacuum apparatus with the aim of boosting the number of ATI electrons which reach the MCP detectors. In the multishot apparatus a nozzle was used to supply the xenon gas jet. The advantage of the nozzle is that it is easy to handle but its drawback is that even a relatively low xenon gas density in the interaction volume requires a high gas load. With a high gas load other parts of the vacuum apparatus including the drift tubes get contaminated by xenon which can damage the MCP detectors, as those require a high vacuum of 10^{-5} mbar pressure at least, for a safe and reliable operation. Another reason for a high vacuum is to ensure collisionless free flight for the electrons in the drift tubes. Therefore the

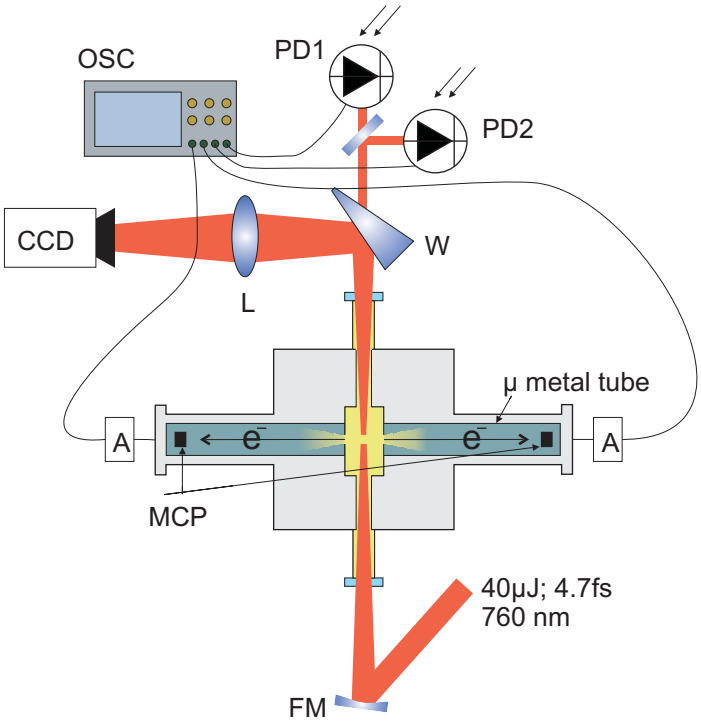

Figure 7.1: Single-shot stereo-ATI phase meter. Two opposing time-of-flight detectors are mounted in a compact vacuum apparatus. A differentially pumped stage is established between the entrance and exit windows in the apparatus (yellow part) with a xenon preasure of $1.6{\cdot}10^{-2}$ mbar. Outside of this part a high vacuum ($4{\cdot}10^{-6}$ mbar) was maintained within the apparatus (blue part) with a turbomolecular pump (not shown) to provide a safe operation for the MCPs and a free flight for the HATI electrons. The horizontally polarized focused laser beam entered the apparatus through the entrance window and ionized the xenon atoms slightly before the focus at an average intensity of $8 \cdot 10^{13}$ W/cm^2. The electrons left the differentially pumped section through two 0.7 mm thin vertical slits and after 15.5 cm of flight in the drift tubes reached the MCP detectors. The drift zone was magnetically shielded with a μ-metal tube (dark blue) with a large opening between the gas inlet and the turbo pump. The voltage from the MCPs were amplified by two wide-band amplifiers (A) and recorded with a digital oscilloscope (OSC). A fast diode (PD1) was used to trigger the oscillosope and the signal of a slow diode (PD2) was also digitized for monitoring the pulse energy fluctuation. The beam exiting the apparatus was split into two with a wedge (W). The front surface reflection was used to image the interaction volume with an achromatoc lens (L) onto a CCD camera. This imaging system was applied to precisely align the laser beam in the phase meter and optimize its intensity.

signal yield i. e. the number of electrons and consequently the number of xenon atoms in the interaction volume had to be increased, without degrading the vacuum in the

drift tubes around the MCP detectors. This was made by replacing the gas nozzle with a differential pumping stage as it is shown in Figure 7.1. A small hollow cube with 2 cm side length was used for that purpose. The cube had an entrance and exit hole on the front and back for the laser beam, and two 0.7-mm-thin vertical slits on the sides for the ejected HATI electrons. The slits held back the electrons generated outside the laser focal region and ensured that only a small gas inlet contaminated the vacuum. The small cube at the two holes with thin tubes was connected inside the vacuum apparatus to the front and back vacuum flanges of the main cube. The entrance and exit vacuum windows were at the ends of two short ISO-KF 25 vacuum tubes attached to the vacuum cube. Increasing the distance from the laser focus was necessary to avoid optical damage. The small volume between the two windows including the small cube and the tubes to the vacuum flange and KF tubes formed a differential pumping stage with a relatively high xenon pressure of $1.6 \cdot 10^{-2}$ mbar, while a high vacuum ($4 \cdot 10^{-6}$ mbar) in the other parts of the apparatus could had been maintained by the turbomolecular pump. The continuous gas supply during the experiment was provided by a high pressure xenon gas bottle which was regulated by a fine dosing vacuum valve. With the differential pumping stage the xenon gas pressure was increased considerably for a higher signal yield while the high vacuum in other parts of the apparatus was maintained. At $1.6 \cdot 10^{-2}$ mbar of xenon pressure space charge effects, which can distort the signal were still negligible.

The main cube and the drift tubes in order to make the phase meter more compact and to reduce the pumped volume were an aluminum ISO-K 100 cube and two 15.5 cm long ISO-K 100 tubes respectively. At this drift tube length the resolution of the TOF and energy spectra were still sufficiently high for an accurate CEP measurement.

The requirement of the time-of-flight spectroscopy is that the ionized electrons have to travel by experiencing no disturbation or deflection on their path to the detector. As the drifting electron is sensitive to the magnetic field it was important to shield the path of the electron from external magnetic fields. In the multi-shot apparatus two tubes made of mu-metal were concentrically inserted into the drift tubes for that purpose, with a few cm of distance from each other in the center, leaving the space unshielded around the gas jet. Unfortunately it was discovered that two tubes in certain cases instead of shielding could rather amplify the magnetic field in the center of the apparatus. Magnetic field lines which could not pass at the tubes could had been directed to pass between the the two mu-metal tubes, resulting in a deflection of the electrons' path. As the magnetic field in the laboratory can be a few times higher than the Earth's magnetic field, especially close to the optical tables, the deflection can be big enough for the electron to miss the MCP detector. Therefore an improvement of the magnetic shielding was indispensable for proper single-shot TOF spectroscopy.

The general solution for magnetic shielding is to use a set of Helmholz coils, which can generate a uniform magnetic field to cancel the external field. The advantage of using a Helmholz coil is that it requires no modification of an existing setup including the vacuum design, which is a sensitive point of the single-shot phase meter. Quick test with coils showed the limitation of this technique as it can cancel only uniform

fields. Around the phase meter due to the optical table and several metal components including the vacuum pump the field is strongly inhomogeneous, therefore the only effective solution that can come into consideration is still a proper mu-metal shielding.

In general it is considered that the more a certain volume is covered with mu-metal the better is the shielding. Following this logic it wouldn't had been possible to establish a proper shielding for the phase meter as the high electron yield requires a highly effective vacuum apparatus which gets in conflict with semi-enclosed volumes inside the vacuum chamber. Luckily it turned out that the generally followed logic is not true in all cases and by proper design both an effective shielding and effective vacuum pumping can be established. If the magnetic lines penetrates into a certain volume they also have to exit the volume and they "don't like to exit" close to point where they entered. This means that even a relatively large opening on the mu-metal tube doesn't degrade the shielding, if a similar opening can not be found by the magnetic lines. While a single opening doesn't degrade the shielding, if it is between the gas source and the turbo pump it can make the vacuum pumping highly effective. Therefore a single mu-metal tube covering the space between the two MCPs with a large opening above the vertical slits of the differentially pumped stage is a suitable shielding for the single-shot phase meter (Figure 7.1). The requirement is that the length is several times larger than its diameter. This way neither of the tube end-openings will form a pair with the central opening for the field lines to pass in and out. With this arrangement both an effective pumping and magnetic shielding have been established. Although this solution is surprisingly simple we haven't found any other example in electron spectroscopic experiments where it has been used. In the contrary, in all the apparatuses we've found in publications the magnetically sensitive volume was almost perfectly covered by mu-metal shields, which severally hindered the vacuum efficiency of the systems and made the use of large vacuum pumps necessary. With our arrangement it became possible to place the turbomolecular pump directly above the gas source which radically increased the efficiency of the pumping and made the apparatus more compact. As no large pump below the device was necessary any longer the single-shot stereo-ATI phase meter could had been put onto the optical table.

Due to the radically improved signal yield by the above changes it become unnecessary to use highly expensive MCP detectors. Instead of the previously used MCPs (Burle BiPolar TOF Detector) almost an order of magnitude less expensive and less sensitive detectors could had been used (Del Mar Photonics MCP-MA34/2) while the recorded spectra due the large number of detected electrons exhibited only a low noise as it can be seen on Figure 7.2.

7.2.2 Digital data acquisition

While the number of electrons reaching the detectors in a single laser shot had been boosted thanks to the the above changes, the old data acquisition system based on electron counting couldn't handle the intense signals. Hence in order to detect the

large number of electrons arriving to the detectors simultaneously in a single laser shot, modification of the acquisition system was also necessary.

Electron counting in TOF spectroscopy works the following way: a start signal from the laser or from an external diode triggers the multiscaler card i. e. a sweep signal is started and the time starts to count. When an electron arrives to the MCP and is multiplied, the multiscaler detects it by recording the arrival time of the signal relative to the start signal. Multiscaler cards are most typically used in sequential mode when a preset number of sweeps are sequentially started (one for each laser shot) and the arrival times of the electrons are recorded and accumulated during the preset number of shots. While this technique due to its very low noise level is perfectly suitable for single-photon or ion counting experiments, where a low signal have to be detected at high repetition rates, it can not handle intense pulses as simultaneously arriving electrons are all counted as one event. Therefore for single shot detection of intense signals a different approach was necessary.

The new data acquisition system used a fully digital approach where instead of single electron counting the signal of the MCP detectors were amplified first and then digitized with a high sampling rate digital oscilloscope. The amplifiers were two high gain amplifiers with a bandwidth of 1.6 GHz and gain of 26 db (Becker&Hickl, HFAC-26). Due to the application of the high gain post-amplifiers the MCPs could had been operated on a lower voltage, which extended the lifetime of the detectors. In order to avoid noise pickup in signal cables the amplifiers were directly connected to the feedthroughs on the end-flanges of the drift tubes. (The MCPs were connected to the other side of the feedthroughs in the vacuum chamber.) The amplified signal then was recorded with a digital phosphor oscilloscope (Tektronix, TDS 7104) with 400 ps temporal resolution. As it is depicted in Figure 7.1 a fast diode triggered the oscilloscope, and additionally to the signal of the left and right MCPs, the signal of a slow-diode was also digitized for monitoring the pulse energy fluctuation. Although this was not used in the current study, in the future this will be exploited for invesigating the phase-energy coupling of the phase stabilization, which has recently become a hot topic in ultrafast laser technology [134–136]. The extended acquisition memory of the digital oscilloscope allowed for recording 4500 of consecutive laser shots. This can be done at repetition rates of 160 kHz, which is significantly higher than the repetition rate of intense few-cycle lasers. Therefore by digitizing the signal of the MCPs it become possible to record intense single shot signals at high repetition rates. In the future the digital oscilloscope will be substituted with a digitizer card that by simultaneously writing and reading two acquisition memory panels will allow to record unlimited number of consecutive laser shots at several hundreds of kHz repetition rates.

As several orders of more electrons bombarded the MCPs in the single shot experiment than previously, it become necessary to protect the detectors from the low energy direct electrons. Those are generated in two orders of magnitude higher numbers than the phase sensitive HATI electrons, which could had radically shorten the lifetime of the detectors. A blocking potential of -25 V allowed only electrons with a kinetic energy of larger than 25 eV to reach the detectors.

7.2.3 Imaging system

In order to reach single shot detection the phase meter had to operate on its absolute peak performance. This required not only a peak performance from the vacuum apparatus and the data acquisition system, but to fully exploit the potential of the phase meter the laser intensity in the interaction volume had to be carefully optimized. To this end an imaging system has been set up that helped to direct the beam into the tiny interaction volume without damaging the MCPs and to optimize the intensity.

The imaging system is depicted in Figure 7.1 showing the experimental setup. The beam exiting the phase meter has been split into two and the front surface reflection from the splitting wedge after refocusing with an achromatic lens has been directed into a CCD camera. The system was aligned so that the center of the interaction zone i. e. the plane of the vertical slits was imaged onto the CCD chip. For the alignment a diffuser was moved into the beam before it entered the apparatus, turning the laser to simple light source. The diffused beam illuminated the differentially pumped cube, and the lens and the camera have been adjusted until the contours of its side walls could had been clearly seen. Thus the camera was watching the interaction volume, the diffuser was moved out and the focused laser beam could had been positioned to centrally propagate between the two slits. Then with a z-scan by monitoring the beam size the intensity was optimized.

This simple imaging system was indispensable for the single-shot experiment. In previous multishot experiments without this system there was no feedback at all about the position and intensity of the laser beam, requiring hours of alignment for optimal performance. Changing from the gas nozzle to differential pumping with a tiny interaction volume where the walls of the cube are only a millimeter away from the laser focus it was necessary to prevent the beam from hitting the walls of the interaction cube. That could had showered the MCPs with electrons and damaged them. As ATI with few-cycle pulses is highly sensitive to the intensity this system proved useful also for monitoring of the laser intensity during the experiment (by knowing the pulse duration from autocorrelation/FROG measurements). Thus a complete alignment of the experimental setup was possible even before switching on the MCP detectors, which were highly vulnerable in the single shot experiment as everything was operating at maximum performance.

7.3 Experimental results

7.3.1 Single shot HATI spectra

With the completely redesigned phase meter the signal yield with more than four orders of magnitude was improved which made possible to record left and right HATI spectra in single laser shots. Moreover with the new data acquisition system the spectra could had been recorded consecutively without missing a single laser shot. Single-shot left and right spectra at the CEP of $\pi/2$, π, $3\pi/2$, 2π are indicated in Figure 7.2 with

red and blue lines respectively. One can readily see that there is a pronounced phase sensitivity while the noise in the spectra is relatively low. This potentially allows for a highly accurate CEP measurement with high repetition rate and thus for CEP tagging.

To retrieve the CEP from the spectra a parameter characterizing the asymmetry between the left and the right spectra was defined. This so called phase asymmetry parameter introduced in [137] was defined as follows: $(P_L - P_R)/(P_L + P_R)$ where P_L and P_R are the number of HATI electrons emitted in the left and the right directions respectively, which in Figure 7.2 would correspond to an integral over the red and blue spectra respectively, starting from ≈30 eV to infinity. The phase asymmetry parameter depends sinusoidally on the CEP as it has been shown numerically [137]. The limitation of a single phase asymmetry parameter is that its sinusoidal dependence vs. the CEP is not a monotone function, therefore two CEP values correspond to one phase asymmetry value. Thus at CEP tagging, where phase-stabilization is not available, and the phase varies randomly from shot to shot, one can not retrieve the CEP this way. Instead a one-to-one correspondence between phase asymmetry and CEP is required. In [133] for this reason multiple phase asymmetry parameters were defined, each for a certain energy window in the HATI spectra. As those mormalized phase asymmetry parameters themselves exhibit a close-to-sinusoidal dependence on the phase but with a certain phase shift with respect to each other, it became possible to establish a one-to-one correspondence between phase asymmetries and CEP, which allowed unambiguous determination of the CEP.

Although a one-to one correspondence has been established, measuring the CEP of non-phase-stabilized laser shots for CEP tagging was still not possible. In the conventional representation [137] the phase asymmetry or multiple phase asymmetries [133] were plotted versus the CEP. For CEP tagging experiments this is not suitable as the CEP of non-phase-stabilized laser pulses are unknown. To overcome this difficulty we used a novel representation that could handle non-phase-stabilized single laser shots: We used two phase asymmetry parameters 1 and 2 for electron energies between 37.9 eV and 57.5 eV and for 57.5 eV and 64.8 eV respectively. On the single shot spectra in Figure 7.2 the integration ranges are colored orange and green. These two phase asymmetry parameters both exhibit a close to sinusoidal dependence with a 60 degree phase shift with respect to each other. We plotted the two phase asymmetry parameters of the consecutively recorded 4500 non-phase-stabilized laser shots on a 2D parametric graph, and obtained an elliptical Lissajous curve. On this curve the polar angle in 360 degree range corresponds to the entire 2π phase range, however the correspondence between the polar angle and the CEP is not linear. In order to obtain the correspondence between them we exploited the fact that the CEP distribution of non-phase-stabilized laser pulses is completely random. Going around the elliptical curve 4500/12=375 shots corresponded to a $2\pi/12$ phase shift. With this first-principle calibration phase differences between laser shots can be immediately determined. A comparison with one-dimensional TDSE simulations gave the indicated CEP ticks around the loop.

A great advantage of the novel representation is that it also enabled the estimation

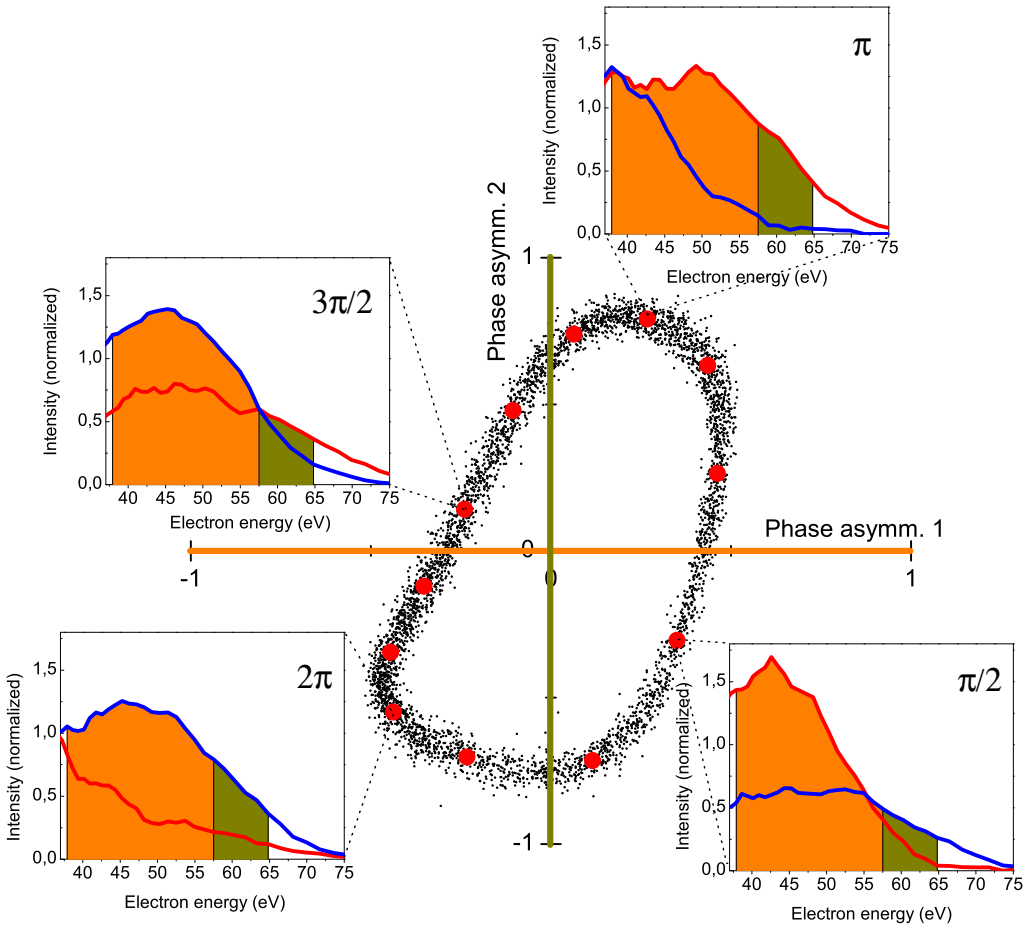

Figure 7.2: Single shot left and right HATI spectra and 4500 consecutive non-phase stabilized laser shots in Lissajous representation. The asymmetry between left (red) and right (blue) spectra shows a pronounced phase asymmetry. To quantify the asymmetry two normalized phase asymmetry parameters were calculated by $(P_L - P_R/P_L + P_R)$ where P_L and P_R are the integrated signal yield in the left and right directions respectively between 37.9 eV and 57.5 eV (shaded orange) for the first, and between 57.5 eV and 64.8 eV (shaded green) for the second parameter. 4500 concecutive non-phase stabilized laser shots on a 2 D parametric plot (phase asymm. 2 vs. phase asymm. 1) distribute around an elliptical curve. CEP values were obtained by "first principle calibration" and by comparison with 1 D TDSE simulations. Measurement precision have been estimated to $\pi/300$ at the CEP of $5\pi/9$.

of the measurement error. While previously in multi-shot CEP measurements with stabilized pulses the error of the measurement and the error of the phase stabilization couldn't had been decoupled, now using non-phase stabilized single shot results it became possible. In the Lissajous figure the CEP changes in tangential direction while the "width" of the elliptical figure origins from the measurement noise. To quantify the error an assumption has been made: the measurement noise in tangential and radial direction are the same. Since with the first-principle calibration the tangential shift around the curve was already converted to a phase shift with this assumption the radial change had been also quantified. It was found that the standard deviation of the measurement error at the best measurement point approaches $\pi/300$ at the CEP of $5\pi/9$.

7.3.2 CEP tagging

By measuring the CEP of non-phase stabilized few-cycle pulses consecutively with an ultra-high precision, it became possible to perform CEP tagging for the characterization of phase dependent processes. A proof-of-principle CEP tagging to demonstrate the power of this technique can be made by the HATI electron spectra those were recorded in the experiment, as it is described below:

On the Lissajous-plot in Figure 7.2 the CEP is increasing with the polar angle. CEP tagging can be performed by arranging the left and right HATI spectra in an ascending order by their polar angles and thus by their corresponding CEPs as it is shown in Figure 7.3 (c) and (d) respectively. This novel method for the characterization of the phase dependence have several advantages over a regular phase scan. In comparison left and right HATI spectra obtained with a phase scan in $\pi/10$ steps with the same pulse parameters (pulse duration, intensity) are shown in Figure 7.3 (a) and (b). (Naturally the right spectra shifted by $90\,^\circ$ CEP are identical with the left spectra. As the two MCPs were not perfectly matching pairs the right spectra are less intense than the left.) The differences between the two methods, phase scan and CEP tagging can be summarized as follows:

- One can readily see that there is a much smoother transition between the spectra in the CEP tagging figures thanks to the high number of recorded shots (4500) and the ultra-high measurement precision. This allows for a much more precise characterization of the investigated phenomenon. CEP tagging can be performed with a precision of $\pi/300$, while attainable accuracy with a phase scan is limited by the phase fluctuation of the stabilized laser, that is at least 278 mrad for a state of the art laser.

- Experimentally the CEP tagging with 4500 laser shots was conducted in 1.5 seconds (laser repetition rate 3 kHz) while the CEP scan with 20 phase steps needed several tens of minutes. This huge difference is due to the fact that CEP tagging with non-phase stabilized pulses (those CEP change from shot-to-shot in a random manner) can be considered as an "ultrafast phase scan". The several

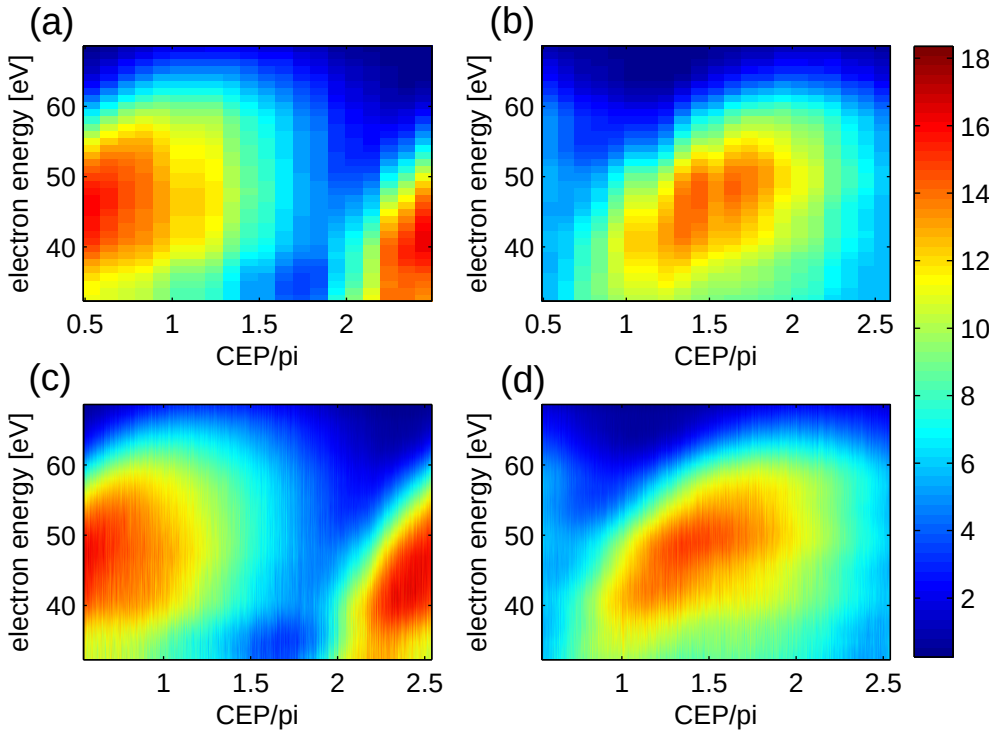

Figure 7.3: CEP tagging vs. phase scan. Left (a) and right (b) multi shot HATI spectra obtained by phase scan in Pi/10 steps and left (c) and right (d) single shot HATI spectra obtained by CEP tagging. CEP tagging enables a far more precise characterization of HATI spectra within orders of magnitude shorter acquisition time: 1.5 s vs. several tens of minutes. Similarly to HATI spectra any phase dependent phenomenon can be characterized with CEP tagging.

orders of magnitude higher acquisition speed dramatically improves feasibility of the experiment. Moreover measurement precision is further increased as during several tens of minutes considerable fluctuation of laser parameters such as intensity, pulse duration and beam pointing occurs.

Phase scan requires phase stabilization which is technically elaborate, heavily affected by well-known inherent fluctuations and to date is not available for larger systems. Therefore studying phase dependent processes at relativistic intensities with state of the art multi-TW few-cycle lasers [9, 10] is only possible by the here introduced CEP tagging method. Furthermore it is possible to run phase dependent experiments also on smaller systems parallel to the single-shot stereo-ATI phase meter as it requires only 40μJ of pulse energy, which is 10% of the laser energy of a typical multi-kHz few-cycle system [138]. Phase stabilization is still important for the majority of experiments where laser shots should be generated with a desired CEP, but for experiments where the entire 2π phase range have to be studied our novel method CEP tagging performs

superior to phase scans.

7.4 Summary

In this chapter we've presented the development of a single-shot stereo-ATI phase meter. Our study was motivated by enabling waveform dependent experiments in the future with recently developed few-cycle multi-TW OPCPA laser systems. Although these lasers hold promise for extending attosecond science to relativistic intensities, as they are not phase stabilized a new measurement method by tagging the CEP of each laser shot is required.

To achieve single-shot performance from the phase meter a four orders of magnitude increase in the signal yield compared to the old multi-shot apparatus was necessary. This has been accomplished by: redesigning the magnetic shielding and the vacuum system to increase the number of electrons arriving to the detectors; developing a data acquisition system to be able to detect a large number of simultaneously arriving electrons in a single laser shot at high repetition rates; installing an imaging system that allows for a precise alignment of the laser beam in the interaction volume and the optimization of the intensity. The single-shot phase meter requires merely 40μJ of pulse energy, which is 10% of the laser energy of a typical multi-kHz few-cycle system [138], therefore it can be used as an online diagnostics at any intense few-cycle lasers.

Single shot HATI spectra at the laser's repetition rate (3kHz) have been recorded consecutively. The spectra exhibit only low measurement noise which has been evaluated using a Lissajous representation. Enabled by the single-shot measurement I demonstrated that CEP tagging can operate as as "ultrafast phase scan" and thus it can be superior to ordinary phase scans performed with a stabilized laser.

Chapter 8

Summary

Preliminaries

With the invention of chirped pulse amplification the generation and amplification of ultrashort laser pulses to petawatt peak powers became possible. Such high-power pulses provide a unique means to investigate matter at extreme conditions. By focusing them into a tiny small spot, peak intensities of 10^{22} W/cm^2 [1] can be generated that can instantaneously transform the surface of any solid target into a hot overdense plasma. At these extreme intensities and target temperatures relativistic interactions come to the fore opening the door to the exploration of a wide range of new phenomena. Experiments theoretically predicted for a long, like high-order harmonics generation from oscillating plasma surfaces, or proton acceleration from thin foil films are now routinely performed in many laboratories. The prerequisite to conduct laser-plasma experiments this kind is to ensure a clean interaction between the exposed solid target and the laser pulse. This means that prior to the arrival of the main laser pulse, radiation with a considerable intensity mustn't expose the target as it can alter the interaction. Unfortunately for technical reasons in the amplification process pedestals and leading prepulses are unavoidably generated. Their focused intensity is only a few orders of magnitude lower than that of the main pulse and thus it is well beyond the damage threshold of any target material. As a result prepulses and pedestal that overtake the main pulse generate a low density preplasma, which expands on the target surface and in place of the steep density gradient solid target the main pulse interacts with the low density preplasma. This unwanted phenomenon has existed since the invention of CPA lasers and has remained the main impediment to study laser-solid interaction at relativistic intensities.

Intensity contrast is the quantity that is used to characterize the temporal cleanness of laser pulses. It is the ratio of the intensity of the main pulse to that of the pedestal. Continuous efforts have been taken to improve the intensity contrast of high-power lasers by several optical methods and by incorporating all effective techniques into a laser system the contrast nowadays approaches 10^8 at best [2]. This is several orders below the desired contrast ratios, as prepulses and the pedestal with an intensity above 10^7 W/cm^2 easily alter the interaction and lasers with focused intensities

beyond 10^{20} W/cm^2 are now commonplace in many laser laboratories. Moreover with continuous developments available peak intensities are steadily increasing, while available laser contrast have been at the same level for more than a decade now. This shows that improving the laser contrast is one of the foremost challenges in high-intensity laser physics.

Plasma mirror (PM) which is an ultrafast self-induced optical shutter was proposed as a contrast improvement technique already in the early nineties. Its operation is based on the ultrafast ionization occurring at high intensities: a laser pulse is focused onto a transparent bulk target, and while the low intensity prepulses and pedestal mainly traverses the target and gets reflected only with the low Fresnel reflectivity, the rising edge of the main pulse with its high intensity generates a highly reflective flat plasma layer. The main pulse cleaned from the pedestal and prepulses is specularly reflected off the plasma layer thus the contrast of the reflected beam is significantly enhanced.

Although PM has been proposed for long as contrast improvement technique, so far only proof-of principle studies have been conducted but no thorough characterization or practical implementation of this technique have been reported yet. My motivation in my Phd studies was: to demonstrate that PM can effectively improve the contrast of high-power lasers, to perform a complete experimental characterization of the PM, and to improve the temporal contrast of the 100 TW laser with the implementation of a double plasma mirror (DPM) setup and completely characterize its operation.

While the first part of my thesis focuses on the improvement of the temporal contrast of sub-picosecond high-power laser pulses – as it has been briefly presented above – the second part of my thesis deals with a fairly different topic, with the development of a single-shot carrier-envelope phase meter.

Thanks to the vast progress in ultrafast laser technology generation of amplified laser pulses comprising merely a few oscillation cycles of the electromagnetic field became possible to the turn of the millennium. The important feature of few-cycle pulses in contrast to multi-cycle ones is that the temporal evolution of the electromagnetic waveform within the laser pulse is accessible. As virtually all strong field phenomena are directly governed by the electromagnetic field, this feature attracted a great scientific interest in recent years.

The quantity that is used to characterize the evolution of the field within the laser pulse is called the carrier-envelope phase (CEP), which is defined as the offset phase between the peak of the electric field and the peak of the pulse envelope. Stabilization of the CEP of high repetition rate few-cycle sources became possible a few years ago using f-to-2f interferometers [5], which had an enormous impact on time resolved laser spectroscopy by enabling pump-probe experiments with attosecond resolution [6, 7]. The major limitation of phase stabilization is that it is technically rather complex and it has been demonstrated only up to 0.2 TW peak powers [8], while few-cycle lasers with multi-10-TW peak powers are already available [9,10]. These unique laser systems hold promise for extending attosecond metrology and spectroscopy to attosecond control

by the generation of energetic isolated attosecond bursts on solid surfaces [11]. Such attosecond pulses would allow for pump-probe experiments with one attosecond pulse releasing the electron and the other controlling its further evolution. However sufficient parameters of the laser pulse's envelope (pulse duration and focused intensity) are already available, due to the lack of phase stabilization conducting waveform dependent experiments at relativistic intensities is still not possible. Therefore the development of a single-shot measurement apparatus that can record the CEP of few-cycle pulses consecutively, and thus would allow for a new measurement method "CEP tagging" with non-phase stabilized lasers, has become a premier challenge in ultrafast optics.

Goals

1. My *first goal* is to perform a complete experimental characterization of a single PM. So far in proof of principle experiments only the time and space integrated (overall) reflectivity was measured which depends on the spatial parameters of the applied laser, therefore such measurements can not be used as an absolute reference. My primary goal was to perform a complete space and time resolved experimental study that can provide the necessary parameters for designing an effective PM system for the 100 TW laser at Laboratoire d'Optique Appliquée.
The experimental characterization aimed for measuring: time and space resolved, time integrated and space resolved (peak) and time and space integrated (overall) reflectivity at various pulse durations. My goal was to measure the plasma triggering threshold at various pulse durations and demonstrate that by applying the optimal fluence on the PM, it can effectively enhance the intensity contrast of high-power laser pulses, while focusability and spatial characteristics of the reflected beam are also improved.

2. My *second goal* is to set up and fully characterize a double plasma mirror system for the 100 TW laser Salle jaune laser at Laboratoire d'Optique Appliquée. My goal was to optimize the fluence on both PMs to exploit the most from the system in order to improve the initial contrast of the laser with several orders of magnitude. My goal was to perform a complete experimental and numerical characterization of the system. In particular I wanted to demonstrate that placing the first plasma mirror into the near field – which is a critical part of the design but unavoidable due to the high pulse energy (2.5 J) – doesn't impair but slightly improves the focusability and more than 40-50% of the laser's initial peak intensity is preserved.

3. My *third goal* is to develop a single-shot carrier-envelope phase meter. F-to-2f interferometers which are commonly used to stabilize the phase of few-cycle lasers can only detect the rate of change of the CEP, but they are blind to its actual value. Measurement of the CEP therefore requires a completely different approach. In recent years several non-optical methods exploiting various phase sensitive phenomena have been demonstrated to retrieve the CEP, but all of them work only on a proof-of-principle level and require several thousands of laser shots for a single measurement

point. Therefore they are applicable only on high repetition rate few-cycle sources with relatively low pulse energies – which are commonplace in many laboratories – as currently only those can be phase stabilized. My goal is to develop the first single-shot measurement apparatus that can record the phase of consecutive non-phase stabilized laser shots, and therefore can be used also on high-power few-cycle lasers, which are non-phase stabilized.

Methods of investigation

1. Complete experimental characterization of a single PM was performed in Saclay Laser Interaction Center (SLIC) with the LUCA laser. This required a very complex experimental setup. I've participated in designing and setting up the experiment, participated in the measurements and I performed the data analysis. Laser pulses with 60 fs of pulse duration, 800 nm central wavelength and 100 mJ of pulse energy were focused onto the surface of transparent bulk quartz and anti-reflection (AR) coated quartz targets. To measure the reflectivity of the PM in function of the laser fluence it was varied in a wide range (between 1-100 J/cm^2). Space and time-integrated (overall) reflectivity was measured with energy meters and space resolved time-integrated (peak) reflectivities were obtained by imaging the PM surface on a high-dynamic CCD camera. Time and space resolved reflectivities were measured by chirping the incident pulses to 1.1 ps. The spectrum of the reflected pulse provided the onset of plasma formation at different incident fluences. Distortion of the beam spatial profile in the far-field and the near-field was measured by imaging the beam in the plane of the PM surface (focal plane), and some distance after the PM.

2. I've participated in the design and construction of the double PM setup, and I completely characterized it. The laser delivers 25 fs pulses with energies up to 2.5 J at 780 nm wavelength with up to 10 Hz repetition rate. Due to the high pulse energy, long focusing mirror had to be used to provide the ideal fluence for the PMs. An f=10 m null telescope created an intermediate focus for the laser beam and recollimated it; near this the PMs were situated both with 45 ° angle of incidence. The first PM was in the near field 14 cm from the focus and the second PM was in the focus. Due to the improved contrast after the first PM the fluence could had been higher on the second PM. The beam was S polarized and the targets were AR coated quartz. I optimized the fluence by changing the radius of curvature of the deformable mirror. I monitored the beam profiles on the PMs and in the final target plane with webcameras and with a high-dynamic CCD camera respectively. I used an optical beam tracing code to model the DPM setup. I also participated in a short proof-of-principle experiment performed for comparing high-order harmonic generation with and without the DPM system. We observed the generated harmonics with an XUV spectrograph.

3. I've conducted the experiment at Max Planck Institute of Quantum Optics using a few-cycle laser system that delivers sub-4 fs pulses with 800 nm central wavelength

at 3 kHz repetition rate. The single-shot stereo-ATI phase meter uses the left/right asymmetry in the yield of high-energy above-threshold-ionization (HATI) electrons along the polarization axis to retrieve the CEP. In order to record the left and right HATI spectra in a single laser a four orders of magnitude increase in the sensitivity was necessary compared to the previous multi-shot apparatus. For that I have made the following major changes in the new design: I redesigned the magnetic shielding and the vacuum apparatus to increase the number of electrons arriving to the detectors; I changed the data acquisition system from electron counting to digital voltage detection to be able to detect a large number of simultaneously arriving electrons in a single laser shot at high repetition rates; I installed an imaging system that allows for a precise alignment of the laser beam in the interaction volume and optimization of the laser intensity.

Results

1. I provided a complete experimental characterization of a single plasma mirror. I measured the peak and overall and the space and time resolved reflectivity of the PM in function of the incident laser fluence. I measured 74% and ≈60% of peak reflectivity on quartz and AR coated quartz targets respectively at 60 J/cm^2 incident laser fluence [139]. Since the contrast improvement factor is the ratio of the reflectivitiy after and before (0.3% for AR) plasma formation, this provides a contrast improvement factor of nearly 200. Improving the contrast of few-TW laser systems with more than two orders of magnitude considerably improves the conditions of several experiments, especially that of high-harmonic generation on solid surface.
With time resolved measurements I showed that the onset of plasma formation and reflectivity increase happens earlier with increasing fluence, and even at the highest applied fluence it is the rising edge of the main pulse that triggers the PM and not the prepulses or the pedestal. I also demonstrated that the PM acts as a spatial filter and improves the spatial profile of the reflected beam. I measured the plasma triggering threshold and found that it is slightly increasing with increasing pulse duration.

2. I provided a complete experimental and numerical characterization of the double plasma mirror system [140]. I optimized the fluence on both PMs and achieved a 47%-57% of peak and 31% of overall reflectivity for the system. I improved the initial contrast of the 100 TW laser by a factor of $5 \cdot 10^4$ to a record high $5 \cdot 10^{11}$.
I've used an optical propagation code to model the optical transport of the beam and found a good agreement between modelled and measured results including beam profiles on both PMs and focus in the final target plane. Extensively studying the fluence distribution on the first PM, which is in the intermediate field, I found that the beam profile as it was expected is somewhat rough. Although this unavoidably leads to some distortion of the reflected beam profile, this slight degradation is overly compensated by the second PM, which was positioned into the intermediate focus, thus it acts as a spatial filter. Due to this, I observed no degradation of beam quality

or focusability in the final target plane, but on the contrary, a slight improvement in the spatial characteristics. As high-power lasers are built to maximize peak intensity on target surface, retaining or rather improving the focusability of the beam is the key feature of the DPM system.
The DPM was engineered as a standard system feature and is easily added or bypassed with a single kinemtic stage in the 100 TW Ti:sapphire research laser. The AR targets can be shifted from shot to shot to provide a fresh undamaged surface for each laser shot.
I've compared high-order harmonic generation with and without the DPM system [141, 142]. Temporally cleaning the pulses with the DPM system a narrow beam of harmonics was generated and the laser light was reflected specularly. Without the DPM no harmonics were observed and the reflected beam was diffuse and inhomogeneous. With this I demonstrated that high contrast pulses produced by the DPM system preserves the steep electronic density gradient, which is compulsory for conducting clean laser-solid interactions.

3. I've developed a single-shot stereo-ATI phase meter, which can measure the CEP of few-cycle laser pulses consecutively [143, 144]. This I've achieved by increasing the sensitivity with more than four orders of magnitude compared to the previous multishot apparatus. With the single-shot phase meter I recorded the CEP of non-phase stabilized laser pulses consecutively for the first time, which demonstrates that the phase meter unlike previous mutishot methods doesn't require phase stabilization. This enables a new measurement method CEP-tagging for studying waveform dependent phenomena with any few-cycle laser system, independently whether the particular laser can be phase stabilized or not. This is particularly important as state-of-the-art multi-10TW few-cycle lasers are not phase stabilized [145]. Therefore this new method will potentially open the door for studying the waveform dependence of laser-solid interactions at relativistic intensities.
With the apparatus I recorded the CEP of each shot of a high-repetition rate (3kHz) laser using 40μJ of pulse energy for the measurement. As it is merely 10% of the pulse energy of a typical multi-kHz few-cycle laser, CEP tagging can be performed also on those sytems. Running the laser non-phase stabilized due to the random fluctuation of the phase, CEP tagging will work as an "ultrafast phase scan" resulting in an acquisition speed that is orders of magnitude higher than that of regular phase scans. This means that for experiments where the entire 2π phase range have to be studied this novel method is far superior to technically elaborate phase scans.
These results were published in [143] and highlighted in press releases at MPQ [146] and at the TU München [147], and also reported in Laser Focused World [148] and by several popular science websites [149]. The CEP measurement method will be incorporated also into Prof. Rick Trebino's well-known lecture notes on Ultrafast Optics [150].

9. fejezet

Összefoglalás

Tudományos előzmények

A csörpölt impulzuserősítés (CPA) felfedezésével lehetővé vált ultrarövid lézerimpulzusok akár petawattos csúcsteljesítményig való erősítése. Ezen extrém nagy teljesítményű lézerimpulzusok új távlatokat nyitottak meg a lézer-anyag kölcsönhatás kutatásában. Az impulzusokat egy céltárgy felületére fókuszálva akár 10^{22} W/cm^2 csúcsintenzitás is elérhetővé vált, ami bármilyen szilárd anyag felületét szinte pillanatszerűen nagy hőmérsékletű és sűrűségű plazmává változtatja. Ilyen extrém intenzitások és céltárgy hőmérsékletek mellett a kölcsönhatás során relativisztikus effektusok lépnek fel és ezáltal számos új jelenség kísérleti tanulmányozása válik lehetővé. A rendkívül magas csúcsintenzitásnak köszönhetően olyan, numerikus szimulációkkal már jó ideje megjósolt kísérleteket mint pl. magasrendű harmonikus keltést oszcilláló plazmafelület-rétegen, vagy proton gyorsítást vékony fóliákról ma már szinte rutinszerűen hajtanak végre számos lézer-laboratóriumban. Az ilyen típusú lézer-anyag kölcsönhatás kísérletek végrehajtásának egyik legfontosabb előfeltétele, hogy a szilárd céltárgy és a lézerimpulzus közötti kölcsönhatás zavartalan legyen. Ez azt jelenti, hogy a lézerimpulzus megérkezése előtt semmilyen nagy intenzitású sugárzás nem érheti a céltárgyat, hiszen az jelentősen befolyásolhatja a kölcsönhatást. Sajnos különböző technikai okokból az erősítési folyamat során egy hosszú ún. piedesztál-impulzus és különálló előimpulzusok keletkeznek. Ezeknek a fókuszált intenzitása általában csupán néhány nagyságrenddel kisebb a főimpulzusénál, ami már bármilyen céltárgy esetén jóval meghaladja az optikai sérülési küszöbértéket. Ennek következtében az előimpulzusok és a piedesztál-impulzus alacsony sűrűségű előplazmát hoznak létre, ami a céltárgy felületén kitágul és így a főimpulzus a meredek gradiensű szilárd céltárgy helyett az alacsony sűrűségű előplazmával találkozik. Ez a nem kívánatos jelenség gyakorlatilag egyidős a nagy teljesítményű CPA rendszerekkel és mind a mai napig a legfőbb akadálya lézer-szilárd anyag közötti kölcsönhatás relativisztikus intenzitáson való tanulmányozásának.

Az impulzusok időbeli tisztaságának karakterizálására szolgáló mennyiség az intenzitás kontraszt, ami a főimpulzus és az piedesztál intenzitásainak arányát adja meg. Az elmúlt több mint két évtizedben számos sikeres és sikertelen próbálkozás történt az intenzitás kontraszt javítására különböző optikai módszerekkel. Ezek közül a hatásosnak

bizonyulókat a lézerbe implementálva a kontraszt ma már a 10^8-os értéket is elérheti. Még azonban ez is több nagyságrenddel alacsonyabb a kívánatos értéknél, mivel az előimpulzusok és a piedesztál-impulzus 10^7 W/cm^2-es intenzitás felett már alapvetően befolyásolhatja a kölcsönhatást, ugyanakkor nagy teljesítményű lézerek 10^{20} W/cm^2-os fókuszált intenzitással ma már több laboratóriumban is megtalálhatóak. Ráadásul a folyamatos fejlesztéseknek köszönhetően az elérhető csúcs-intenzitás folyamatosan növekszik, míg az elérhető legnagyobb kontraszt gyakorlatilag egy évtizede változatlan. Ez mutatja, hogy a lézer kontrasztjának javítása jelenleg a nagy intenzitású lézerfizika egyik legnagyobb kihívása.

A plazma tükör (angol rövidítés után: PM), ami nem más mint egy ultragyors optikai zár, amit maga a lézerimpulzus hoz létre, már a kilencvenes évek elején felmerült potenciális kontraszt javító módszerként. Működése a nagy intenzitásokon lejátszódó ultragyors ionizáción alapul: a lézerimpulzust egy átlátszó céltárgyra fókuszálva, amíg az alacsony intenzitású piedesztál-impulzus és különálló előimpulzusok áthaladnak a céltárgyon, illetve csak az alacsony Fresnel-reflexióval verődnek vissza, addig a főimpulzus eleje a nagy intenzitásával egy nagy reflexiójú sima plazma réteget hoz létre a céltárgy felületén. A főimpulzus megtisztítva a piedesztál-impulzustól és előimpulzusoktól tükörszerűen reflektálódik a plazma rétegen, s ezáltal a visszavert nyaláb kontrasztja jelentősen javul.

Habár a PM-et már jó ideje javasolták a kontraszt javítására eddig jóformán csak a működési elvet demonstráló kísérleteket történtek, de sem a PM kiterjedő karakterizálása sem gyakorlati alkalmazása még nem történt meg. A tézisem első részében a fő célkitűzéseim éppen ezek voltak, vagyis: annak demonstrálása, hogy a PM hathatósan meg tudja növelni egy nagy teljesítményű lézer kontrasztját, a PM teljes kísérleti karakterizálása, valamint egy 100 TW-os lézer kontrasztjának javítása egy dupla plazma tükör (angol rövidítés után: DPM) implementálásával és annak teljes karakterizálása.

Ahogy az a fenti bevezetőből kiderült, a tézisem első része a szub-pikoszekundumos lézerimpulzusok intenzitás kontrasztjának javításával foglalkozik. A tézisem második részében egy ettől némileg eltérő területtel foglalkozom, egy egylövéses hordozó-burkoló fázis detektor kifejlesztését mutatom be.

Az ultragyors lézertechnológia rendkívül nagy fejlődésének köszönhetően az ezredfordulóra lehetővé vált olyan erősített lézerimpulzusok létrehozása, amelyek időben annyira rövidek, hogy bennük az elektromágneses hullám már csak néhány oszcillációt végez. Ezek az ún. néhány ciklusos impulzusok egyik legfontosabb tulajdonsága a több ciklusosokhoz képest, hogy az elektromágneses hullám időbeli lefutása a lézerimpulzusban hozzáférhető. Mivel jóformán minden nagy intenzitású lézer-anyag kölcsönhatást közvetlenül az elektromágneses mező irányít, ezért a néhány ciklusos impulzusok ezen tulajdonságuknak köszönhetően az utóbbi időben a tudományos érdeklődés középpontjába kerültek.

Az elektromágneses tér lézerimpulzuson belüli időbeli lefutását az ún. hordozó-burkoló fázis (angol rövidítés után: CEP) adja meg, amit az elektromos tér csúcsa és a burkológörbe csúcsa közötti ofszet fázisként definiálnak. Nagy ismétlési frekven-

ciájú néhány ciklusos lézereknél ezt a paramétert pár éve sikerült stabilizálni f-to-2f interferométer segítségével, ami rendkívül nagy hatással volt az időfelbontású lézersektroszkópiára azáltal, hogy lehetővé tette attoszekundumos felbontású pumpa-próba kísérletek kivitelezését. Azonban a fázisstabilizálás jelentős fogyatékossága, hogy technikailag rendkívül összetett, és eddig csupán 0.2 TW-nál kisebb teljesítményű lézereken sikerült alkalmazni, holott ma már több 10 TW-os csúcsintenzitású néhány ciklusos lézerek is léteznek. Ezekkel a maga nemükben egyedülálló lézerrendszerekkel várhatóan nagy energiájú izolált attoszekundumos impulzusokat lehet majd szilárd céltárgyon való harmonikuskeltéssel létrehozni, ilyen impulzusok pedig várhatóan majd megnyitják az utat az attoszekundumos metrológia és spektroszkópia kísérletek attoszekundumos kontrollá való továbbfejlesztése felé. Nagy energiájú attoszekundumos impulzusokkal ugyanis olyan pumpa-próba kísérleteket lehet majd végezni, amikben az egyik attoszekundumos impulzus ionizálja az elektront míg a másik kontrollálja a további pályáját. Habár az ehhez szükséges lézerimpulzusok a burkológörbe különböző paramétereiket tekintve (úgymint impulzushossz és fókuszált csúcsintenzitás) már léteznek, fázisstabilizálás hiányában elektromágneses hullámformától függő kísérletek relativisztikus intenzitásokon továbbra sem végezhetőek. Ezért egy olyan egylövéses mérőműszer kifejlesztése, amelyik egymást követő lézerimpulzusok hordozó-burkoló fázisát tudja detektálni, és ezáltal a „fázis-címkézését" mint új mérési módszert teszi lehetővé fázisstabilizálatlan lézerekkel, az ultragyors optika egyik legnagyobb kihívásává vált.

Célkitűzések

1. Az *első célkitűzésem* a PM teljes kísérleti karakterizálása. Korábban a PM működését alapszinten demonstráló kísérletekben csak az időben és térben integrált reflexiót mérték, ami az adott lézernyaláb profiljától is függ, ezért ezek a mérések nem szolgálhattak referenciaként plazmatükrök felállításánál. Az elsődleges célom a PM teljes tér és időfelbontású karakterizálása kísérletileg, s ezáltal a szükséges paraméterek megmérése a Laboratoire d'Optique Appliquée-ben (LOA) található 100 TW-os lézeren egy PM-rendszer felállításához.

A karakterizálás célja: időben és térben felbontott, időben integrált térben felbontott (csúcs) és térben és időben integrált (átlagolt) reflexió mérése különböző impulzushosszakon. Továbbá célom volt a plazma triggerelési küszöbérték megmérése szintén különböző impulzushosszakon és demonstrálni, hogy plazma tükrön az optimális energiasűrűséget alkalmazva a nagy-teljesítményű lézerek kontrasztja jelentősen javítható, úgy hogy emellett a visszavert nyaláb fókuszálhatósága és térbeli profilja is javul.

2. A *második célkitűzésem* az LOA 100 TW-os lézeréhez egy dupla plazma tükör felállítása és annak teljes karakterizálása. A célom hogy az energiasűrűséget mindkét PM-en optimalizálva a lézer intenzitás kontrasztját több nagyságrenddel megnöveljem. Továbbá célom volt a rendszer teljes kísérleti és numerikus karakterizálása. Legfontosabb célom annak demonstrálása volt, hogy az első PM-et a közeli mezőbe helyezve – ami

a tervezés szempontjából kritikus, de elkerülhetetlen lépés volt a nagy impulzusenergiák miatt (2.5 J) – nem rontja sőt kis mértékben javítja a nyaláb fókuszálhatóságát, s emellett az impulzus csúcsintenzitásának több mint 40-50%-a megmarad visszaverődés után.

3. A *harmadik célkitűzésem* egy egylövéses hordozó-burkoló fázis detektor kifejlesztése. Az f-to-2f interferométerek amelyeket rendszeresen alkalmaznak a néhány ciklusos lézerek fázisának stabilizálására, csupán a fázis változásának mértékét tudják detektálni, de a fázis valós értékét nem. A fázis mérése tehát az interferométerekétől teljesen eltérő megközelítést igényel. Az elmúlt években jó néhány, különböző fázis szenzitív jelenségeken alapuló nem optikai módszert mutattak be, amelyek képesek ugyan a mérésekből kinyerni a fázis mértékét, de ezek a módszerek meglehetősen kezdetlegesek, és egyetlen mérési ponthoz több ezer egymás utáni lövésre van szükségük. Következésképpen ezeket a módszereket csak a jelenleg széles körben használt kis impulzusenergiájú, nagy ismétlési frekvenciájú néhány ciklusos lézereken lehet alkalmazni, mivel jelenleg csak azok fázisstabilizálhatóak. Ezért célul tűztem ki az első egy lövéses hordozóburkoló fázis detektor kifejlesztését, amely egymás utáni nem-fázisstabilizált lövések fázisának mérésére is képes lesz, s így alkalmazható lesz nagy energiájú néhány ciklusos lézereken is, amelyek nem fázisstabilizáltak.

Vizsgálati módszerek

1. A PM teljes kísérleti karakterizálása a Saclay Laser Interaction Center (SLIC)-ben történt a LUCA lézerrel. A teljes karakterizáláshoz egy rendkívül komplex kísérleti elrendezésre volt szükség. Részt vettem a kísérlet tervezésében és felállításában valamint a mérésekben és én végeztem a kísérleti adatok kiértékelését. Lézerimpulzusokat (impulzushossz 60 fs, központi hullámhossz 800 nm, impulzusenergiája 100 mJ) fókuszáltunk átlátszó kvarc valamint anti-reflexiós (AR) réteggel bevont kvarc lemezekre. A plazma tükör reflexiójának méréséhez az energiasűrűséget széles tartományban változtattuk (1-100 J/cm^2 között). Térben és időben integrált (átlagolt) reflexiót energiamérővel mértünk, az időben integrált térben felbontott (csúcs) reflexiójának méréséhez a PM felszínét egy nagy dinamikájú CCD kamerára képeztük le. Időben és térben felbontott reflexió méréséhez csörpöltük az impulzusokat, amelyek így 1.1 ps hosszúak lettek. A visszavert nyaláb spektrumából a plazma keletkezésének kezdetére lehetett következtetni különböző lézer energiasűrűségértékeknél. A nyalábprofil torzulása a visszavert nyaláb leképezésével történt: a távoli mező vizsgálatához a PM felszíne, a közeli mezőhöz egy attól távolabbi sík került leképezésre.

2. Részt vettem a dupla plazma tükör rendszer tervezésében valamint átfogóan karakterizáltam a rendszert. A lézer 780 nm központi hullámhosszon 25 fs hosszú 2.5 J energiájú impulzusokat bocsátott ki 10 Hz-es ismétlési frekvenciával. A nagy impulzusenergia miatt a plazma tükrökön az optimális energiasűrűség biztosításához nagyon

hosszú fókuszáló tükröt használtunk. Egy f=10 m hosszú null-teleszkóp hozta létre a köztes fókuszt majd kollimálta újra a nyalábot. A köztes fókusz körül helyezkedett el a két PM, mindkettő 45°-os beesési szöggel. Az első PM a közeli mezőben volt a fókusztól 14 cm-re, a második pedig a fókuszban. Az első PM után már nagyobb volt a kontraszt így a másodikon magasabb lehetett az energiasűrűség. A nyaláb S polarizált volt, a céltárgy AR réteggel bevont kvarc. Az energiasűrűséget a deformálható tükör görbülti sugarának változtatásával optimalizáltam. A nyaláb profilokat a PM-eken egyszerű webkamerákkal a végső fókuszban pedig nagy dinamikájú CCD kamerákkal figyeltem meg. Egy optikai sugár követő szoftvert használtam a DPM modellezésére. Emellett részt vettem egy rövid kísérletben amiben magasrendű harmonikus keltését hasonlítottuk össze a DMP rendszerrel valamint nélküle. A harmonikusokat egy XUV spektrográf detektálta.

3. A kísérleteket a Max-Planck-Instituts für Quantenoptik-ban végeztem egy néhány ciklusos lézert használva, amely szub-4 fs-os impulzusokat bocsált ki 800 nm-es központi hullámhosszal és 3 kHz-es ismétlési frekvenciával. Az egylövéses fázisdetektor a nagy energiájú küszöb feletti ionizációs elektronok polarizációs tengely menti ionizációjánál fellépő bal/jobb aszimmetriát használja fel a fázis mérésére. Ahhoz, hogy a bal és jobb oldali elektron spektrumokat egyetlen lövésből detektálni lehessen, a korábbi multishot fázisméterhez képest több mint négy nagyságrendes érzékenység növelésre volt szükség. Ezért az egylövéses detektor tervezésekor a következő alapvető változtatásokat végeztem el: a mágneses árnyékolást és a teljes vákuumkamrát újraterveztem, hogy ezáltal növeljem a detektorokba érkező elektronok számát; megváltoztattam az adatrögzítési technikát az elektronok számlálása helyett az MCP-k erősített feszültségének digitalizálására, és ezáltal lehetővé tettem egy lézerimpulzus által kiváltott nagy számú közel egyidejűleg érkező elektron detektálását, akár egymás utáni nagy ismétlési frekvenciával kibocsáltott lézerimpulzusoknál is; egy leképező rendszert állítottam fel ami lehetővé teszi a lézernyalábnak a kölcsönhatási zónában való pontos pozícionálását és intenzitásának optimalizálását.

Új tudományos eredmények

1. Plazma tükör teljes kísérleti karakterizálását végeztem el. Megmértem a csúcs, az átlagolt, valamint az időben és térben felbontott reflexiót a beeső nyaláb energiasűrűségének függvényében.
60 J/cm^2-es beeső lézerintenzitásnál kvarc esetén 74%-os, AR bevonatú kvarc esetén ≈60%-os csúcsreflexiót mértem. Mivel a kontraszt javulás egyenlő a plazma keletkezése utáni és előtti (0.3% AR céltárgynál) reflexiók hányadosával, ez közel 200-szoros kontraszt javulást jelent [139]. TW-os csúcsteljesítményű lézerek kontrasztjának több mint két nagyságrenddel történő növelése számos kísérlet körülményeit jelentősen javítja, különösen szilárd anyagon történő magasrendű harmonikus keltését.
Időfelbontású mérésekkel megmutattam, hogy a plazmakeltés vmint a reflexió emelke-

dése a beeső lézernyaláb energiasűrűségének növelésével egyre korábban történik meg, és még a legmagasabb alkalmazott energiasűrűségnél is az impulzus eleje triggereli a PM-et és nem az előimpulzus vagy a piedesztál-impulzus. Megmutattam, hogy a PM térbeli szűrőként működik s így a visszavert nyaláb profilját javítja. Megmértem a plazma triggerelési küszöb-energiasűrűséget, és azt találtam, hogy a lézer impulzushosszával kis mértékben emelkedik.

2. Egy dupla plazma tükör rendszer átfogó kísérleti és numerikus karakterizálását végeztem el [140]. A beeső lézernyaláb energiasűrűségét mindkét PM-en optimalizálva 47%-57%-os csúcs és 31%-os átlag reflexiót mértem. A 100 TW-os lézer kontrasztját $5 \cdot 10^4$-el megnövelve rekord nagyságú $5 \cdot 10^{11}$-es kontrasztot értem el.
Egy optikai terjedést szimuláló program segítségével modelleztem a nyaláb terjedését és jó egyezést találtam a kísérleti eredményekkel, beleértve a nyalábprofilokat a PM-eken és a fókuszt a végső céltárgy síkjában. Alaposan megvizsgáltam az energiasűrűség eloszlását az első PM-en, ami a közeli mezőben van és azt találtam, hogy a nyaláb profilja ahogyan az várható volt, némileg inhomogén. Habár ez elkerülhetetlenül a visszavert nyaláb torzulását okozza, ezt nagyban kompenzálja a második PM ami a köztes fókuszban helyezkedett el s így térbeli szűrőként funkcionált. Ennek köszönhetően a DPM rendszer a nyalábprofil minőségét és fókuszálhatóságát nem rontja, sőt éppen ellenkezőleg, a végső fókusz profilja még valamelyest jobb is az eredetinél. Mivel a nagy teljesítményű lézerek fejlesztésének legfőbb célja a céltárgy felszínén minél nagyobb intenzitás elérése, ezért a fókuszálhatóság megőrzése illetve javítása a DPM rendszer legfontosabb tulajdonsága.
A DPM rendszer a 100 TW-os titán-zafír lézerrendszer integráns része, ami egyszerűen egy eltolható tükörtartó állvány elmozdításával a rendszerből kicsatolható, illetve hozzáadható. Az AR-rel bevont kvarc lemezeket számítógéppel kontrollálva lövésről-lövésre lehet mozgatni, így minden egyes lövés friss még sérületlen felszínre esik a plazma tükrökön.
Összehasonlítottam a harmonikuskeltést a DPM rendszer használatával valamint nélküle [141, 142]. Az impulzusokat „időben tisztítva" a DPM rendszerrel egy vékony harmonikus nyalábot sikerült létrehozni, valamint a céltárgy tükörszerűen reflektálta a lézernyalábot. A DPM nélkül nem sikerült magasrendű harmonikust kelteni, valamint a visszavert nyaláb diffúz és inhomogén volt. Ezzel demonstráltam, hogy a DPM-el keltett nagy kontrasztú impulzusok megőrzik a szilárd céltárgy meredek elektronikus gradiensét, ami tiszta lézer-szilárd anyag kölcsönhatások kivitelezéséhez elengedhetetlen.

3. Kifejlesztettem egy egylövéses hordozó-burkoló fázis detektort ami egymás utáni néhány ciklusos lézerimpulzusok fázisát képes mérni [143,144]. Ezt úgy értem el, hogy a műszer érzékenységét a korábbi több lövéses detektorhoz képest több mint négy nagyságrenddel növeltem meg. Az egylövéses hordozó-burkoló fázis detektorral elsőként sikerült felvennem egymás utáni fázisstabilizálatlan lövések fázisát, ami jól mutatja, hogy az általam kifejlesztett mérőműszernek a korábbi több lövéses módszerektől el-

térően a méréshez nincs szüksége fázisstabilizálásra. Ezáltal egy új mérési módszert a fázis címkézést tettem lehetővé, amivel hullámformától függő jelenségek tanulmányozása vált lehetővé bármilyen néhány ciklusos lézerrendszeren, függetlenül attól, hogy adott lézer fázisstabilizálható-e vagy sem. Ennek rendkívüli jelentőségét az adja, hogy a jelenleg a technika csúcsát képviselő több-10-TW-os néhány ciklusos lézerek fázisstabilizálatlanok. Várhatóan tehát ez a mérési módszer [145] lehetővé fogja tenni relativisztikus intenzitásokon végzett lézer-szilárd anyag kölcsönhatás elektromágneses hullámformától való függésének tanulmányozását.
A mérőműszerrel egy 3kHz ismétlési frekvenciájú lézer minden egyes lövésének fázisát detektáltam mindössze 40μJ-os impulzusenergiát használva a méréshez. Miután ez csupán 10%-a a széles körben elterjedt több-kHz-es ismétlési frekvenciájú lézerek energiájának, ezért fázis címkézés végezhető ezeken a rendszereken is. A lézert fázisstabilizálás nélkül járatva a lézer fázisának lövésről lövésre való véletlenszerű fluktoációja fázis címkézésnél egyfajta „ultragyors fázis szeknnelésként” fog funkcionálni, ami a korábbi fázisstabilizált impulzusokkal végzett fázis szkenekhez képest nagyságrendekkel gyorsabb kísérleteket eredményez. Tehát olyan kísérleteknél ahol a fázis függést a teljes 2π tartományban szeretnénk vizsgálni, ez az új mérési módszer lényegesen előnyösebb lesz a technikailag nehezen kivitelezhető fázis szkeneknél.
Ezek az eredmények [143]-ben kerültek publikálásra, valamint az ismertetésükre az MPQ és a Müncheni Műszaki Egyetem egy-egy sajtóközleményt bocsátottak ki [146, 147], valamint beszámolt róluk a Laser Focused World [148] és számos ismeretterjesztő weblap [149]. Továbbá a fázis mérési módszer Prof. Rick Trebino jól ismert Ultragyors Optika előadásjegyzeteiben [150] is ismertetésére fog kerülni.

Bibliography

[1] S-W. Bahk, P. Rousseau, T. A. Planchon, V. Chvykov, G. Kalintchenko, A. Maksimchuk, G. A. Mourou, V. Yanovsky Opt. Lett. **29**, 2837. (2004)

[2] K. Osvay, M. Csatári, I. N. Ross, A. Persson, C. G. Wahlström, Laser and Particle Beams **23**, 327. (2005)

[3] R. Szipöcs, K. Ferencz, Ch. Spielmann, F. Krausz, Opt. Lett. **19**, 201. (1993)

[4] M. Nisoli, S. De Silvestri, O. Svelto, R. Szipöcs, K. Ferencz, Ch. Spielmann, S. Sartania, F. Krausz, Opt. Lett. **22**, 522. (1997)

[5] A. Baltuska, Th. Udem, M. Uiberacker, M. Hentschel, E. Goulielmakis, Ch. Gohle, R. Holzwarth, V. S. Yakovlev, A. Scrinzi, T. W. Hänsch, F. Krausz, Nature **421**, 611. (2003)

[6] M. Uiberacker, Th. Uphues, M. Schultze, A. J. Verhoef, V. Yakovlev, M. F. Kling, J. Rauschenberger, N. M. Kabachnik, H. Schröder, M. Lezius, K. L. Kompa, H.-G. Muller, M. J. J. Vrakking, S. Hendel, U. Kleineberg, U. Heinzmann, M. Drescher, F. Krausz Nature **446**, 627. (2007)

[7] A. L. Cavalieri, N. Müller, Th. Uphues, V. S. Yakovlev, A. Baltuska, et al. Nature **449**, 1029 (2007)

[8] H. Mashiko, Ch. M. Nakamura, C. Li, E. Moon, H. Wang, J. Tackett, Z. Chang, Appl. Phys. Lett. **90**, 161114. (2007)

[9] S. Witte, R. Th. Zinkstok, A. L. Wolf, W. Hogervorst, W. Ubachs, K. S. E. Eikema, Optics Express **14**, 8168 (2006)

[10] F. Tavella, Y. Nomura, L. Veisz, V. Pervak, A. Marcinkevicius, F. Krausz, Opt. Lett. **32**, 2227. (2007)

[11] G. D. Tsakiris, K. Eidmann, J. Meyer-ter-Vehn and F. Krausz, New J. Phys. **8**, 19 (2006)

[12] G. G. Paulus, F. Lindner, H. Walther, A. Baltuska, E. Goulielmakis, M. Lezius, F. Krausz, Phys. Rev. Lett. **91**, 253004. (2003)

[13] P. Agostini, F. Fabre, G. Mainfray, G. Petite, N. K. Rahman, Phys. Rev. Lett. **42**, 1127. (1979)

[14] C. E. Cook, Proceedings of the IRE **48**, 310. (1960)

[15] D. Strickland, G. Mourou, Opt. Comm. **56**, 219. (1985)

[16] O. E. Martinez, IEEE J. Quantum Electron. **QE-23**, 59. (1987)

[17] P. Maine, D Strickland, P. Bado, M. Pessot, G. Mourou, IEEE J. Quantum Electron. **24**, 398. (1988)

[18] M. D. Perry, D. Pennington, B. C. Stuart, G. Tietbohl, J. A. Britten C. Brown, S. Herman, B. Golick, M. Kartz, J. Miller, H. T. Powell, M. Vergino, and V. Yanovsky Opt. Lett. **24**, 160. (1999)

[19] C. N. Danson, et al. Nucl. Fusion **44**, S239. (2004)

[20] Y. Kitagawa, et al. IEEE J. Quantum Electron. **40**, 281. (2004)

[21] J. Hecht, Laser focus World **42**, 105. (2006)

[22] M. Tabak, J. Hammer, M. E. Glinsky, W. L. Kruer, S. C. Wilks, J. Woodworth, E. M. Campbell, M. D. Perry, R. J. Mason, Phys. Plasmas **1**, 1626. (1994)

[23] M. H. Key, K. Estabrook, B. Hatchett, D. Hinkel, J. Kilkenny, J. Koch, et al. Phys. Plasmas **5**, 1966. (1998)

[24] R. A. Snavely, M. H. Key, S. P. Hatchett, T. E. Cowan, M. Roth, T. W. Phillips, M. A. Stoyer, E. A. Henry, T. C. Sangster, M. S. Singh, S. C. Wilks, A. MacKinoon, A. Offenberger, D. M. Pennington, K. Yasuike, A. B. Landon, B. F. Lasinkski, J. J. Johnson, M. D. Perry, E. M. Campbell, Phys. Rev. Lett. **85**, 2945. (2000)

[25] B. Dromey et al. Nature Physics **2**, 456. (2006)

[26] R. Lichter, J. Meyer-ter-Vehn, and A. Kukhov, Phys. of Plasmas, **3**, 3425. (1996)

[27] J. D. Bonlie, F. Patterson, D. Price, B. White, P. Springer Appl. Phys. B **70**, S155. (2000)

[28] D. Umstadter, S.-Y.Chen, A. Maksimchuk, G. Mourou, R. Wagner, Science **273**, 472. (1996)

[29] A. G. Zhidkov, A. Sasaki, T. Tajima, T. Aguste, P. D'Olivera, S. Hulin, P. Monot, A. Ya. Faenov, T. A. Pikuz, I. Yu. Skobelov, Phys. Rev. E**60**, 3273. (1999)

[30] J. D. Kmetec, C. L. Gordon, III, J. J. Macklin, B. E. Lemmof, G. S. Brown, S. E. Harris, Phys. Rev. Lett. **68**, 1527. (1992)

[31] P. Norreys, M. Santala, E. Clark, M. Zepf, I. Watts, F. N. Beg, K. Krushelnick, M. Tatarakis, A. E. Dangor, X. Fang, P. Graham, T. McCanny, R. P. Singhal, K. W. D. Ledingham, A. Creswell, D. C. W. Sanderson, J. Magill, A. Machacek, J. S. Wark, R. Allott, B. Kennedy, D. Neely, Phys. of Plasmas, **6**, 2150. (1999)

[32] S.-Y.Chen, A. Maksimchuk, D. Umstadter, Nature **396**, 653. (1998)

[33] G. Steinmeyer, D. H. Sutter, L. Gallmann, N. Matuschek, U. Keller, Science **286**, 1507. (1999)

[34] K. Yamane, Z. Zhang, K. Oka, R. Morita, M. Yamashita, A. Sugoro, Opt. Lett. **28**, 2258. (2003)

[35] E. Goulielmakis et al. Science **320**, 1614. (2008)

[36] A. Zewail, J. Phys. Chem. A **104**, 5660. (2000)

[37] F. Krausz Physics World, **14**, 41. (2001)

[38] P. B. Corkum Phys. Rev. Lett. **71**, 1994 (1993)

[39] M. Drescher, M. Hentschel, R. Kienberger, G. Tempea, Ch. Spielmann, G. A. Reider, P. B. Corkum, F. Krausz, Science **291**, 1923. (2001)

[40] M. Drescher, M. Hentschel, R. Kienberger, M. Uiberacker, V. Yakovlev, A. Scrinzi, Th. Westerwalbesloh, U. Kleineberg, U. Heinzmann, F. Krausz, Nature **419**, 803. (2002)

[41] M. Hentschel, R. Kienberger, Ch. Spielmann, G. A. Reider, N. Milosevic, T. Brabec, P. Corkum, U. Heinzmann, M. Drescher, F. Krausz, Nature **414**, 509. (2001)

[42] R. Kienberger, M. Hentschel, M. Uiberacker, Ch. Spielmann, M. Kitzler, A. Scrinzi, M. Wieland, Th. Westerwalbesloh, U. Kleineberg, U. Heinzmann, M. Drescher, F. Krausz, Science **297**, 1144. (2002)

[43] P. B. Corkum, F. Krausz, Nature Physics **3**, 381. (2007)

[44] J. Itatani, J. Faure, M. Nantel, G. Mourou, S. Watanabe, Opt. Comm. **148**, 70. (1998)

[45] S. Luan, M. H. R. Hutchinson, R. A. Smith F. Zhou Meas. Sci. Technol **4**, 1426. (1993)

[46] A. Tien, M. Nantel, G. Mourou, D. Kaplan, M. Bouvier, Opt. Lett. **22**, 1559. (1997)

[47] D. Grischkowsky, A. C. Balant, Appl. Phys. Lett. **41**, 1. (1982) 41, 1 (1982)

[48] J. P. Heritage, R. N. Thurston, W. J. Tomlinson, A. M. Weiner, R. H. Stolen, Appl. Phys. Lett. **47**, 87. (1985)

[49] M. D. Perry, F. G. Patterson, J. Weston, Opt. Lett. **15**, 381. (1990)

[50] K. Yamakawa, C. P. J. Barty, H. Shiriga, Y. Kato, IEEE J. Quantum Electron. **27**, 288. (1991)

[51] K. Yamakawa, H. Shiriga, Y. Kato, C. P. J. Barty, Opt. Lett. **16**, 1593. (1991)

[52] Y.-H. Chuang, D. D. Meyerhofer, S. Augst, H. Chen, J. Peatross, S. Uchida, J. Opt. Soc. Am. B, **8**, 1226. (1991)

[53] J. D. Kmetec, J. J. Macklin, J. F. Young, Opt. Lett. **16**, 1001. (1991)

[54] J-L. Tapié, G. Mourou, Opt. Lett. **17**, 136. (1992)

[55] R. S. Marjoribanks, F. W. Budnik, L. Zhao, G. Kulcsár, M. Stainer, J. Mihaychuk, Opt. Lett. **18**, 361. (1993)

[56] B. E. Lemoff, C. P. J. Barty, Opt. Lett. **18**, 1651. (1993)

[57] A. Sullivan, W. E. White, Opt. Lett. **20**, 192. (1995)

[58] G. Cheriaux, P. Rousseau, F. Salin, J. P. Chambaret, B. Walker, L. F. Dimarou, Opt. Lett. **21**, 414. (1996)

[59] M. Pittmann, S. Ferré, J. P. Rousseau, L. Notebaert, J. P. Chambaret, G.Chériaux, Appl. Phys. B **74**, 529. (2002)

[60] I. N. Ross, P. Matousek, M. Towrie, A. J. Langley, J. L. Collier, Opt. Comm. **144**, 125. (1997)

[61] I. N. Ross, J. L. Collier, P. Matousek, C. N. Danson, D. Neely, R. M. Allott, D. A. Pepler, C. Hernandez-Gomez, K. Osvay, Appl. Opt. **39**, 2422. (2000)

[62] I. Jovanovic, B. J. Comaskey, C. A. Ebbers, R. A. Bonner, D. M. Pennington, E. C. Morse, Appl. Opt. **41**, 2923. (2002)

[63] G. Kurdi, K. Osvay, M. Csatári, I. N. Ross, J. Klebniczki, IEEE J. Sel. Top. Quant. Electr. **10**, 1259. (2004)

[64] F. Tavella, A. Marcinkevicius, F. Krausz, New J. Phys. **8**, 219 (2006)

[65] G. Veres, G. Kocsis, E. Rácz, S. Szatmári, Appl. Phys. B **78**, 635. (2004)

[66] H. C. Kapteyn, M. M. Murnane, A. Szoke, and R. W. Falcone, Opt. Lett. **16**, 490. (1991)

[67] D. M. Gold, H. Nathel, P. R. Bolton, W. E. White and L. D. Woerkom SPIE Short Pulse High-Intensity Lasers and Applications **1413**, 41. (1991)

[68] S. Backus, H. C. Kapteyn, M. M. Murnane, D. M. Gold, H. Nathel, and W. White Opt. Lett. **18**, 134. (1993)

[69] D. M. Gold, Opt. Lett. **19**, 2006. (1994)

[70] Z. Bor, B. Rácz, G. Szabó, D. Xenakis, C. Kalpouzos, and C. Fotakis Appl. Phys. A **60**, 365. (1995)

[71] B. Hopp, Z. Tóth, K. Gál, Á. Mechler, Zs. Bor, S. D. Moustaizis, S. Georgiou, C. Fotakis Appl. Phys. A **69**, 191. (1999)

[72] Z. Tóth, B. Hopp, Á. Mechler, Z. Bor, S. D. Moustaizis, A. Athanassiou, S. Georgiou, C. Kalpouzos, and C. Fotakis Laser Physics **10**, 241. (2000)

[73] R. P. Feynman, R. B. Leighton, M. Sands, The Feynman lecture notes on physics: section **59.3**

[74] M. Geissler, G. Tempea, A. Scrinzi, M. Schnürer, F. Krausz, T. Brabec, Phys. Rev. Lett. **83**, 2930 (1999)

[75] Y. Nomura, L. Veisz, K. Schmid, T. Wittmann, J. Wild, F. Krausz, New J. Phys. **9**, 9 (2007)

[76] L. Veisz, Y. Nomura, K. Schmid, F. Krausz, T. Wittmann, Lasers and Electro-Optics Europe, 2005. CLEO/Europe DOI10.1109/CLEOE.2005.1568200 page:422 (2005)

[77] F. F. Chen, Introduction to Plasma Physics and Controlled Fusion, Plenum Press (1984)

[78] R. J. Goldston, P. H. Rutherford, Introduction to plasma physics, Institute of Physics publishing (2000)

[79] D. Giulietti, L. A. Gizzi X-ray emission from laser-produced plasmas, La Rivista del Nuovo Cimento, (1998)

[80] V. L. Ginzgurg, The propagation of electromagnetic waves in plasmas 2ed., Pergamon Press (1970)

[81] B. N. Gershman, V. L. Ginzgurg, N. G. Denisov, Uspekhi fizicheskikh nauk **82**, 561 (1957)

[82] N. G. Denisov, Soviet Physics, JETP **4**, 544 (1957)

[83] W. L. Kruer, The Physics of Laser Plasma Interactions, Addison-Wesley publishing company (1988)

[84] K. Mima, H. A. Baldis, A. Nishiguchi, H. Tabake, C. Yamanaka, Laser plasma theory and simulations, Harwood Academic Publishers (1994)

[85] D. Du, X. Liu, G. Korn, J. Squier, G. Mourou, Appl. Phys. Lett. **64**, 3071. (1994)

[86] B. C. Stuart, M. D. Feit, A. M. Rubenchik, B. W. Shore, M. D. Perry, Phys. Rev. Lett. **74**, 2248 (1995)

[87] B. C. Stuart, M. D. Feit, S. Herman, A. M. Rubenchik, B. W. Shore, M. D. Perry, Phys. Rev. B. **53**, 1749 (1996)

[88] B. C. Stuart, M. D. Feit, S. Herman, A. M. Rubenchik, B. W. Shore, M. D. Perry, J. Opt. Soc. Am. B. **13**, 459 (1996)

[89] B. C. Stuart, M. D. Feit, S. Herman, A. M. Rubenchik, B. W. Shore, M. D. Perry SPIE Short Pulse High-Intensity Lasers and Applications **2714**, 616. (1996)

[90] H. Varel, D. Ashkenasi, A. Rosenfeld, R. Herrmann, F. Noack, E. E. B. Campbell, Appl. Phys. A **62**, 293. (1996)

[91] M. Lenzner, J. Krüger, S. Sartania Z. Cheng, Ch. Spielmann, G. Mourou, W. Kautek, F. Krausz, Phys. Rev. Lett. **80**, 4076 (1998)

[92] A-C. Tien, S. Backus, H. Kapteyn, M. Murname, G. Mourou, Phys. Rev. Lett. **82**, 3883 (1999)

[93] W. Kautek, J. Krüger, M. Lenzner, S. Sartania, Ch. Spielmann, F. Krausz, Appl. Phys. Lett. **69**, 3146 (1996)

[94] K. K. Thornber, J. Appl. Phys. **52**, 279. (1981)

[95] L. V. Kledysh, Sov. Phys. JETP **20**, 1307 (1965)

[96] O. Wood, II,W. T. Silfvast, H. W. K. Tom, W. H. Knox, R. L. Fork, C. H. Brito-Cruz, M. C. Downer, P. J. Maloney Appl. Phys. Lett. **53**, 654. (1988)

[97] S. E. Harris, J. D. Kmetec Phys. Rev. Lett. **61**, 62 (1988)

[98] M. M. Murnane, H. C. Kapteyn, R. W. Falcone Phys. Rev. Lett. **62**, 155 (1989)

[99] N. H. Burnett, H. A. Baldish, M. C. Richardson G. D. Enrigh Appl. Phys. Lett. **31**, 172. (1977)

[100] E. A. McLean, J. A. Stamper, B. H. Ripin, H. R. Griem, J. M. McMahon, S. E. Bodner Appl. Phys. Lett. **31**, 825. (1978)

[101] R. L. Carman, C. K. Rhodes, R. F. Benjamin Phys. Rev. A **24**, 2649. (1981)

[102] M. Zepf, G. D. Tsakiris, G. Pretzler, I. Watts, D. M. Chambers, P. A. Norreys, U. Andiel, A. E. Dangor, K. Eidmann, C. Gahn, A. Machacek, J. S. Wark, and K. Witte Phys. Rev. E **58**, R5253. (1998)

[103] P. Gibbon, Phys. Rev. Lett. **76**, 50 (1996)

[104] A. Pukhov, J. Meyer-ter-vehn, Appl. Phys. B **74**, 355. (2002)

[105] J. Faure, Y. Glinec, A. Pukhov, S. Kiselev, S. Gordienko, E. Lefebre, J.-P. Rousseau, F. Burgy and V. Malka, Nature **431**, 541. (2004)

[106] J. Faure, C. Rechatin, A. Norlin, A. Lifschitz, Y. Glinec and V. Malka, Nature **444**, 737. (2006)

[107] A. Giulietti, P. Tomassini, M. Galimberti, D. Giulietti, L. A. Gizzi, P. Koestler, L. Labate, T. Cecccotti, P. D'Oliveira, T. Auguste, P. Monot, P. Martin, Phys. Plasmas **13**, 093103. (2006)

[108] S. P. D. Mangles, A. G. R. Thomas, M. C. Kaluza, O. Lundh, F. Lindau, A. Persson, Z. Najmudin, C-G Wahlström, C. D. Murphy, C. Kamperiddis, K. L. Lancaster, E. Divall and K. Krushelnick Plasma Phys. Control. Fusion **48**, B83 (2006)

[109] T. Tajima, J. M. Dawson, Phys. Rev. Lett. **43**, 267 (1979)

[110] A. J. Mackinnon, M. Borghesi, S. Hatchett, M. H. Key, P. K. Patel, H. Campbell, A. Schiavi, R. Snavely, S. C. Wilks, and O. Willi Phys. Rev. Lett. **86**, 1769 (2001)

[111] I. Spencer, K. W. D. Ledingham, P. McKenna. T. McCany, R. P. Singhal. P. S. Foster, D. Neely, A. J. Langley, E. J. Divall, C. J. Hooker, R. J. Clarke, P. A. Norreys, E. L. Clark, K. Krushelnick, J. R. Davis Phys. Rev. E. **67**, 046402 (2003)

[112] M. Kaluza, J. Schreiber, M. I. K. Santala, G. D. Tsakiris, K. Eidman, J. Meyer-ter-Vehn, and K. J. Witte Phys. Rev. Lett. **93**, 045003 (2004)

[113] T. Boehly, Y. Fisher, D. D. Meyerhofer, W. Seka, J. M. Soures and D. K. Bradley Phys. Plasmas **8**, 231. (2001)

[114] K. B. Wharton, C. D. Boley, A. M. Komasho, A. M. Rubenchik, J. Zweiback, J. Crane, G. Hays, T. E. Cowan, T. Ditmire, Phys. Rev. E **64**, 025401 (2001)

[115] I. B. Földes, G. Kocsis, E. Rácz, S. Szatmári, G. Veres, Laser and Particle Beams **21**, 517. (2003)

[116] S. Szatmári, Appl. Phys. B **58**, 211. (1994)

[117] B. Dromey, S. Kar, M. Zepf, P. Foster, Rev. Sci. Instrum. **75**, 645. (2004)

[118] W. E. Lamb Jr., Phys. Rev. 134 (6A), A1429 (1964)

[119] U. Keller, et al. Opt. Lett. **17**, 505 (1992)

[120] P. M. Paul, et al. Science **292**, 1689 (2001)

[121] K. Varjú, et al. Phys. Rev. Lett. **95**, 243901 (2005)

[122] T. Remetter, P. Johnsson, J. Mauritsson, K. Varjú, et al. Nature Physics **2**, 323 (2006)

[123] E. Goulielmakis, M. Uiberacker, R. Kienberger, A. Baltuska, V. Yakovlev, A. Scrinzi, Th. Westerwalbesloh, U. Kleineberg, U. Heinzmann, M. Drescher, F. Krausz, Science **305**, 1267 (2004)

[124] G. Szabó, Z. Bor, A. Müller, Opt. Lett. **13**, 746 (1988)

[125] D. J. Kane, R. Trebino, IEEE J. Quan. Electron **29**, 571. (1993)

[126] T. M. Fortier, P. A. Roos, D. J. Jones, S. T. Cundiff, R. D. R. Bhat, J. E. Sipe, Phys. Rev. Lett. **92**, 147403. (2004)

[127] M. Kress, et al. Nature Phys. **2**, 327. (2006)

[128] C. A. Haworth et al. Nature Phys. **3**, 52. (2007)

[129] A. Apolonski et al. Phys. Rev. Lett. **92**, 073902. (2003)

[130] S. Chelkowski, A. D. Bandrauk, Phys. Rev. A. **71**, 053815 (2005)

[131] G. G. Paulus, F. Grasbon, H. Walther, P. Villoresi, M. Nisoli, S. Stagira, E. Priori, S. De Silvestri, Nature **414**, 182. (2001)

[132] F. Lindner, G. G. Paulus, H. Walther, A. Baltuska, E. Goulielmakis, M. Lezius, F. Krausz Phys. Rev. Lett. **92**, 113001 (2004)

[133] M. G. Schätzel, F. Lindner, G. G. Paulus, H. Walther, E. Goulielmakis, A. Baltuska, M. Lezius, F. Krausz, Appl. Phys. B **79**, 1021. (2004)

[134] C. Li, E. Moon, H. Wang, H. Mashiko, Ch. M. Nakamura, J. Tackett, and Z. Chang, Opt. Lett. **32**, 796. (2007)

[135] C. Li, E. Moon, H. Mashiko, H. Wang, Ch. M. Nakamura, J. Tackett, Z. Chang, Appl. Opt. **48**, 1303. (2009)

[136] H. Wang, E. Moon, M. Chini, H. Mashiko, C. Li, Z. Chang, Opt. Expr. **17**, 12082. (2009)

[137] S. Chelkowski, A. D. Bandrauk, Phys. Rev. A. **70**, 013815 (2004)

[138] A. L. Cavalieri, E. Goulielmakis, B. Horvath, W. Helml, M. Schultze, M. Fieß, V. Pervak, L. Veisz, V. S. Yakovlev, M. Uiberacker, A. Apolonski, F. Krausz, R. Kienberger, New J. Phys. **9**, 242 (2007)

[139] G. Doumy, F. Quéré, O. Gobert, M. Perdrix, Ph. Martin, P. Audebert, J. C. Gauthier, J.-P. Geindre, and T. Wittmann, Phys. Rev. E **69**, 026402 (2004)

[140] T. Wittmann, J. P. Geindre, P. Audebert, R. S. Marjoribanks, J. P. Rousseau, F. Burgy, D. Douillet, T. Lefrou, K. Ta Phuoc, and J. P. Chambaret, Rev. Sci. Instrum. **77**, 083109. (2006)

[141] R. S. Marjoribanks, J. P. Geindre, P. Audebert, T. Wittmann, G. Doumy, P. Martin, M. Perdrix, F. Quere, P. Monot, D. Douillet, T. Lefrou, K. T. Phuoc, S. Sebban, J. P. Rousseau, F. Burgy, B. Cross, 2005 Quantum Electronics and Laser Science Conference (QELS) **3**, 2021 (2005)

[142] R. S. Marjoribanks, P. Audebert, J. P. Geindre, T. Wittmann, J. C. Gauthier, Ph. Martin, O. Gobert, M. Perdrix, F. Quere, G. Doumy, P. Monot, P. D'Oliveira, D. Douillet, K. T. Phuoc, S. Sebban, J. P. Rousseau, F. Burgy, B. Cross, American Physical Society, 46th Annual Meeting of the Division of Plasma Physics, 2004APS..DPPCO2015M

[143] T. Wittmann, B. Horvath, W. Helml, M. G. Schätzel, X. Gu, A. L. Cavalieri, G. G. Paulus, R. Kienberger, Nature Physics **5**, 357 (2009)

[144] T. Wittmann, B. Horvath, W. Helml, M. G. Schätzel, X. Gu, A. L. Cavalieri, G. G. Paulus, R. Kienberger, Conference on Ultrafast Phenomena, 2008, THU2P.1

[145] T. Wittmann, M. G. Schätzel, F. Lindner, G. G. Paulus, A. Baltuska, M. Lezius, A. Marcinvevicius, F. Tavela, F. Krausz IAMPI, 2006, Szeged, poster P23

[146] http://www.mpq.mpg.de/cms/mpq/en/news/press/09_04_19.html

[147] http://portal.mytum.de/pressestelle/pressemitteilungen/news_article.2009-04-18.8174740109/newsarticle_view

[148] Ultrafast-pulse Diagnostics: Single-shot technique measures CEP for few-cycle pulses, Laser Focus World, June 2009

[149] http://www.world-of-photonics.net/link/en/21644171
http://www.laseropto.de/index.php?id=5&artid=3261&np=2&L=1
http://www.analytica-world.com/news/d/99906/
http://idw-online.de/pages/de/news310446
http://www.chemie.de/news/d/99906/

[150] http://www.physics.gatech.edu/frog/lectures/index.html

Acknowledgements

I would like to thank all the people who helped me to achieve the results presented in this thesis. Since the experimental work was conducted in three different laboratories with a help of a great many collaborators, let me apologize in advance if some names are unintentionally omitted.

First of all I would like to acknowledge my supervisor Prof. Béla Rácz at the Department of Optics and Quantum Electronics at the University of Szeged for his constant support and for helping me whenever I had problems.

I'm indebted to Prof. Zsolt Bor, the former head of the Department for orienting me towards laser physics at the third year of my university studies. I am grateful to Prof. Gábor Szabó for supporting my Erasmus stipend to the Friedrich Schiller University of Jena, where I could gain knowledge about multi-TW lasers and strong-field laser physics.

I would like to thank Patrick Audebert for supervising my work at the Laboratoire pour l'Utilisation des Lasers Intenses. His healthy criticism and scientific guidance helped me to gain a deeper understanding in physics in general.

I thank Prof. Ferenc Krausz for giving me the opportunity to work in his group at the Max Planck Institute of Quantum Optics and for his thoughtful suggestions from his knowledge and experience. I'm indebted to Prof. Reinhard Kienberger for his patience and support during my work, and Prof. Gerhard Paulus for introducing me CEP measurements and for helping me to develop the single-shot stereo-ATI detector. I thank Bálint Horváth for his great enthusiasm and particular endurance in the lab work and particularly during the data analysis that allowed us not to give up but to go on even when everything seemed entirely hopeless.

I would like to say thank you also to: Jean-Paule Geindre at LULI, Philip Marin, Gilles Doumy at CEA Saclay, Jean-Paul Chambaret, Jean-Philippe Rousseau, Frédéric Burgy, Denis Douillet, Thierry Lefrou, Kim Ta Phuoc at LOA, Michael Schätzel and Wolfram Helml at MPQ.

Last but not least, I would like to thank my family for all their help and for supporting me any time in any possible way.